Structure Activity Relationships in the Fracture of Hybrid Covalent/Metallosupramolecular Organogels

by

Jennifer L. Hawk

Department of Chemistry
Duke University

Date:_____

Approved:

_____
Stephen L. Craig, Supervisor

_____
Michael C. Fitzgerald

_____
Richard A. MacPhail

_____
Stefan Zauscher

Dissertation submitted in partial fulfillment of
the requirements for the degree of Doctor of Philosophy in
the Department of Chemistry in the Graduate School
of Duke University

2014

ABSTRACT

Structure Activity Relationships in the Fracture of Hybrid

Covalent/Metallosupramolecular Organogels

by

Jennifer L. Hawk

Department of Chemistry
Duke University

Date:_____

Approved:

_____
Stephen L. Craig, Supervisor

_____
Michael C. Fitzgerald

_____
Richard A. MacPhail

_____
Stefan Zauscher

An abstract of a dissertation submitted in partial
fulfillment of the requirements for the degree
of Doctor of Philosophy in the Department of
Chemistry in the Graduate School
of Duke University

2014

Abstract

Hybrid polymeric networks constructed using both covalent and reversible cross-links have been shown to be effective in preventing fracture and ultimately failure in polymeric materials. The prevention of failure has been largely attributed to the ability of the reversible cross-links to dissipate energy without breaking the covalent cross-links. The ability to rationally design materials that optimize this strategy would benefit from quantitative and systematic studies of the relationship between the number and strength of reversible interactions and the failure behavior of hybrid networks. This dissertation describe studies of fracture under compression in a family of hybrid networks, in which the timescale of reversible cross-linker dissociation is varied over several orders of magnitude, whereas the covalent components are kept constant.

Polymeric networks were constructed with 4-vinylpyridine. Bimetallic pincer Pd and Pt complexes were inserted into the network, forming reversible metal-ligand bonds that cross-link pyridine residues. The additional reversible cross-links prolong the lifetime of the hybrid networks under compressive strain when compared to their covalent counterparts. The observed failure behavior is dependent on the rate at which the networks are compressed as well as the strength of reversible interaction. Most interestingly, the addition of very dynamic and weak reversible interactions, so weak as to make no measurable contribution to bulk modulus, still leads to enhanced fracture

strains. The failure of the covalent component within these hybrid networks was probed directly by incorporating a mechanophore that emits light upon chain scission. It was confirmed that the addition of these dynamic and weak reversible cross-links delays the catastrophic bond scission events associated with failure in the materials.

Dedication

"Most people are familiar with the basics of rheology from experience with diarrhea or perhaps rheostats." - Janmey, and Schliwa 2008.

This dissertation is dedicated to my colon, Eglon. May he rest in peace.

Contents

List of Tables

List of Figures

List of Symbols and Abbreviations:

E_c = compressive modulus

ε_b = % strain at break under compression

σ_b = maximum stress at break

v_c = compression velocity

$\dot{\varepsilon}_i$ = average initial compression strain rate

ϕ_{rel} = relative volume fraction

ε_{em} = % strain where the maximum light emission is observed

DN = double networks

IPN = interpenetrating networks

PAMPS = 2-acrylamido-2-methylpropanesulfonic acid

PAAm = poly(acrylamide)

AFM = atomic force microscopy

QELS = quasi-elastic light scattering

TEM = transmission electron microscopy

CoPM = coordination polymer multilayer

ROMP = ring-opening metathesis polymerization

PVP = Poly (4-vinyl pyridine)

DMAP = dimethylaminopyridine

DMSO = dimethyl sulfoxide

DBH = 1,6 – dibromohexane

DPEA = *9,10*-Bis(phenylethynyl)anthracene

Acknowledgements

I could not have made it through graduate school without the love and support of so many people. A short acknowledgements section hardly seems to capture the gratitude in my heart for all of these people, but I will try my best to express my appreciation for everything they have done for me over the years.

I would first like to thank everyone who has helped me on the professional side of things. Thank you so much Steve Craig, for helping and guiding me over the years. You encouraged me from the first day I met with you to become the "scientist I wanted to become." I really believe you have supported me in that. You allowed me to participate in teaching and training opportunities that prepared me for my dream job after Duke. I would also like to thank my teaching mentors over the years, Todd Woerner, Jim Bonk, and Dick MacPhail. I knew when I came to Duke that I wanted to become an educator and these men demonstrated what being a teacher looks like on a day to day basis. The lessons I learned from them will always stay with me. I would also like to thank the Duke University Chemistry Department for the practical support of resources and collaborations.

I would like to thank Zach Kean for his help and collaboration on the work discussed in Chapter 4. His synthetic chemistry abilities are a gift. His inspiration and insight into the dioxetane work was invaluable. His practical help with the camera and

analyzing the light data are greatly appreciated. I would also like to thank Zach for making awesome smoke "machines" for our lab dance parties. I would also like to thank Donghua Xu for his helpful discussion and contributions to the work described in my dissertation.

In addition to the practical and professional support from the Department, my personal interactions with fellow students in the Department has been a great blessing. When I first came to Duke, I had older graduate students who took me under their wing and became my big brothers and sisters in Chemistry. Claire Siburt and Sarah Crider, thank you so much for all of the meals, sleepovers, and venting sessions. Your support through graduate school has been great. You told me how to pass my pre-lim, showed me how to get a job, and how to be a "big kid". David Loveless and Jared Heymann, you guys taught me all about Duke Basketball, "that Christian guy", T's, and battle doming. You taught me how to enjoy life outside of a chemistry lab and I will never forget that.

Julie Pollock, you were my first friend in grad school. We met the first day of orientation at breakfast. I remember being scared and unsure of what this chapter of my life held….then I met you. We had similar goals and backgrounds and you just felt like a friend. I know our friendship has grown and changed over the years, but so many of my first memories at Duke involve you. I'm so grateful to share such a big part of my life with you. Robert Harris, thanks for drinking whiskey and watching basketball with

me in my old age. Thanks for all of the postgame milkshake runs, encouraging me to get mad at chemistry, allowing me to work on projects around your house to blow off steam, and cooking me chili. You were a steadfast friend in some of the roughest times of my life. Ariel Geer, you brought the spark of youth to me in the last few years at Duke. You are so perky and happy. I love hugging you. Thanks for all of the lunch time talks and laughter. I would also like to thank "all my Ladies" (Amanda, Ashley, and Adria), for the dance parties and crazy times in the Craig Lab.

CRAIG LAB LOVE! Wow – I don't even know how to put this into words. I would like to thank all of the past and present generations of the Craig Lab. The old guard (Raj, David, Farrel, and Mike) was rough and gruff, but still got me through my pre-lim. You harassed me and showed me the ropes at the same time. Jeremy, Ashley, Hope, Zach, Donghua, Junpeng, and Bobin you guys have been great. I wish you all the best in whatever you end up doing. John Overcash, "my" undergrad, thanks for helping me get data to pass my pre-lim, talking science when we couldn't figure something out, and buying me computers whenever I need a new one!

The support I received outside of lab meant so much to me as well. I would like to take this time to thank the people who aren't affiliated with the Chemistry program. First, I would like to thank my Dissertation Spouse, Stephanie Holmer. D.S. we did the two worst things in life together – we wrote our dissertations and we exercised together. Thanks for all of the countless hours of talking over life, boys, and science. You

supported me when I was at my lowest points in life and loved me even when I was a hot mess. I can't even really explain the ways you supported me, but you always did and that was awesome. I would also like to thank my nanimals - The Sheep, The Duck, and The Big One - for their support over the years. You made up my home and brought love, laughter, and beauty into my life. Thanks for all of the meals, puppy piles, and adventures. Pearl and Jenny – you are the two people who have pretty much known me the entire time I've been here at Duke. You are the thread that ties together the different "eras" of my time in Durham. I met you the first weekend I came to Duke, and you have been around ever since. Thanks for reminding me what good Midwesterners are like and for driving back and forth to Raleigh. Nate Massey, thanks for the use of the LBH for work parties. You always offered practical support when needed. Thanks for the rides, the tech support and oreos and ice cream. You challenged me with questions and poked fun at the ridiculousness in life. You got to know me towards the end of this process, but you took that with a grain of salt and became my friend anyway.

I would like to take the time to thank the InterVarsity Grad Christian Fellowship here at Duke. GCF has been such a great group of people. While the individuals have changed over the years, the group has remained a constant support in my life. GCF constantly challenged me to think about my faith, my career, and my life. Steve Hinkle has guided and counseled me through so much over the years, and his leadership has been a great inspiration. And last, but certainly not least, I would like to thank my

Family – Mom, Dad, Lisa, Andrew, Melissa, Timmy, Hilary, Emma, Wyatt, and Kenzie. You have kept me going through the thick and thin. Thanks for all the love, support, texts, calls, trips back and forth to N.C., flowers, and Take5 bars.

1. Introduction to Polymer Networks

Many versatile and useful materials are currently built using polymer networks. Polymer networks, like all materials, can experience failure when subjected to load, and recent studies have focused on strategies for making networks that can withstand greater stresses and strains.[1-5] Among the strategies is the incorporation of reversible, supramolecular interactions into a covalent network – a class of materials hereafter referred to as *hybrid networks*, and which have been shown to be useful in many different applications.[6-9]

This dissertation examines how the addition of weak interactions influences the stress and strain that a given covalent gel can withstand before rupturing. The focus is on the development and characterization of new hybrid networks constructed with a common covalent component and a modular reversible component whose dynamics can be varied across a range of dissociation time scales. The goal was to elucidate the structure activity relationships that dictate the fracture of the gels under strain, with a specific emphasis on the dynamics of the reversible component.

Following a brief introduction to different types of polymer networks and some of their limitations in this chapter, Chapter 2 presents pincer complexes as tools for physical and materials applications, including their role as probes of polymer physics – a capacity in which they are used in work described in the remainder of the dissertation. Chapter 3 describes how the addition of even very weak and highly dynamic reversible

cross-linking can have an unexpected and substantial impact on the maximum strain that a covalent gel can sustain before breaking. The mechanism of the improvement in properties is explored further in Chapter 4, from the perspective of the covalent network framework. Work discussed in Chapter 5 further suggests that the dynamics of the reversible components also directly influence the relaxation behavior of the hybrid networks under compression. Finally, Chapter 6 looks ahead to remaining prospects and questions that have arisen from the work.

1.1 Covalent Polymer Networks

The first polymeric network was reported by Baekeland in 1909.[10] These initial networks were hard and insoluble, and they demonstrated that permanent networks could be formed using covalent chemistry. Covalent networks have since been studied extensively and developed for various functions. Many models have been developed to describe the elasticity[11] and behavior of networks under stress and strain.[2, 12] An array of synthetic methods can be used to form networks of different compositions and properties.

Polymeric gels are formed when polymer networks are swollen in liquid.[13] Gels can be designed for various applications using appropriate combinations of polymers and solvents.[14-16] Hydrogels, for example, are a class of gels that are swollen in water and exhibit many interesting properties,[17] especially for biological applications including: drug delivery,[18] joint fluid[19], tissue engineering,[20-21] contact lenses,[22] and cornea

replacements.[23] Organogels are gels that are swollen in organic solvents and also have many applications. Some organogels have biological compatibility and are used for drug delivery[24], edible food options[25], and enzyme immobilization in membranes.[26] Organogels can also be used for non-health related functions such as light harvesting[27] and electronically active soft materials.[28]

Interpenetrating networks (IPN) or double networks (DN) comprise two different networks that are physically interlocked but not covalently linked together.[29] An initial network is formed first and then the components of the second network are introduced to the system. The second network is then cross-linked around and through the initial network. The two networks cannot be separated unless covalent bonds are broken, but they are not covalently linked together.[30] IPNs offer several advantages over single network structures. For example, a highly deformable network can be combined with a network of a higher modulus. The combined IPN may exhibit higher elasticity than the second network, while also having a higher modulus than the first network.[29, 31]

Gong *et al.* have developed DN hydrogels with drastically increased strength under compression when compared to their single network components.[32] Single networks comprised of either poly(2-acrylamido-2-methylpropanesulfonic acid) (PAMPS) or poly(acrylamide) (PAAm) and a DN comprised of both PAMPS and PAAm were compressed. Figure 1 shows a comparison of a single network and a DN before and after being exposed to a high compressive strain.

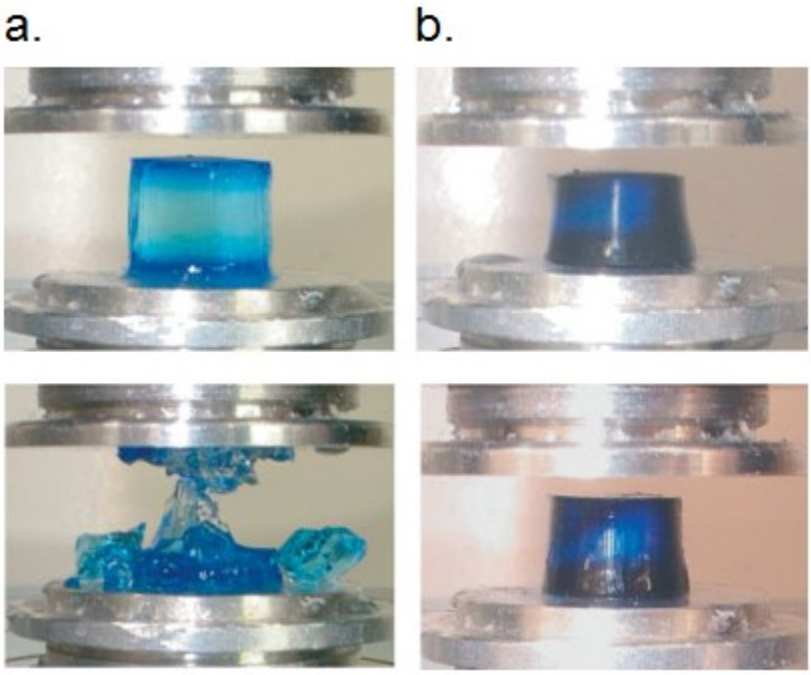

Figure 1: Single and double networks before and after compression
a. A hydrogel comprised of a single PAMPS network fractures at 0.4 MPa. b. When a DN hydrogel comprised of both PAMPS and PAAm is compressed to the same stress, it survives. Figure was reproduced from reference 32 with permission from Copyright @ 2003 John Wiley and Sons.

The DNs were able to withstand more than 20 times the amount of applied stress withstood in either of the individual networks. The most dramatic increase in ultimate strength of the DN came when the first network was highly cross-linked and the second was more lightly cross-linked. The DN combines the stiffness of the highly cross-linked first network with the ability to easily dissipate stress through the fluidity/viscosity of the loosely cross-linked second network.

Similarly, Liao and coworkers recently developed three dimensional IPNs with a complex woven structure that mimics the material properties of articular cartilage.[33] When compared with either just the woven scaffold, or the single network hydrogels, the composite of both the woven scaffold and interpenetrating hydrogel best approximated the material properties of articular cartilage, showing improvements in strain recovery, compressive modulus, dynamic modulus, and coefficient of friction over either of the single components.

1.2 Reversible Polymer Networks

In addition to the plethora of covalent networks, many networks are formed through reversible supramolecular interactions.[34-38] These reversible networks (physical gels) can be built using any of the various supramolecular interactions including host-guest complexes,[39] hydrogen bonding,[40-42] metal-ligand associations,[8, 43-46] van der Waals interactions or π-π interactions.[47-48] These reversible interactions break and reform on timescales that depend on the interactions used. Reversible networks offer an intriguing answer to the problem of failure observed in purely covalent networks, because the reversible interactions are inherently reversible *reform* after they break. Many reversible networks have been referred to as "self-healing" because of this ability to reform either autonomously or in response to external stimuli.[49-55]

Hydrogen bonds are often used to build reversible polymer networks because of the specific directionality of their interactions. Sijbesma and coworkers developed a

reversible network that relies on the formation of a set of quadruple hydrogen bonds between monomer units.[40, 56] The polymer systems linked with hydrogen bonds showed improved control over the network architecture when compared to randomly cross-linked covalent networks. The hydrogen bonded systems also had a high level of control over the degree of branching, and distance between cross-linkers within the network. Additionally, due to the directionality in the hydrogen bonding, these systems showed little aggregation within the bulk material. [40, 42]

Polymer networks constructed with only reversible interactions often experience creep or flow over time.[49, 57] In 2008, Cordier *et al.* built a supramolecular network comprising monomers that associate via either two or three hydrogen bonds. These networks demonstrated amazing self-healing properties: they could be cut clean through with a razor blade and then put back together and stressed after healing. The one major limitation of this system is its inability to resist creep.[49]

While DNs demonstrate an interesting way to change the properties of a material and can successfully combine the properties of two covalent networks, they still often experience failure under large or repeated strains. Reversible networks offer an improvement over covalent networks with their ability to heal without stimuli or intervention. The purely reversible networks, however, face their own limitations when it comes to recovering shape after a strain event. Hybrid networks offer an interesting solution to the problem of failure in covalent networks.

1.3 Hybrid Polymer Networks

When a material experiences an applied force (stress), it is deformed (strain). Once the material can no longer support the applied stress, it fails. When thinking about ways to overcome the problem of failure, there are two main approaches. One approach is to repair the failure after it has taken place, and the other is to prevent the failure from happening. Many groups have been developing self-healing polymers that repair after failure. While this work is very promising, there are current limitations with the self-healing systems. Many systems require heat[58] or light[59] to induce repair. Other systems can only heal for a limited number of cycles before running out of healing agent.[60] Given those limitations, it is important to develop materials that prevent failure from occurring in the first place.

When a polymer network is stressed, the applied energy can either be stored as elastic energy that can be recovered at a later time or dissipated through heat, friction,[61] or the breaking of bonds.[62-63] If the applied force is too great for the network chains to support, then the chains break. In a covalent network, this correlates to covalent bond scission. As more and more individual bonds and chains break, they begin to form microcracks. With continued stress, these micro cracks eventually grow to form larger and larger cracks until the material fails and can no longer support the applied stress.

As discussed above, both covalent and reversible networks have positive features and limitations. Drawing inspiration from the DNs, one can envision systems

that combine different types of interactions to overcome specific design flaws, or for specific applications. As defined in this dissertation, hybrid polymer networks comprise a permanent covalent component and a reversible component. Much as the DNs or IPNs combine the properties of two different covalent networks, the hybrid networks combine those of its components. The covalent component provides a lasting structure to the material that prevents creep or changes in shape in response to applied stresses. The reversible interactions might offer either a mechanism of energy dissipation,[64-65] or a mechanism for autonomous repair within the network.[66]

For example, Kushner *et al.* reported that the incorporation of hydrogen bonding domains into larger polymers improved the toughness and adaptive properties of the polymers.[67] They were also able to build three dimensional structures that mimic the structure of the muscle protein *titin*[68] (Figure 2). In addition, these polymers are able to withstand repeated extension cycling and showed increased strength, toughness, and elasticity that mimic the material properties of the natural protein. [68] The incorporation of weak reversible interactions leads to the enhanced mechanical properties.

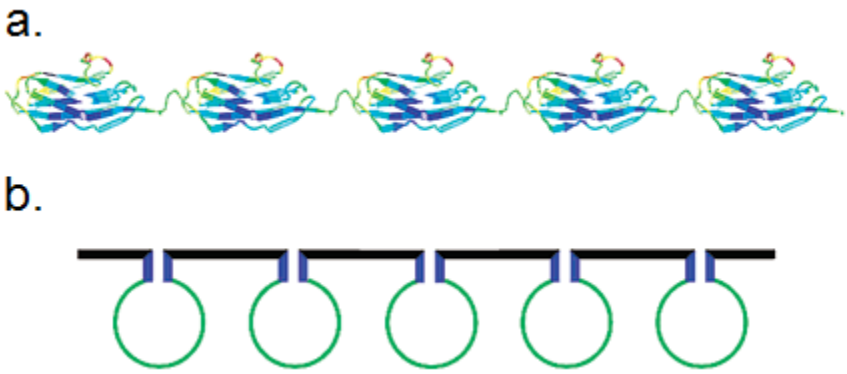

Figure 2: Comparison of *titin* folded structure and the designed modular polymer a. The protein *titin* is composed of repeating domains that open sequentiallyunder tension. b. The proposed concept for a polymer mimic of the natural occurring *titin*. The polymer system should loop on itself due to reversible interactions. Figure was reproduced from reference 68 with permission from Copyright © 2004 The American Chemical Society.

Hydrogen bonds have also been used to build hybrid networks for use in films and coatings.[69-70] Wietor *et al*. replaced covalent cross-links in polyester-polyurethane coatings with hydrogen bonding moieties. The addition of these hydrogen bonding units improved both the strength and toughness of the networks. The reversible hydrogen bonds also provided a mode of relaxation within the network that can act as a preemptive healing mechanism that is completely autonomous and repeatable over many cycles.

In addition to forming hybrid systems with hydrogen bonding, metal and ionic interactions have been used to form reversible cross-links within polymeric networks.[71-72] Sun *et al* developed tough and stretchable hydrogels by combining Ca^{2+} ions for cross-

linking alginate chains with covalently cross-linked polyacrylamide networks.[72] When tensile stress was applied to the alginate gels, they showed a pronounced hysteresis and a lasting shape deformation. In contrast, the covalently cross-linked polyacrylamide gels showed very little hysteresis, and the material recovered its shape after the load was removed. The hybrid networks comprising both the covalently cross-linked polyacrylamide and the ionically cross-linked alginate showed significant hysteresis, but the persistent shape deformation was drastically decreased when compared with the pure alginate gels. The hybrid networks also survived to both higher stresses and strains at failure than either of the individual parent networks. This work demonstrated that the incorporation of the reversible cross-links provided a mechanism for easy energy dissipation that could be recovered after the strain event. Additionally, this energy dissipation may lead to the prevention of failure under specific conditions.

Henderson *et al* were also able to produce hydrogels with enhanced strength under tensile loading by ionically cross-linking polymer triblocks.[71] They were able to capitalize on the d-block elements' ability to form complexes with carboxylate ligands. These metal-ligand interactions are highly stable yet reversible interactions within the network. They studied a range of metal-ligand bonds formed from different divalent metals (Zn, Ca, Ni, Co, and Cu). Under tension, the ionically cross-linked gels are similar to DN hydrogels, in that they dissipate energy and survive high strains, but unlike the DN hydrogels the dissipation is recoverable. They are able to withstand

fatigue testing previously unattainable by traditional covalent DNs and show increased toughness. Additionally, it was shown that the ionic cross-linking depends on the concentration of metallic cross-linker incorporated into the polymer networks. Stronger cross-links made for stiffer gels, but the weaker cross-links were able to dissipate energy in a manner that led to higher fatigue resistance. Further elucidation of these types of structure-activity relationships is one goal of the work described in this dissertation.

1.4 Summary

As discussed above, polymer networks are useful for a wide range of applications. Covalent, reversible, and hybrid networks each offer unique properties that can be harnessed to face specific design criteria. In particular, hybrid networks offer a desirable platform for enhanced properties, motivating the pursuit of predictive structure activity relationships. While keeping the major covalent component of the network constant, I wanted to develop and characterize a hybrid network that could easily incorporate reversible components with drastically different dynamic behavior. Previous work in the Craig research group[73-84] has shown that *bis*-functional pincer complexes offer a wide range of dynamic behavior in supramolecular polymer chains, networks, and brushes. The individual dynamic behaviors of the pincer complexes that form reversible cross-links influence the bulk mechanical and viscoelastic properties of these systems. Early work studying hybrid networks[85] created with these pincer complexes revealed a clear structure activity relationship between the cross-linker

dynamics and the rheological properties of the hybrid networks . I set out to further characterize the structure activity relationship of several hybrid networks under compression.

Chapter 2 highlights and discusses several unique applications of pincer complexes with regard to building complicated architectures and probing kinetic contributions to bulk properties in reversible and hybrid networks.

Chapter 3 discusses the work developing and characterizing several different hybrid networks using a family of *bis*-functional pincer complexes. Initially, it was demonstrated that hybrid networks can be constructed and show enhanced failure properties when compared with their covalent counterparts. The hybrid networks survive to higher stresses and strains than the pure covalent networks. These are properties that are attributed to the addition of the reversible components. Later studies show that the rate at which these hybrid networks are compressed influences their failure properties. Lastly, the covalent component is kept consistent while the dynamics of the reversible component are varied to study the resulting changes in the failure properties under compression. Perhaps most interestingly, the reversible components do not have to contribute to the overall properties of the gels (such as modulus), but can still prevent failure from happening.

Chapter 4 goes on to further characterize the failure behavior of the covalent network after the incorporation of the highly dynamic and weak reversible components.

Mechanochemical probes are utilized to monitor when the covalent network begins to fail as a function of applied compressive strains. The mechanically active probes emit light when the covalent bonds are ruptured. The resulting light emission behavior indicates that the addition of the reversible components delays covalent bond breakage in the network. Later in Chapter 5, relaxation dynamics and repeated compression testing are carried out on another family hybrid networks. This family of networks is based on a different covalent network and was studied to further characterize the versatility of the observed structure activity relationships in different covalent networks.

2. Physical Applications of Pincer Complexes*

* Sections of this chapter have previously been published[86]

Pincer complexes are chelating agents that coordinate three adjacent coplanar sites around a transition metal. The work described in this dissertation is enabled by the use of pincer *N,C,N*-palladium and -platinum complexes, where the common thee atom notation is used to indicate the three atoms that formt he pincer around the transition metal. Organometallic pincer complexes are typically employed as tools for synthetic and catalytic chemistry, but they have also found numerous uses in physical applications (including those in this dissertation). This chapter reviews the alternative, non-synthetic uses of pincer complexes, including their role as a mechanistic probe in supramolecular polymer chemistry that provided a foundation for the work reported in Chapters 3-5.

The numerous physical applications discussed in this chapter derive from the ability of pincer complexes to participate in metal-ligand coordination events that offer both selectivity and strength. Pincer complexes that contain either Pd^{II} or Pt^{II} metal centers are often used because of their particular affinities for pyridines, nitriles, and phosphines.[87] As described below, the accessibility and diversity afforded by these metal-ligand coordination events provides opportunities for applications in polymer science, nanoscience and materials science.

The utility of pincer complexes in materials applications can broadly be divided into two categories: one in which they provide a purely (or largely) structural component, and a second in which they contribute a specific behavior of function that translates into material properties. Many applications obviously fall into both categories, but this categorization is employed in the organization of this chapter. At the level of structural manipulation, the metal-ligand coordination of the pincer complexes can be used as the primary mechanism to bring together small individual units to build a larger structure. Examples include the construction of various nanostructures such as metallodendrimers [88] and complex rosette architectures.[89] These specific interactions have also been used to functionalize existing polymer chains with specifically designed pendant ligand groups.[90] Placement of the pincer complexes along the polymer chains allows for easy side chain modifications.

On the functional end of the spectrum, pincer complexes can be used as a probe for understanding the kinetic influences of physical (i.e., supramolecular) associations on polymer properties.[82] Systems to which the probes have been applied include linear polymers,[82] networks,[84] cross-linked brushes,[73] films, [91] and gels.[92] By making small changes in the chemical structure of the pincer complexes, the kinetics of the interaction can be varied.[83] Studying the resulting changes in physical properties offers insight into the role of the kinetics of these metal-ligand associations, bearing direct relevance for future material design. The complexes have also found use in polymer

mechanochemistry, further highlighting their versatility. This chapter will explore the utility of the pincer complexes in: creating complex structures through metal-ligand coordination, applications in molecular and material design, and investigation of the dependence of physical properties on molecular kinetics.

A principle physical and materials application of pincer complexes is to employ their ligand coordination behavior as a construction tool. Pincer complexes have been successfully used to create a number of desired structures. These structures range in complexity from simple supramolecular chains,[82] to complex nanostructures,[93] surface patterns,[94] and even thin films.[95] In addition to building new structures, pincer complexes can be employed to modify existing structures such as polymer backbones.[87] In these pursuits, pincer coordination offers some advantages over other traditional synthetic methods, and those advantages will be discussed in the context of specific examples, where appropriate.

2.1 Building Metallodendrimers

Current fabrication technologies often strive to create ever smaller structures. Often, methods for fabricating nanomaterials rely on a top down approach that can be complemented by using chemistry to build up from the atomic level. In bottom up materials design, specific and directional supramolecular interactions are often utilized as the glue through which to achieve the desired geometries of the nanostructures.[96] Self-assembly of this type is a popular and effective method for bottom-up synthesis,

and pincer complexes have proven to be useful in this regard, by relying on the physical interactions of the metal-ligand coordination to drive assembly. Dendrimers are one example of nanostructures "with highly branched architecture leading to spherical shapes combined with high molecular weights" [97] that have been built successfully using branched pincer complexes.

There are two main methods for constructing metallodendrimers. One is a purely divergent technique. A divergent synthesis requires starting from the center of the structure and building out layer by layer,[98] and it is by far the most common assembly technique. Divergent methods have been used in other construction motifs outside of self-assembly. Utilizing pincer complexes in divergent synthesis, is a simple, yet elegant way to build different types of metallodendrimers. Additional complexity can be incorporated into the metallodendrimers by utilizing a convergent assembly method.[98] Convergent assembly brings previously established structures together. A beautiful example of convergent construction is demonstrated when metallodendrimer wedges are brought together using additional hydrogen bonds.[98] There are many other examples of convergent assembly methods that rely on covalently cross-linked wedges or other coordination techniques.

Whether utilizing a purely divergent or a combination of divergent and convergent techniques, pincer-based self-assembly of metallodendrimers is a prime example of the pincer's usefulness as a construction tool. Pincer complexes offer a

consistent and reliable platform for building intricate supramolecular structures. In this section, some of the physical implications and considerations of using pincer complexes to build metallodendrimers is explored.

The first example of pincer complexes being used to build dendritic nano-spheres with well controlled size distribution was demonstrated in 1995 by Huck *et a.l*[96] The core structure was a traditional tridentate pincer complex coordinated to the nitrile of an organic ligand. The coordination geometry of nitriles and similar ligands to the pincer Pd^{II} center is that of a square planar complex. The smallest unit (monomer) of a repeating dendritic structure was constructed by including three coordination - ready prongs: two pincer complexes and one cyanomethyl group (Figure 3).

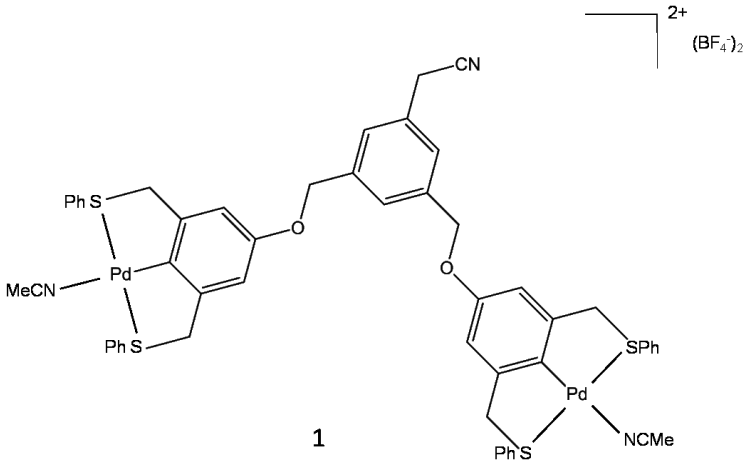

Figure 3: Chemical structure of the repeating unit used to form metallodendrimers. The repeat unit contains 2 prongs made with pincer complexes, and the third prong with a ligand for coordination to tother units.

When a solution of the repeat unit **1**, Figure 3, is heated in nitromethane, the coordinating solvent molecules (acetonitrile) evaporate and the cyanomethyl group from a separate unit is replaced as the 4th coordinating ligand around one of the Pd^{II} centers. This coordination of the nitrile from one monomeric unit to the pincer motif of another results in a continuous branching pattern, shown out to the 2nd level in Figure 4. [98]

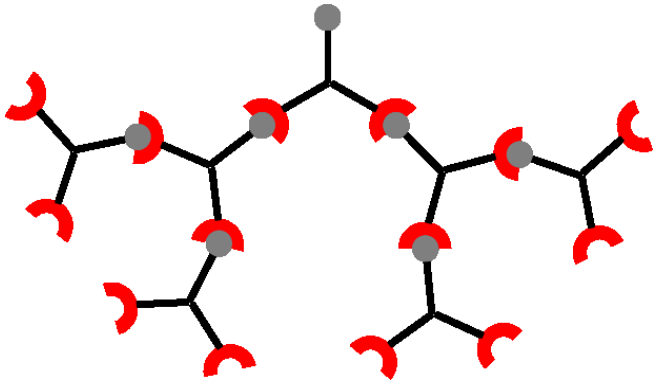

Figure 4: Cartoon representation of a self-assembled metallodendrimer
Th metallodendrimer is built out to the second level. Curved wedges and balls represent pincer complexes and coordinationg ligands, respectively.

The coordination can be followed using FT-IR spectroscopy to monitor the shift in the characteristic peak of the C≡N bond; the un-coordinated nitrile stretch at 2250 cm^{-1} shifts to a value of 2290 cm^{-1} upon coordination. [99] The addition of small amounts of acetonitrile breaks the dendrimers apart and regenerates the original monomer. This result highlights how the spheres retain the reversibility of the pincer complex, in contrast to the irreversible nature of covalent bonds. As with other supramolecular

interactions, reversibility of this sort is one of the main advantages achieved when using pincer complexes as a construction tool. Reversibility provides both advantages in synthesis (error correction) and performance (*e.g.*, stimulus response) that might be useful for certain applications.

Further characterization allowed the size and shape of the presumed dendritic assemblies to be determined. Quasi-elastic light scattering (QELS) indicated that the hydrodynamic diameter of the assemblies in solution is 200 nm.[99] In addition, the assemblies were deposited onto surfaces and characterized by atomic force microscopy (AFM) in the solid state; the diameter of the spheres measured by AFM on the surfaces was on average 205 nm, in excellent agreement with the solution measurements. Both gold and glass surfaces were employed in the AFM experiments to show that the material of the surface did not dictate the size or shape of the assemblies. Lastly, transmission electron microscopy (TEM) was used to determine the size of the globular structures that resulted after the evaporation of the solution on a carbon-coated copper grid. The TEM results gave diameters in the range of 150-200 nm, a value that is consistent with both the QELS and AFM data. Branching was shown to be essential to the building of these spheres; when non-branched complexes of similar composition were exposed to the same assembly conditions, no globular structures were observed by TEM.[99]

The initial work described above demonstrated that pincer complexes are useful building blocks for the divergent construction of dendritic nano-spheres, proving a new construction motif and concept for the synthesis of dendritic architectures. The relative ease of construction and multiple handles for structural variation on the molecular level suggested that pincer complexes might be used to produce more complicated and intricately designed structures. Further studies, described below, determined what factors influenced this method of construction and what limitations are inherent to the methodology.

In later work, Huck *et. al.* [88-89] showed that they could extend the concepts developed in the first metallodendrimer system to build larger systems with the same repeating unit. They were also able to investigate what variables dictated the size of these branching structures. A modified approach was taken, built upon a similar but slightly modified repeat unit. Unlike the first system, comprised of only the repeating unit, the metallodendrimer synthesis was initiated from a core unit that remains at the center of the dendrimer throughout its synthesis.

This core unit is similar in structure to the repeat unit **1** utilized above, but it has three pincer Pd^{II} complexes instead of two. The pincer complexes are initially protected with a chloride ligand, as chloride is not displaced by nitrile and it therefore prevents coordination by cyano groups from the other monomers.

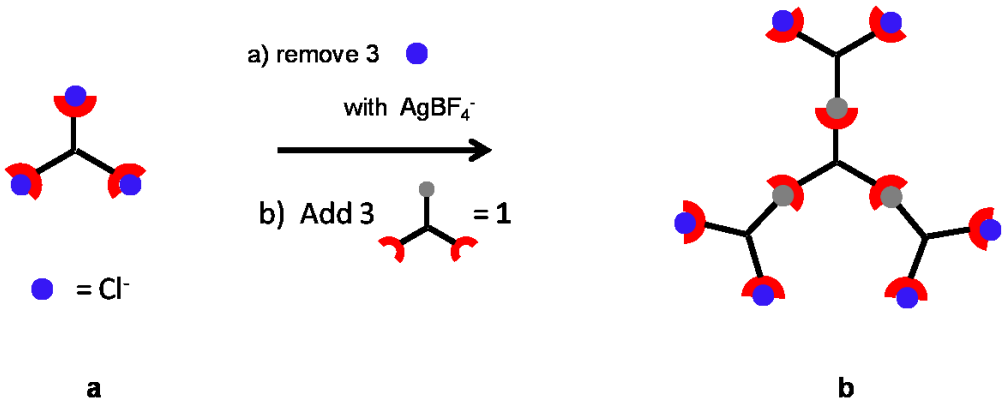

Figure 5: Representation of dendrimer construction using a core unit
The three prongs of the core unit (a) are identical and the first layer of the divergent dendrimer (b) built with a branched pincer structure. The chloride ions act as a protecting group that inhibits undesired coordination. Curved wedges represent the pincer moieties.

Growth is then activated with the addition of a silver salt of a weakly coordinating anion, *e.g.*, $AgBF_4$. The precipitation of AgCl leaves behind the non-coordinating BF_4^-, which allows a cyano-substituted, *bis*-PdCl pincer complex to add to the three sites of the core (Figure 5). The deprotection/coordination cycle can be repeated to add additional generations or layers,[88] and the methodology provides a very controlled process for iterative, divergent metallodendrimer synthesis. Although not discussed further here, the larger blocks constructed using this approach can be further combined using hydrogen bonds to build rosette structures.[89] The ability to simultaneously exploit hydrogen bonding and pincer-ligand coordination as orthogonal assembly motifs has also been advantageous in polymer modification, as discussed in later sections.

The counter ion that is introduced during the deprotection step influences the limiting sphere size that can be obtained with this methodology.[93] When larger polyatomic ions (ClO_4^-, PF_4^-, $CF_3SO_3^-$, *p*-$MeC_6H_4SO_3^-$, and BPh_4^-) were introduced as their corresponding silver salts, the bulkier counter ions tended to be limited to smaller assemblies, as characterized by QELS, AFM, and TEM. The authors speculate that the correlation is a result of the overall charge distribution of the assembly, presumably as a consequence of the larger ions eventually becoming unable to fit inside the highly charged dendrimer or because the larger anions are less effective at shielding a growing number of cation-cation repulsions.

Several common characteristics are seen in the dendritic systems, including that they meet the obvious requirement that each individual building block or repeating unit must contain all of the necessary information for complete self-assembly (i.e. both the pincer and the ligand).[100] The orientation and components of these units can be varied, but they must be able to form the branched structures without additional materials or outside intervention. By building the individual units to contain all the necessary information, the ultimate assembly process is simplified and allows for structures to form quickly and easily.

Whereas the core pincer metal-ligand construction motif is held constant, different specific pincer complexes can be used to make similar metallodendrimers of varying structures. The SCS - pincer structure has traditionally been used for self-

assembly applications, but the pincers can be converted to PCP structures in order to incorporate different transition metals. In addition to Pd^{II}, Ni^{II} and Pt^{II} have been effectively used to build other dendritic structures. These metals all have similar behavior, due to a shared square planar coordination geometry.[97]

Overall, a wide variety of structures can be built with various pincer complexes, which have shown themselves to be highly useful for the construction of metallodendrimers. By harnessing the metal-ligand coordination event, they provide a simple and specific interaction that is robust under many conditions. Although the focus of this chapter is on applications at the interface of polymers and materials, please note that a range of other self-assembled structures have been formed using pincer coordination.[101-104]

2.2 Building Films and Surface Patterns with Pincer Complexes

Because pincer coordination complexes can be quite strong, easy to work with, and maintain the reversible nature desired for construction, they offer an intriguing combination of potential uses within the materials arena. They offer a useful method for the physical construction of systems that have mechanical integrity, so that ultimately they might be developed into useful materials. The structural integrity of pincer-based metallodendrimers, for example, allows them to be spin-cast from solution to form molecularly thin films, which offer a wide variety of potential applications in material

science.[95] Metallodendrimers of the 5th generation (Figure 5) generated films of ~ 4 nm thickness as characterized by AFM and TEM (Figure 6).

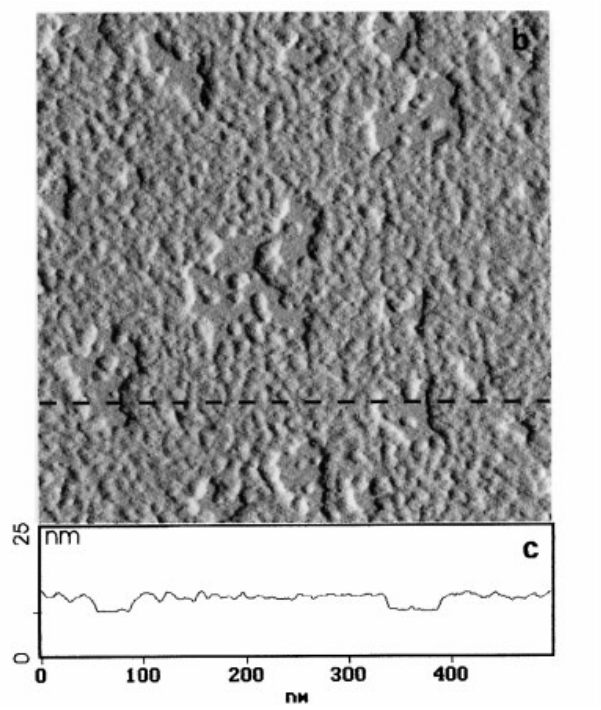

Figure 6: Tapping scanning force micrographs of a non-closed molecular film
The molecular film was prepared by spin-casting a dilute solution of dendrimers in nitromethane onto a freshly cleaved surface. The dendrimers formed out to the 5th generation. Figure was reproduced from reference 94 with permission from Copyright @1998 John Wiley and Sons.

Another application of pincer-based assembly is found in surface patterning, for which existing techniques are often time consuming and costly. Developing a fast and simple method for functional surface patterning is an ongoing goal in the field of nanoscience. Metallodendrimers were linked to a surface by modifying them with long sulfide chains for attachment to gold surfaces.[94] These dendrimer tethers can then be

inserted into a self-assembled monolayer on a gold surface at defect sites (essentially holes in the monolayer) that form during monolayer self-assembly. The dendrimer attachment pattern can be characterized using AFM. [94] The overall density and positions of the dendrimers are controlled using different techniques for the monolayer. Direct positioning of pendent groups using pincer complex affinity was posited to be useful for future surface patterning techniques.[94]

In addition to serving as a critical structural unit in metallodendrimers for film and surface pattern fabrication, pincer complexes have also been employed as the primary structural "glue" for multilayer film deposition. The so-called Coordination Polymer Multilayer (CoPM) technique features polymer chains with pincer units incorporated along the backbone.[105] The CoPM strategy is shown in Figure 7. The pincer complex is linked via a tether to the backbone of a polymer synthesized by ring-opening metathesis polymerization (ROMP). The coordinating pyridine ligand is displayed as a side chain functionality on the second polymeric component, poly(vinyl pyridine) (PVP). CoPMs are synthesized by the alternating deposition of these two complementary polymeric components, in a process inspired by electrostatic layer-by-layer deposition. The ability to construct the CoPMs arises directly from the Pd^{II} pincer's responsiveness, inertness towards unwanted functionalities, and specific strength of coordination towards pyridine, in addition to its chemical compatibility with the ROMP conditions. The CoPMs are comparable in strength, durability and stability to

their covalent multilayer counterparts. Interestingly however, the CoPMs exhibit many responsive behaviors that are similar to polyelectrolyte multilayers, whose durability is not as great.[105]

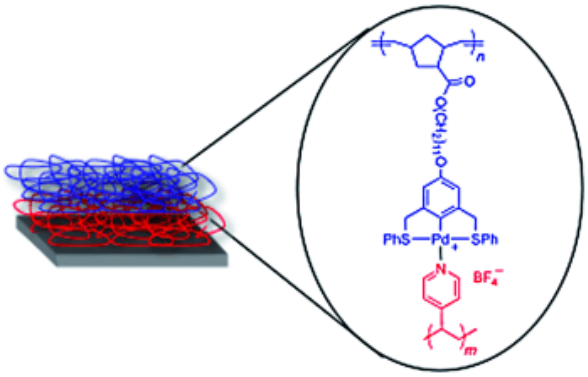

Figure 7: Representation of Coordination Polymer Multilayer (CoPM)
The CoPM is built up on gold. The pincer ligand coordination responsible for building the layers is emphasized within the figure. Figure was reproduced from reference 105 with permission from

In contrast to building multilayers from polymer chains with the pincer monomers in the backbone, small molecule pincer complexes have also been used to cross-link layers of PVP chains.[91] The combination of PVP and pincer cross-linkers produces uniform films in non-aqueous environments. The structure and properties of these films can easily be modified by changing the solution concentrations, molecular weight of the PVP chains, adding competing ligands or changing the pH. Figure 8, shows how different layers of polymers can be brought together by the coordination of the free small molecule, *bis*-pincer complex. Both types of multilayers offer interesting potential for building films of different desired properties.[91]

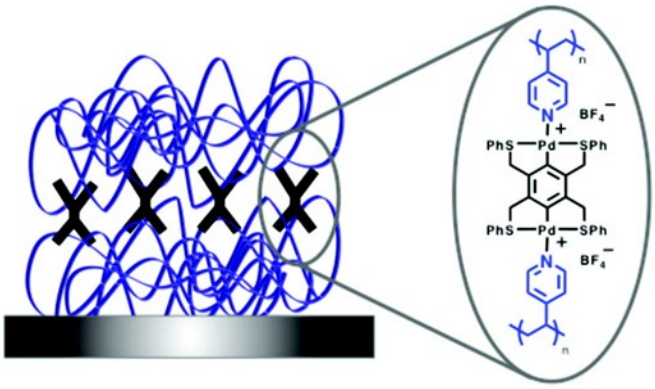

Figure 8: Representation of PVP layers held together with *bis*-pincer complexes Two separate PVP layers were brought together with the small molecule *bis*-pincer complexes. Each end of the *bis*-pincer complex coordinates to a ligand from different layers. Figure was reproduced with permission from reference 91 Copyright © 2008 American Chemical Society.

2.3 Functionalizing Existing Polymer Chains

There is a growing desire within the field of polymer chemistry for fast synthesis and easy post-synthetic polymer modification. Often, traditional methods of synthesis and additional side chain modifications rely on covalent chemistry. These reactions often require extensive steps and subsequent purification. If the reactions are not quantitative, unwanted side reactions and other modifications can take place along the polymer chain. The use of non-covalent chemistry has recently gained popularity for its ability to offer selectivity in associations as well as simplicity as a side chain modification technique.[87] These associations can be useful in constructing novel molecular architectures. By incorporating specific pincer complexes as functional side chains along a polymer backbone, secondary functionalization can be obtained through metal-ligand coordination. The use of pincer coordination complexes offers faster and

more selective functionalization of polymer backbones than traditional covalent reaction pathways, and the inherent robustness of the pincer complexes is passed on to the parent polymers.[87] Other variations on this theme have also been reported, including the simultaneous use of pincer coordination and pseudorotaxane formation as a tool for block copolymer modification.[106]

The first use of pincer complexes as a tool for post-synthetic polymer modification was reported by Pollino *et al*.[87] In order to take advantage of pincer coordination in this context, it is important to identify with what specificity the coordination events take place and what types of modifications can be made. Initially, Pollino *et al.* constructed random copolymers within which to demonstrate the viability of the approach and to characterize this method of functionalization.[87] Random copolymers were built with two different side chain functionalities: Pd^{II} pincer units and units capable of hydrogen bonding. The complementary partners for the pincer complexes were a range of pyridine ligands, while the hydrogen bonding units on the polymer had a separate partner motif with which to associate. The orthogonality of the pincer-pyridine coordination and the hydrogen bonding offered the chance for rapid and specific multi-functionalization. As noted in previous sections, pincer-Pd^{II}-pyridine coordination is characteristically reversible, spontaneous, simple and self-repairing (in that an undesired association tends to reverse quickly and give way to a desirable association event) in nature, and the system's potential to self-correct in this way was

important in the context of the desired application, which involved two distinct but simultaneous non-covalent functionalization events. To better determine if the pyridine – pincer interactions were truly orthogonal to the hydrogen bonding interactions, a set of three different methodologies was employed.[87]

This first methodology successfully showed that the pincer metal-ligand interaction is both selective and spontaneous. The pyridine ligand was added to the copolymer solution, and the pyridine ligand could only be observed to associate with the desired pincer complex, and not the hydrogen bonding unit. The second methodology revealed that a stepwise multifunctionalization was possible. The pyridine and hydrogen bonding ligands were added sequentially. The same final functionalized state was achieved regardless of the order of addition, and the extent of pyridine coordination matched that obtained in the absence of the hydrogen bonding unit. Finally, the authors reported that the same final state was obtained again if both types of ligands were added at the same time. Not only was the final state the same, but the rate of formation did not change as a function of order of addition. This combination of studies, shown schematically in Figure 9, demonstrated the concept of non-covalent polymer multifunctionalization and showed that the orthogonal binding properties of pincer coordination and hydrogen bonding units, exploited in dendritic assembly as discussed in earlier examples in this chapter, provides a useful tool also for the post-synthetic modification of linear polymers.

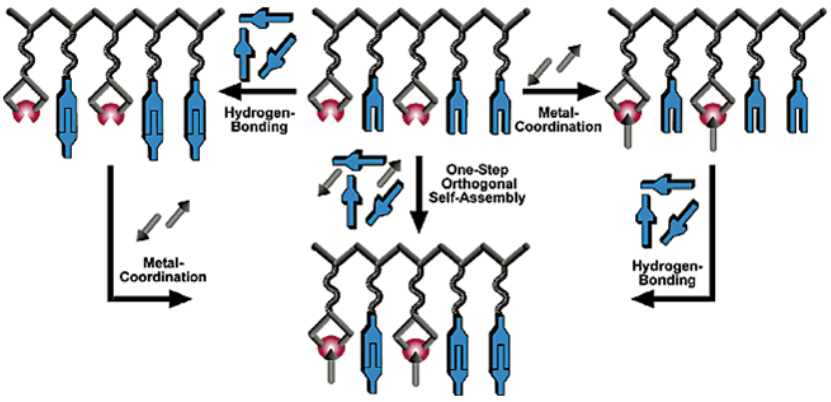

Figure 9: Cartoon representation of the orthogonal self-assembly
The orthogonal self-assembly utilized both metal –ligand associations and hydrogen bonding associations in a random copolymer backbone. Figure was reproduced from reference 87 with permission from Copyright © 2004 American Chemical Society.

It is well established that modifying the blocks in a copolymer can directly influence the physical properties of that polymer. However, as discussed above, traditional methods of post-synthetic modification can be costly, time consuming, and random in modification, sometimes destroying previously established "blockiness". As a result, it was potentially useful to know if the approach used to modify random copolymers could be directly extended to block copolymers without undesired side effects. By using non-covalent coordination with the pincer complexes, block copolymers can be orthogonally modified to produce specific changes in physical properties without compromising the original block structure of the polymer chain.[90]

Similar to the random co-polymers of the previous section, Nair *et al.* designed a polymer backbone with two types of blocks. One contained the pincer complex (for

metal-ligand coordination) and the other contained a unit capable of hydrogen bonding. The pincer coordination event was extended to a nitrile group that was also shown to successfully bind to the pincer complex, either in the presence or absence of the potentially competing hydrogen bonding ligand. Figure 10 shows the three-point hydrogen bonding pair **2**, as well as the two different pincer complexes (with pyridine **3** and nitrile **4**) whose effectiveness was demonstrated in the block copolymer systems. This was the first example of a fast and easy non-covalent functionalization of block copolymers with defined architectures of two blocks. Overall, the order and compositions of the blocks do not influence the coordination events between the pincer complexes and their complementary ligands.[90]

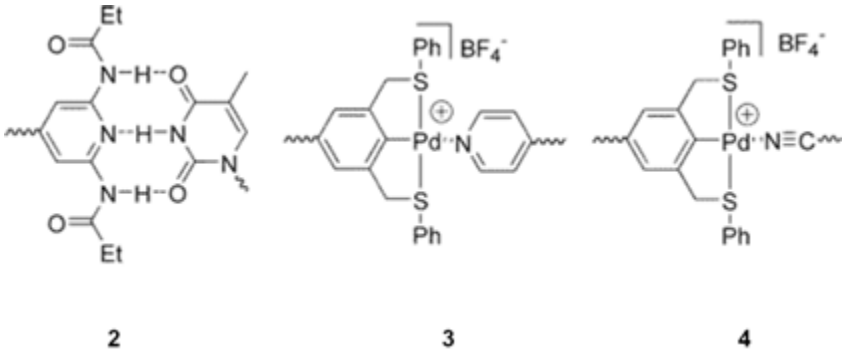

2 3 4

Figure 10: Three different self-assmebly motifs
These motifs were all used in the study of post-synthetic polymerization multifunctionalization: (2) three-point hydrogen bonds, (3) pincer complex coordinated to pyridine, and (4) pincer complex coordinated to nitrile. Figure was reproduced from reference 90 with permission from Copyright © 2006 American Chemical Society.

The initial state (bound to polymer vs. free in solution) of the ligand and metal did not influence the self-assembly (Figure 11), and orthogonality vs. hydrogen bonding was preserved in the reversed coordination cases.

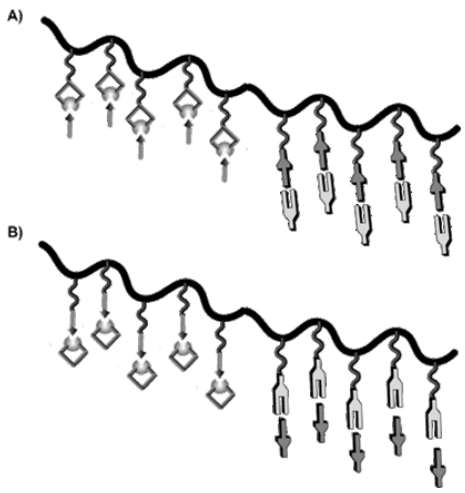

Figure 11: The representation of two different combinations of recognition units
A) Shows a block copolymer backbone containing the pincer units as the recognition units, and B) shows a block copolymer backbone containing the ligands as the recognition units. Figure was reproduced from reference 90 with permission from Copyright © 2006 American Chemical Society.

Of course, the ultimate goal in functionalizing either block or random copolymers is to modify the properties. There were two observed changes in the thermal properties of these polymers. First, metal coordination leads to a decrease in the glass transition temperature of the polymer, an observation the investigators attributed to the disruption in the original intermolecular forces between polymer chains. Second,

the thermal stability drops when the polymers are coordinated to the ligands. Further work is necessary to accurately relate these changes in properties to the various structural changes that accompany functionalization, a general concern for polymer property prediction as increasingly complex functional groups are used more and more frequently in polymer science.[90]

More complex polymer structures were built using two different hydrogen bonding motifs in addition to the pincer complex.[107] Similar to the early systems, the functionalization behavior of these polymers was once again studied. As before, the presence of additional functional groups caused no observed change in the association constants of any of the individual coordination sites. The pincer groups were shown to coordinate rapidly and reversibly to the ligands, and functionalization was achieved without the need for subsequent purification. The multiple coordination events occurred independently of each other, and the order in which they were added did not influence their properties; pincer-ligand coordination was not disrupted by the hydrogen bonding groups, nor did it disrupt the association of those motifs.[107]

To probe the physical properties of these modified terpolymers, a solvent study was carried out.[108] It was observed that by changing the solvent, one coordinating group could be selectively removed from the chain, with the addition of another coordinating ligand. These induced disassembly events can ultimately lead to tunable control over the polymer's properties. All previous studies carried out in halogenated solvents

showed that the three coordination events were orthogonal, but when the solvent is changed to a chloroform/dioxane mixture, the hydrogen bonding is disrupted by the addition of the ligand that can coordinate with the pincer complexes. It was determined that the dioxane competes with and ultimately decreases the strength of the hydrogen bonding events. The pincer –ligand interaction however, is robust in all solvents and is not susceptible to solvent disruptions. It was further determined that the presence of free silver ions from the pyridine – pincer ligand exchange disrupts the hydrogen bonding. This disruption is not dependent on the anion of the silver salt or the solvent that the silver salt is added with. This same disassembly can also be triggered by changing the polarity of the solvent.[108] The pincer complexes offer a robust method of modifying polymer chains and ultimately changing the physical properties of these systems.

2.4 Probing the Kinetic Influence of Pincer Coordination

As described earlier in this chapter, pincer coordination is a useful and versatile motif through which a wide variety of polymeric structures and materials can be constructed, but pincer complexes have also proven to be useful probes of fundamental physical behaviors of polymeric materials. The context of the studies is the increasing use of self-assembly as a route to complex, supramolecular structures and materials.[109] As the number of accessible supramolecular structures grows, relating the properties of

an assembly to those of the supramolecular constituents that define the assembly becomes increasingly important. As reviewed by Raymond [110], the dynamics of supramolecular assemblies are a particularly rich means by which chemists might engineer properties such as: catalysis [111-114], templation effects [39, 115], interconversion of assemblies [116], and kinetic compartmentalization.[117]

In the context of polymer science, the use of supramolecular bonds as defining components of a material is distinguished from the use of covalent bonds by the reversibility of the former. In other words, it is the dynamic properties, rather than the equilibrium structure, of the supramolecular interactions that often contribute to new polymer properties. In order to probe mechanism at the molecular level, however, the effects of dynamics must be differentiated from the effects of equilibrium thermodynamics. This differentiation is a challenge with most reversibly-assembled systems, for example those based on hydrogen bonding, because association typically occurs at or near the diffusion rate, and the equilibrium association constant and rate constant for dissociation are therefore strongly anti-correlated. In polymer science, the inverse correlation of these two descriptors subtly but intrinsically frustrates efforts to determine their relative importance. High association constants lead to larger structures and slower dynamics of the intact equilibrium structure, while slower dissociation rates lead to slower reversible dynamics within the material. Dynamic properties, whether controlled by equilibrium structure or main-chain reversibility, are slowed by both

mechanisms. A method for decoupling the two therefore offers the potential for a rich investigation into the fundamental importance of the reversible interaction.

It is in this context that pincer coordination has proven to be extremely useful. NCN-Pincer compound **8** (Figure 12) and analogs have been synthesized and studied extensively by van Koten.[101] With other organometal motifs [118-119], they have found use in supramolecular chemistry by Reinhoudt, van Koten, and others.[98, 120-121] The reversibility takes place through ligand exchange, which in square planar Pd^{II} and Pt^{II} occurs through a sterically congested associative mechanism. Bulk in the N–alkyl substituents R should therefore slow the exchange, but have only a minimal impact on the ligand association thermodynamics. The expected decoupling of kinetics and thermodynamics were confirmed in room temperature NMR spectra of the R = Me and Et complexes. At identical concentrations (DMSO–d6; 1 mM in 8a/b, 3 mM in 9), effectively identical ratios of free and bound 9 are observed; the measured association constants are 1.6 and 1.3 x 103 M^{-1}, respectively, for 8a and 8b. While the spectrum of 8b•9 is sharp, however, that of 8a•9 shows broad peaks that are indicative of exchange near the NMR timescale. Heating the NMR sample to only 30 °C leads to coalescence of the peaks and corresponds to an exchange rate of 100 s^{-1} at that temperature. In contrast, the same peaks in 8b•9 remain separated until 90° C, above which the reduced concentration of bound ligand makes coalescence impossible to identify clearly. The orthogonal control of dissociation dynamics relative to complexation thermodynamics

can be viewed as a "macromolecular analog of the kinetic isotope effect," and its use in a variety of mechanistic physical studies is the focus of this section.[82]

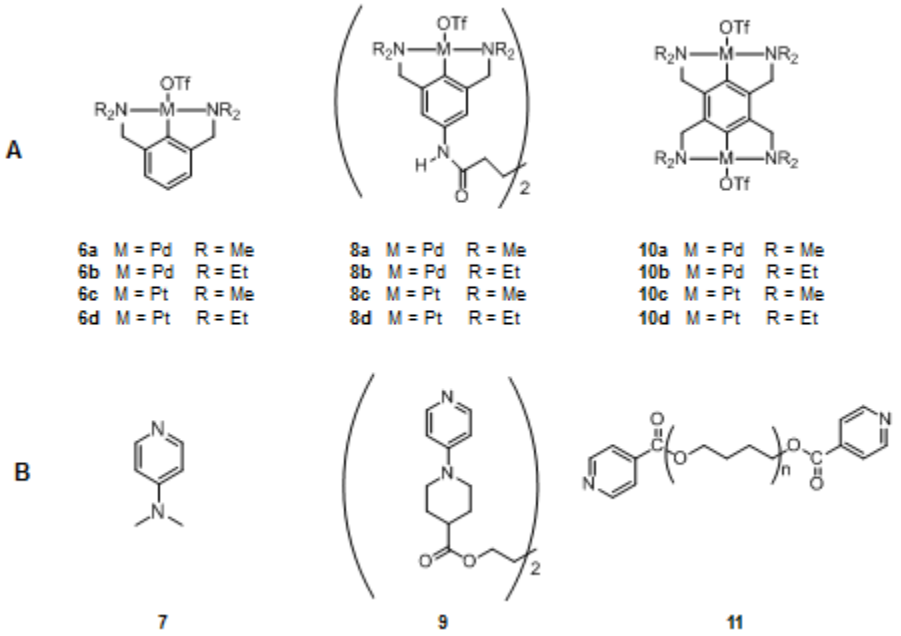

Figure 12: Chemical structures of pincer complexes and pyridine ligands
(A) Several different pincer complexes used in kinetic studies with different metals and R groups, and (B) various pyridine derived ligands which can coordinate to the different pincer complexes.

It has previously been discussed how covalent polymer chains can be modified non-covalently by using side chain pincer coordination, but similar pincer associations are also useful for building the main chain structure by attaching the pincer complexes and ligands to the ends of difunctional polymers and small molecules. [82] The metal-ligand associations between chain ends leads to longer, reversible polymer chains. A

specific example is shown in Figure 13. Mixing a solution of bis-pincer complex **10** with another containing stoichiometric bis-pyiridine capped chains led to an increase in the viscosity of the system, indicating that the longer chains (Figure 13) had formed.[82] Similar effects were observed when analogous ditelechelic polymers are mixed. As described above, the main chain dissociation kinetics can be varied through the *N*-alkyl substituent on the NCN pincer complex. Changing the ligand exchange rate by approximately 2 orders of magnitude has no effect on the viscosities of the polymer solutions across a range of concentrations and molecular weights, demonstrating that the viscosity is determined by the equilibrium structure, and not the main chain dynamics, of the linear polymers.

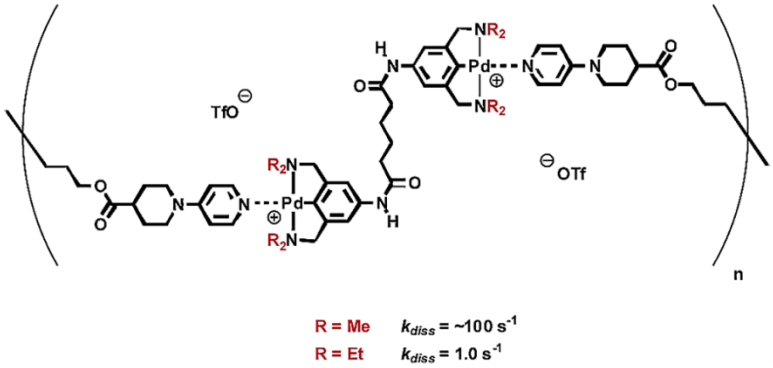

Figure 13: Example of pincer coordinations to form supramolecular polymer chains This *bis* functional pincer molecule (**8a** or **8b**) was used to form chains with structure **9**. Figure was reproduced from reference 82 with permission from Copyright © 2003 American Chemical Society.

Supramolecular polymers often have impressive solid state mechanical properties [122-125], and identifying the extent to which the reversibility of the supramolecular interaction contributes, and the mechanism by which it does, to those properties, is of great interest. In some cases, direct rheological characterization [47, 126-127] offers some insight. In case of the pincer-based linear polymers, reasonably strong and quite tough fibers of **10a/b•11** (structure **11** cross-linked with either **10a** or **10b**) have been hand-drawn from solution. A rudimentary study of the fiber mechanical properties of one specific pincer-based polymer reveal tensile strengths of ~100 MPa and strains at break of roughly 70 %. Importantly, the tensile strength of **10a•11** fibers are identical, within experimental error, to those of the **10b•11** fibers, providing compelling evidence that the nucleophilic displacement mechanism that governs failure under load in solution (as measured by single-molecule force spectroscopy [128]), is not operative in the solid state.[129] The absence of the typical associative ligand displacement pathway in the fibers is likely tied to their significant tensile strength, since the likely alternative failure mechanisms (chain disentanglement and/or purely dissociative scission of the coordination bond) would be comparable to those in conventional, covalent polymers.[129]

2.5 Reversible Networks Using Pincer Complexes

Not only can pincer complexes be incorporated into polymer backbones to induce physical changes, but the *bis*-pincer small molecules can be used to cross-link polymer chains to form reversible networks.[84] When the *bis*-pincer complexes are added

to solutions of PVP, the multiple pincer-pyridine coordination events act as cross-linkers, leading to the formation of reversible networks (Figure 14).[84] These systems provide excellent model systems for exploring the fundamental behavior of supramolecular polymer networks in general.

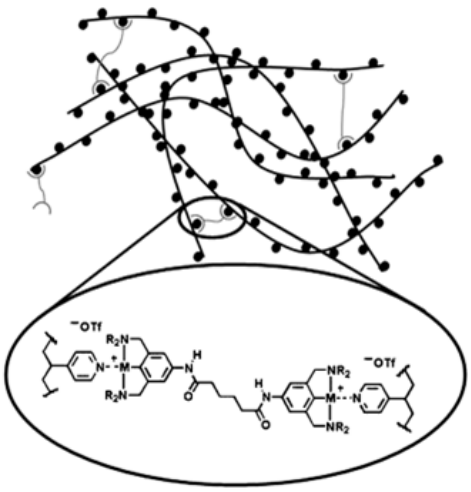

Figure 14: Representation of a reversible network
The reversible network is comprised of cross-links between pyridine ligands **7** in PVP chains through coordination with the *bis*-pincer complexes **10**. Figure was reprodcued from reference 84 with permission from Copyright © 2005 John Wiley and Sons.

The network physical properties were monitored as the small molecule pincer cross-linkers were added to the PVP solutions.[83] As the concentration of cross-linkers went up, there was a concomitant increase in the sample viscosity, indicating the formation of reversible networks. The viscosity increase is reversed upon the addition of dimethylaminopyridine (DMAP), which outcompetes the pyridine side chains for the pincer complexes and disrupts the cross-linking. Furthermore, the addition of a mono-

functional, rather than a *bis*-functional pincer complex to solutions of PVP leads to no observed increase in viscosity. Clearly, the *bis*-functionality of the pincer complexes, and the associated cross-linking, is responsible for the changes in the physical properties. Figure 15 shows the relationship between viscosity and the cross-linkers added (**18a** and **18b**).

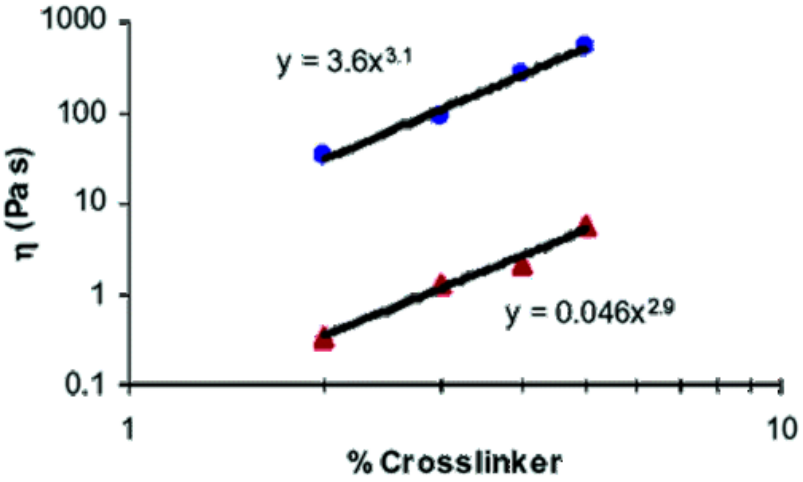

Figure 15: Steady shear viscosity as a function of cross-linker
Percent crosslinker was measured for **8a** (●) and **8b** (▲) in 100mg/mL of 8●PVP in DMSO. Figure was reproduced from reference 83 with permission from Copyright © 2005 American Chemical Society.

While the pincer complexes are useful for forming the reversible networks, it is important to study the influence of the kinetics and thermodynamics of the system as well. As demonstrated with the main chain studies, k_d (as defined in Figure 16) is important in defining many of the physical properties. When pincer complexes of slightly different chemical structures were compared, a drastic difference in properties was observed. The resulting viscosities of the different networks scale with the k_d of the

specific pincer complex used. When comparing two systems with nearly identical values of K_{eq} but significantly different values for k_d, the viscosities are still drastically different. This indicates that it is the lifetime of the cross-links that ultimately dictate the viscosity of the solution and not the strength of the interaction.

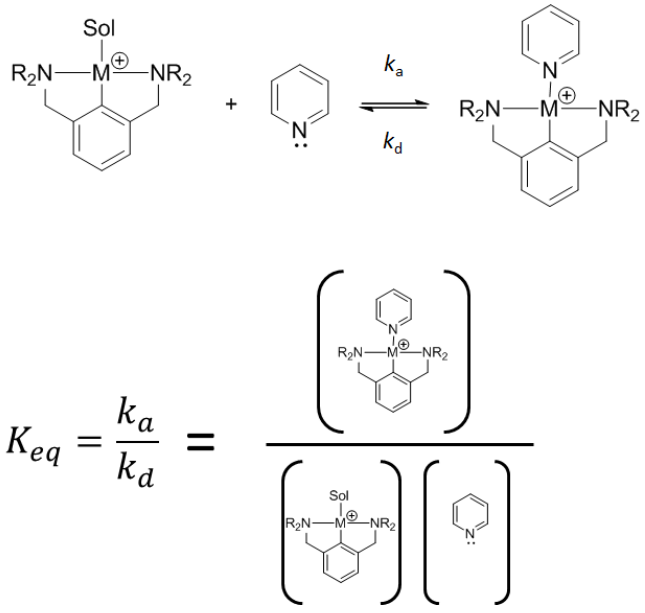

Figure 16: Thermodynamic and kinetic parameters of the reversible interaction

Changing the steric bulk of the pincer complex influences the kinetics of the interaction, but the thermodynamics of the interaction can be controlled with the metal in the complex. By changing the Pd^{II} to Pt^{II} the thermodynamic strength of the interaction increases even. When different pincer complexes with different K_{eq} values were used, however, the mechanical response still scaled with the k_d. When the entire family of cross-linkers was compared (k_d ranging from 0.0006 s^{-1} to 1450 s^{-1}) all relative

viscosities scaled with the k_d and not K_{eq}. Clearly, the chemical structure of these pincer complexes dictates the properties and physical functions of these reversible networks.[83]

Within this family of pincer-based networks, the role of reversible molecular dynamics on material response was explored through the steric effects in the pincer alkylamino ligands, both within the Pd complexes **8a**-**b** and the slower, more strongly coordinating Pt complexes **8c**-**d**. As with the linear polymers, the independent control of kinetics is effective and particularly useful; cross-linkers **8a** and **8b** are structurally identical components within the network, and so their similar thermodynamics (K_{eq} = ~30 M^{-1} for **6a•7** and **6b•7**) ensure that the extent and nature of cross-linking is essentially the same in the two samples (or between Pt(II) pincer molecules **8c–d**; where $K_{eq} = 8 \times 10^3$ M^{-1} for **6c●7** and 4×10^3 M^{-1} for **6d●7**).

Above a critical concentration of cross-linkers, the absolute and relative behaviors of the various networks are quite different, both qualitatively and quantitatively. As seen in Figure 15, the viscosity increases by up to several orders of magnitude over a relatively narrow range of cross-linking content, and past this transition the materials behave like weak gels. This change in properties is attributed to a sol-to-gel transition, and once the macroscopic network is formed, the macroscopic mechanical response of the gel requires that the cross-links dissociate.

The central role of cross-link dissociation is seen in the relative viscosities at cross-linker concentrations beyond the sol-gel transition. In this regime, the relative

viscosities of the samples are proportional to the lifetime ($\tau=1/k_d$) of the coordinative metal–pyridine bonds that define the cross-links [83, 130]; for example, the zero shear viscosity of 100 mg mL^{-1} **8a**•PVP is a factor of 80 less than that of the isostructural network **8b**•PVP (Figure 12). The difference of a factor of ~ 80 in the network viscosities is within experimental error of the difference in the ligand exchange rates, and a full spectrum of dynamic mechanical behavior is similarly well correlated. The frequency-dependent storage and loss moduli, G' and G'', for networks of either **9a**•PVP or the related **9b**•PVP, are reduced to a single master plot when scaled by the corresponding ligand exchange rates, measured on model systems [83]. In other words, the full range of physical mechanical behavior of the networks can be tied back to a single molecular event, the dissociation of a pyridine ligand from a pincer complex. The same relationship is valid for both the Pd (e.g., **9a/b**) and Pt (**9c/d**) cross-linkers, even though the equilibrium association constants for the Pt complexes are roughly a factor of 10^2 higher than those of the corresponding Pd complexes.

Polymer networks formed via weak associations often have quite rich behavior under shear. Depending on the specific system and its environment, networks might grow less viscous once forced to flow (shear thinning, the most common example of which is found in striking a bottle of ketchup to get its contents to flow more easily), or they might become more viscous under induced flow (shear thickening, observed in quicksand and in concentrated cornstarch-water suspensions). Such responses are

classified as “non-linear rheology”, and the important point for purposes of this chapter is that the molecular mechanisms that dictate the various responses are often unclear. The kinetic control afforded by the pincer complexes has proven to be quite useful in establishing the details of these processes, and in fact have uncovered hidden and unanticipated polymer physics.

The nonlinear rheological properties of the pincer-PVP networks depend on the concentration of the PVP. When the networks are formed from less concentrated solutions of PVP (specifically, at concentrations in which the polymer chains are not entangled with each other), the application of shear above a critical shear rate leads to shear thickening [80]. As with the linear rheology, a change in cross-link dissociation rate provides immediate insight into the phenomenon, because the shear rate at which the shear thickening begins is proportional to the stress-free lifetime of the pincer-pyridine bond. The onset and magnitude of the shear thickening depends on the amount of cross-linkers added, and further experimental work has identified the primary mechanism of shear thickening to the shear-induced transformation of intramolecular cross-linking to intermolecular cross-linking, as shown in Figure 17.

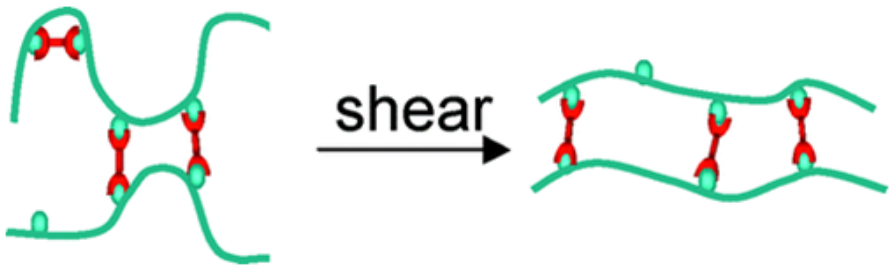

Figure 17: Representation of the mechanism of shear thickening
The shear thickening was observed in pincer cross-linked PVP networks. Figure was reproduced from reference 80 with permission from Copyright © 2010 American Chemical Society.

The story changes somewhat when the concentration of the PVP is higher, so that the PVP polymer chains are wrapped around each other in addition to being bound to each through the pincer complexes. The kinetic control of pincer-pyridine dissociation becomes especially useful in this complex environment. Under steady shear, however, the scaling relationships in the semidilute unentangled regime break down dramatically. This breakdown is not only in the quantitative scaling behavior, but even in the qualitative shear response of different systems: shear thinning is generally observed for samples with cross-linkers that have a faster dissociation rate (e.g., **10a**), while shear thickening is still observed for cross-linkers that have a slower dissociation rate (e.g., **10b**). Clearly, the picture is much more complicated than that of the systems with lower concentrations of PVP. In addition, the change in fundamental mechanism was not predicted by any existing theories of shear thinning and shear thickening, and it is difficult to imagine how the effect of cross-linker dynamics might have been observed without the ability to vary the kinetics in otherwise identical systems that is afforded

through the pincer complexes.[77] Further mechanistic work suggested that two critical processes compete in the time after a cross-linker dissociates: the cross-linker tries to re-associate, and at the same time the now freed polymer chain segment tries to orient in a way that would permit additional intermolecular cross-linkers to form. When cross-linker re-association is rapid, the polymer does not have time to orient for new cross-link formation under the shear flow and shear thinning, rather than shear thickening, results.[81]

The pincer complexes have also been used to shed light on how more complex material mechanical properties might be programmed via a combination of multiple supramolecular interactions. Pincer-PVP networks were formed similarly to the systems discussed in previous sections, but with the incorporation of combinations of multiple types of cross-linkers. The mechanical properties of mixtures of cross-linkers look not like the average of the multiple species, but instead a combination of both, showing that the response to an applied stress occurs through sequential, individual dissociation and re–association events.[74] Representative characterization is shown in Figure 18, and similar effects are observed for different pair wise mixtures of cross-linkers as well as a network with three different cross-linkers. In all cases, the frequency onsets and magnitudes of the transitions are anticipated by the behavior of networks with a single cross-linker, and therefore depend on the intrinsic properties of the individual supramolecular interactions themselves.

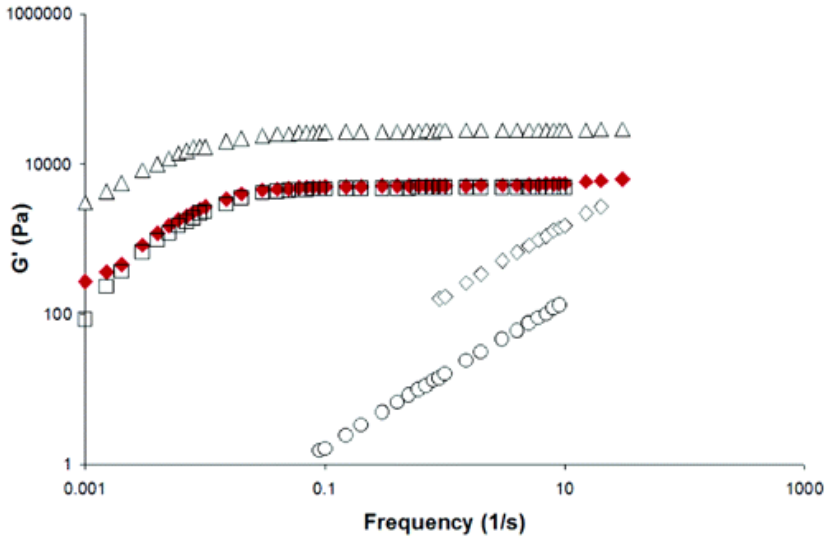

Figure 18: Plot of storage modulus, G', versus frequency for several samples
Reversible network samples included: (♦) 2.5% + 2.5% (**10b** + **10c**)•PVP, (•) 2.5% **10c**•PVP, (Δ) 5% **10c**•PVP, (o) 2.5% **10b**•PVP, and (◊) 5% **10b**•PVP. All networks were 10% by total weight in DMSO, 20 °C. Figure was reproduced from reference 74 with permission from Copyright © 2005 American Chemical Society.

The programmability demonstrated by the pincer complexes is less important in terms of applications of these specific materials than in its general implication for supramolecular materials science, that an understanding of isolated molecular behavior is often directly relevant to materials in which there is an interplay of multiple interactions and time scales. In this case, the behavior is that of transient networks, in which the independent relaxations of stress–bearing entanglements determine the dynamic mechanical response of a network.[131-133] The independence of the cross-links has significant consequences for the rational, molecular engineering of viscoelastic properties. When cross-linking is created through very specific interactions, the chemical

control of properties follows. As long as the strength of the association is great enough to make the cross-linkers active, the dynamics of cross-link dissociation, rather than further details of its thermodynamics, are the key design criterion. As a result, quite complex materials mechanical response can be programmed if one has suitable knowledge of the small molecular behavior.

As previously discussed, the pincer-based reversible networks offer many advantages when it comes to designing networks The networks were further used to demonstrate and characterize sensitive stimulus-response, by taking advantage of the dramatic change in properties that accompanies the sol-to-gel transition (Figure 19).[130] For a fixed PVP concentration, the sol-gel transition occurs at the same concentration across the family of different pincer structures (**10a-c**) in a solution of PVP. The important point is the one mentioned above, that the viscosity changes by several orders of magnitude over a modest change in active cross-linker concentration, suggesting that networks at or near the transition concentration should be very sensitive to external stimuli that influence the extent of active cross-linking.[130]

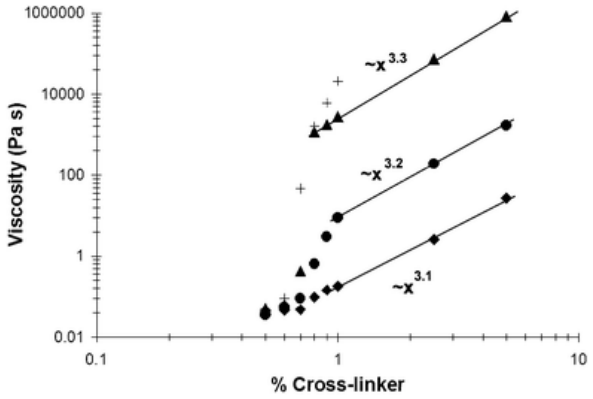

Figure 19: Viscosity as a function of % Cross-linker for various networks
The transient networks were formed from PVP with pincer complexes: **10a**●PVP (♦), **10b**●PVP (●) and **10c**●PVP (▲). Figure was reproduced from reference 75 with permission from Copyright © 2007 Royal Society of Chemistry.

This expectation was confirmed by monitoring the sample viscosity as a function of different added agents to the solution. For example, one specific pincer network had an initial zero-shear viscosity of ~ 1000 Pa●s. The viscosity drops by up to several orders of magnitude, however, in response to relatively small quantities of acids, bases, or other ligands that inhibit the pincer-pyridine coordination (Figure 20). In some cases, the decrease in viscosity can be reversed by removing the competing ligand or treating the system with an additional stimulus. The work indicates the potential to engineer at the molecular level supramolecular and pincer-based networks for use as chemoresponsive systems.[130]

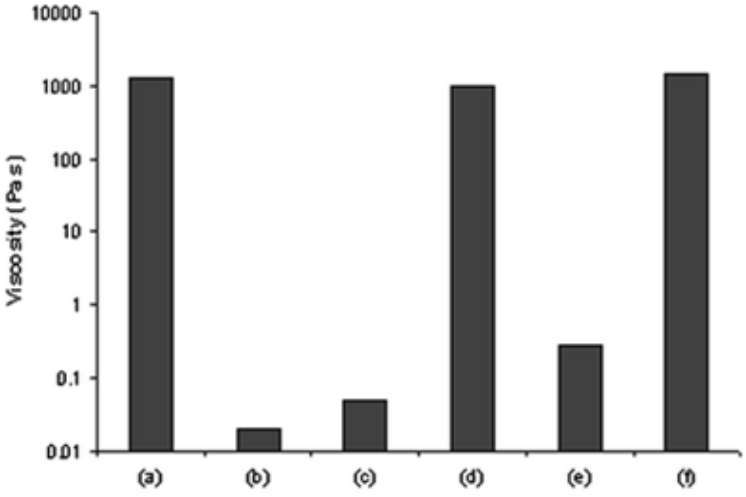

Figure 20: A chart demonstrating the chemoresponsive nature of a network
The network was formed by cross-linking PVP with pincer complex **10c** with the following treatments: (a) initial viscosity, (b) a + NaCl, (c) a + sulfuric acid, (d) c + NaHCO3, (e) a + triflic acid, and (f) e + NaHCO3. Figure was reproduced from reference 75 with permission from Copyright © 2007 Royal Society of Chemistry.

2.6 Hybrid Networks: Combination of Covalent and Reversible Cross-linkers

The previous examples of pincer-based networks feature pincer-pyridine coordination as the only active cross-linking interaction. One of the advantages of the reversibility of the coordination is that the networks formed are 'self-healing', in the sense that if the networks are fractured or cut, they will reorganize and regain their initial structure. This 'healing' behavior is enabled by the same dissociation/re-association processes that allow the networks to flow over extended periods of time (and in many cases the repair and the flow are really the same process). It is therefore interesting to consider the physics enabled by incorporating reversible interactions in

combination with permanent covalent bonding, where the former might provide reversibility, repair, and added toughness, while the latter provides a permanent structure that will not flow over long time scales.

With that motivation, the same pincer motifs discussed in the previous sections were incorporated into a family of hybrid polymer gels in which covalent cross-links create a permanent, stiff scaffold onto which the reversible metal–ligand coordinative cross-links are added.[92] The hybrid gels exhibit frequency-dependent mechanical properties that are different from those of the parent, covalent-only gel (Figure 21). On long timescales, the pincer complexes are dynamic and do not contribute to the storage modulus of the gels, but on shorter time scales they remain intact and the storage modulus increases measurably as a result. The underlying relaxation can be directly attributed to the dissociation and reassociation of the supramolecular pincer cross-linker by employing the same kinetic variation strategy used to good effect in the reversible-only networks. The structural similarity of the related pincer complexes and their comparable pyridine coordination thermodynamics ensures that the equilibrium structures of the two gels are effectively identical. The time scales at which the various cross-linkers begin to contribute to material mechanical properties, however, are not identical, but instead reflect the intrinsic dissociation rates of the various pincer complexes. In the hybrid systems, as in the mixed reversible-only systems, the

individual supramolecular cross-links bear stress and act as largely independent contributors to the dynamic mechanical properties.

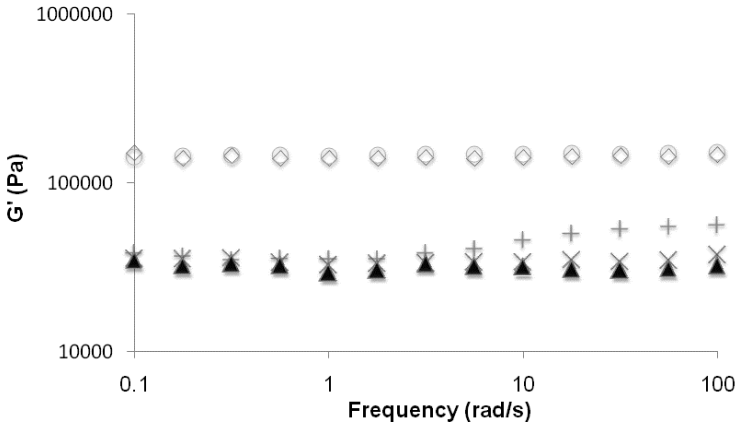

Figure 21: Storage modulus as measured by the oscillatory rheology
The sample gels were comprised of covalent and hybrid DMSO gels: "pure" covalent gel (×); gel•**10a** (●); gel•**10b** (▲); gel•**10c** (Δ); gel•**10d** (○). Figure was reproduced from reference 92 with permission from Copyright © 2006 The Royal Society.

Looking ahead, these and related hybrid networks offer the opportunity for future mechanistic studies of important, but complex, processes whose mechanistic origins are still poorly understood, including: gel fracture [134] self-repair [49], and energy dissipation.[135] Studies in these areas would follow cleanly from the structure-activity studies described above, and should benefit from the groundwork laid by the prior efforts. The shear thinning and shear thickening behavior described in earlier sections shows how pincer complexes can be used as effective probes of highly complex responses for which conclusive molecular interpretations are often not available.

2.7 General Conclusions

As testified by the bulk of pincer chemistry covered in literature and discussed above, pincer complexes have gained popularity largely through their ability to effect chemical transformations. Nonetheless, the ease of synthesis and handling, stability in a wide range of chemical environments, and the availability of handles for structural manipulation has provided a wealth of opportunities to use pincer complexes in a range of physical applications. They have been used to build complicated nanostructures and metallodendrimers by both convergent and divergent techniques. They have provided a mechanism for rapid and selective post-synthetic modification of random and block copolymers, and as the glue for new classes of multi-layer thin films with impressive stability. They have served as probes of fundamental polymer physical behavior, and played a key role in seminal discoveries and demonstrations in the burgeoning field of polymer mechanochemistry. Looking ahead, it seems likely that pincer complexes will provide additional benefits to research in materials science, and for the same reasons that they have been so useful to date: they are compact, functional, and dependable, with metallosupramolecular coordination behavior that functions reliably even in complex environments. Their past utility in the context of materials is therefore not surprising, nor is likely to be their future use in a growing range of physical applications. As will be discussed further in this dissertation, pincer complexes have been used to create new polymeric materials building from the topics discussed in this

chapter. These new materials exhibit desired enhanced mechanical properties when compared to materials that lack the pincer complexes.

3. Failure Behavior of Hybrid Networks

3.1 Initial Characterization of PVP Networks

As was discussed in Chapter 1, hybrid networks are suited for a wide range of applications in the field of material science. By adding weak or reversible interactions to an existing network, a number of potentially useful properties can be specifically designed. In particular, the incorporation of reversible interactions can improve both the fracture toughness and strain at break of a gel,[65] and I set out to characterize the structure activity relationships that are responsible for the improved mechanical properties. Our initial objective was to investigate how the dynamics of reversible components within the same covalent network influence the failure behavior of the hybrid networks. As described in Chapter 2, the pincer complexes offer a mechanism by which to probe directly those contributions. To that end, hybrid networks were fabricated similar to those described in Section 2.6.[85]

Poly(4-vinyl pyridine) (PVP) was cross-linked with 1,6-dibromohexane (DBH) to form a covalent networks. PVP has several advantages as the choice of polymer backbone: (1) it is a commercially available polymer that can be used as received from the supplier; (2) it is readily cross-linked; (3) it has no significant intramolecular interactions in DMSO, which acts as a near theta solvent; (4) the pyridine functionality is a good ligand for reversibly cross-linking through the pincer complexes, which can be

used to tune the cross-linking dynamics as described in Section 2.6. Figure 22 below shows the proposed scheme for the covalent cross-linking reaction.

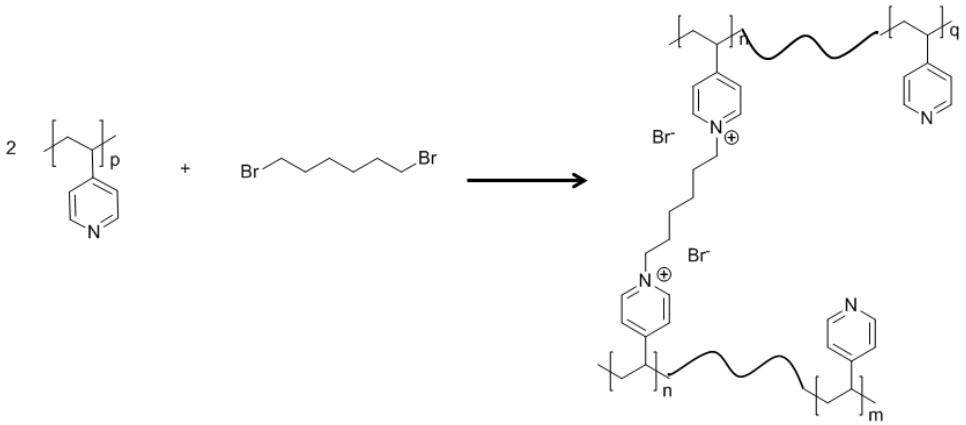

Figure 22: Covalent cross-linking of PVP with DBH; singly reacted DBH not shown

To form the covalent networks, PVP (M_w = 60, 000 as reported by supplier; actual M_w likely varies[79]) was dissolved in DMSO (100 mg/mL). DBH was then added in one of several stoichiometric amounts, from approximately 1% cross-linker up to 56% cross-linker, where the percent cross-linker is reported as functional group equivalents of alkyl bromide (two per cross-linker) to pyridine.

Solutions with varying DBH concentrations were placed in small vials, and then allowed to either sit at room temperature, or sit in an oil bath at 90 °C. Not surprisingly, the addition of heat did in fact speed up the cross-linking and produced self-supporting gels faster than allowing them to sit at room temperature. Table 1 summarizes the results of the heated samples compared to the samples left at room temperature after 15 minutes.

Table 1: Observed changes in 100 mg/mL PVP in DMSO;
Properties vary as a function of cross-linker equivalents and temperature; reaction time = 15 min.

[R-Br] : [pyr]	~ 90 °C	Room Temperature
3%	Liquid and flows freely	Liquid and flows freely
7%	Self-supporting with jelly like consistency	Liquid and flows freely
30%	Self-supporting and can be manipulated	Liquid and flows freely
56%	Self-supporting; stiffer than 30% R-Br	Liquid and flows freely

The samples reacted at room temperature showed no visible gelation over the 15 minutes, but three of the four heated solutions (7, 30, and 56%) produced self-supporting gels, and the observed stiffness of the gel, as characterized by touch, increased with the concentration of DBH. In contrast, all of the samples left at room temperature showed no visible gelation over the 15 minutes. With these guidelines in hand, glass molds (approximately 25 mm x 75 mm x 1 mm) were used to fabricate films of desired thickness. Within this framework, then, the concentrations of PVP and DBH were studied to characterized how they influenced the compressive modulus (E_c) of the formed gels. The goal was to identify gels that could be: 1) easily manipulated, 2) punched into disks, and 3) tunable in terms of compressive modulus (E_c) by varying the

amount of covalent cross-linker. A series of gels were made with different concentrations of PVP and DBH. The gels were punched into 5 mm circular disks and compressed between parallel plates with a constant compression velocity (v_c) of 10 μm/s. The gels are on average 1380 ± 13 μm high, and so this velocity corresponds to an initial strain rate ($\dot{\varepsilon}_i$) of 7.25 x 10^{-3} s^{-1}. A representative stress-strain curve is shown in Figure 23.

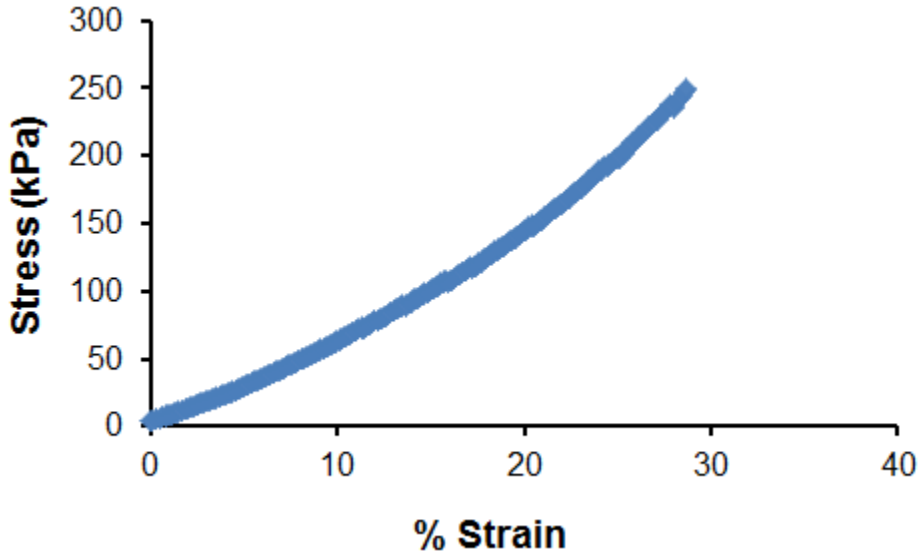

Figure 23: Representative compression curve for a PVP/DBH gel
A 5 mm gel made from 300 mg/mL PVP and 5% DBH was swollen in DMSO and compressed between parallel plates at $\dot{\varepsilon}_i$~ 7.25 x 10^{-3} s^{-1}.

For our studies the compressive moduli, E_c, were obtained from the low-strain region of the curve for each network, and shown in Figure 24 as a function of the concentration of PVP and DBH. We attribute the curvature in the stress/strain plots to the deformation of the gels under compression. As the gels are compressed, their cross-sectional area increases, and since stress = load/area, the true stress is less than the

engineering stress plotted. Similarly, the instantaneous height of the gel decreases with compression, meaning the true strain is greater than the engineering strain reported. In model calculations (not shown), these two effect account for much of the deviation from linearity. Of course, uniaxial compression is more complicated than this simple picture, but no attempt was made to treat the data with more comprehensive models such as those of Mooney and Rivlin[136-137] or Gent and Thomas.[138]

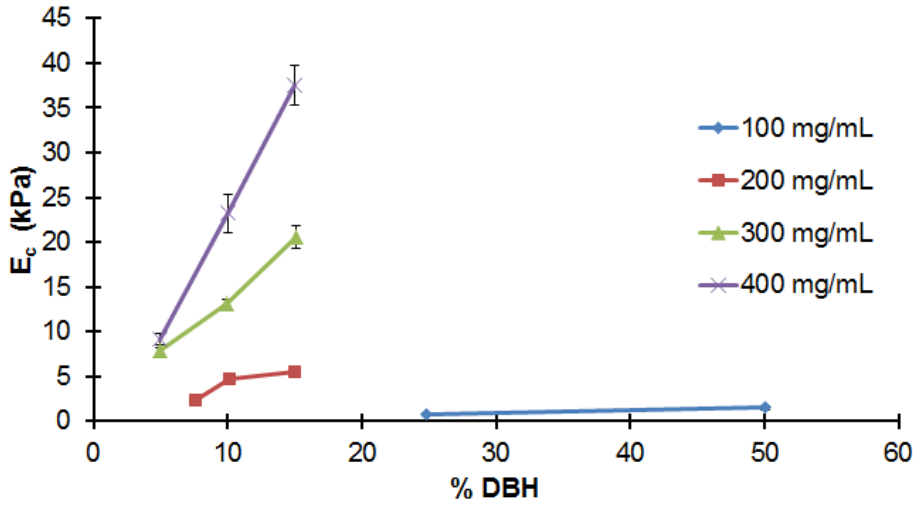

Figure 24: E_c as a function of PVP and DBH concentration
Networks were swollen in DMSO and 5 mm disks were punched from the polymer slabs (1380 ± 13 μm thickness) and compressed at $\dot{\varepsilon}_i = 7.25 \times 10^{-3}$ s^{-1}. % DBH is calculated as the ratio of R-Br (two per cross-linker) to pyridine units.

It should be noted that the compression testing that constitutes the bulk of the experiments carried out in this chapter and Chapter 4 are constant velocity, and not constant strain rate, experiments. The dimensions of the gels change as they are compressed, and so the instantaneous strain rate changes over the course of the

experiment. For ease of interpretation and referencing, the compression rates have been converted to an initial strain rate ($\dot{\varepsilon}_\iota$), where $\dot{\varepsilon}_\iota$ is calculated from the average initial height of the gels (h_{avg}) and the compression velocity as shown in Equation 1. Strain (ε) is reported throughout as engineering strain, calculated from the initial height of the gels (h_o) and the current height (h) using Equation 2.

Equation 1: Definition of average initial strain rate ($\dot{\varepsilon}_\iota$)

$$\dot{\varepsilon}_\iota = \frac{v_c}{h_{avg}}$$

Equation 2: Definition of engineering strain (ε)

$$\varepsilon = \frac{(h_o - h)}{h_o} \times 100\%$$

For the remainder of this dissertation, the strain rate will be reported in terms of $\dot{\varepsilon}_\iota$. See Table 8 in Section 3.7.3 for a summary the relationship between v_c and $\dot{\varepsilon}_\iota$.

The gels made with 300 mg/mL of PVP in DMSO and 2% cross-linking produced robust gels that could be easily manipulated when swollen in DMSO, and this combination of PVP and DBH, referred to hereafter as **N1**, became the standard platform recipe for the majority of the studies discussed in this chapter.

3.2 Creating a Hybrid Network

Reversible pincer cross-linkers wer incorporated into **N1** to examine the effect of cross-linker dynamics. Initial studies employed cross-linker **10d**, which has a low k_d (pincer – pyridine dissociation rate constant, see Figure 16) and therefore remains intact

for a longer period of time. Figure 25 reproduces the structures of complexes **10a-d** that were originally shown in Figure 12 in Chapter 2. Figure 16 (Chapter 2) depicts the reversible interaction that will be utilized and whose thermodynamic and kinetic parameters are summarized in Table 2.

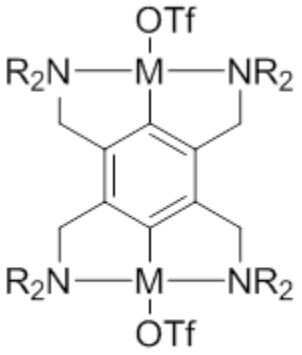

10a M = Pd R = Me
10b M = Pd R = Et
10c M = Pt R = Me
10d M = Pt R = Et

Figure 25: Structure of the *bis*-functional pincer complexes used in this study

Table 2: Dissociation rate and associatoin equilibrium constants (k_d and K_{eq})
For pyridine coordination to **10a-d**, DMSO, room temperature.[83]

Structure	M	R	k_d (s^{-1})	K_{eq} (M^{-1})
10a	Pd	Me	1450	33
10b	Pd	Et	17	29
10c	Pt	Me	0.026	4000
10d	Pt	Et	0.0006	8000

Hybrid networks (**N1●10d** as shown in Figure 26) were formed by transferring , 5 mm disks of **N1** to vials containing solutions of 5 mM or 25 mM **10d** in DMSO and soaking them for 3 or 6 days. After their respective soaking times, the disks were

compressed to determine E_c. Table 3 reports the average E_c as a function of soak time and concentration of **10d**.

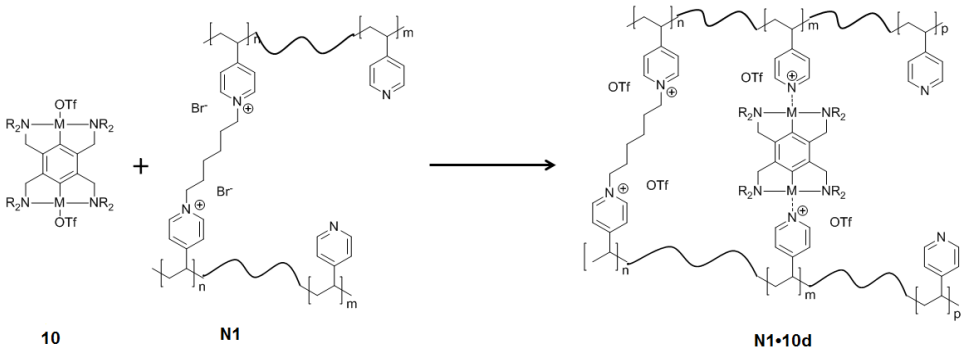

Figure 26: Structure of hybrid networks; singly reacted DBH not shown

Table 3: Ec of N1 as a function of soak time and concentration of 10d

Soak Time	0 mM	5 mM	25 mM
0 Days	2.0 ± 0.2	2.1 ± 0.2	2.1 ± 0.2
3 Days	1.8 ± 0.2	11.0 ± 1.4	23.9 ± 2.5
6 Days	1.9 ± 0.2	13.6 ± 1.1	38.0 ± 3.2

As seen in Table 3, E_c increases with both the amount of cross-linker in the initial solution and the time spent in the solution. The increase in E_c reflects an increase in active, stress-bearing cross-links. UV-Vis studies were carried out to monitor the

concentration of the soaking solution as a function of time (see Appendix 1). It was determined that after 6 days the concentration has effectively reached equilibrium.

3.3 Failure Under Compression

I next set out to characterize the failure behavior of the hybrid gels under compression. For comparison, a new covalent network **N2** was formed from 300 mg/mL PVP in DMSO like **N1**, but with 10% DBH instead of 2%. Disks from the **N1**, **N2**, and **N1•10d** were each compressed at $\dot{\varepsilon}_t = 1.5 \times 10^{-4}\ s^{-1}$ until failure was observed (see below) or until the maximum normal force for the instrument was reached.

In each compression, the stress eventually reaches a maximum value beyond which there is a sharp drop off. This drop corresponds to a macroscopic failure event that is visually evident (e.g., cracking and breaking of the gel). For the remainder of this dissertation, the strain at the point of maximum stress as the strain at break, or ε_b, will be reported as a percentage (%). Figure 27 shows an **N1** disk before and after being compressed to failure, and Figure 28 shows representative compression curves for **N1**, **N2**, and **N1•10d**. Average values of E_c and ε_b for **N1, N2**, and **N1•10d** are shown in Table 4.

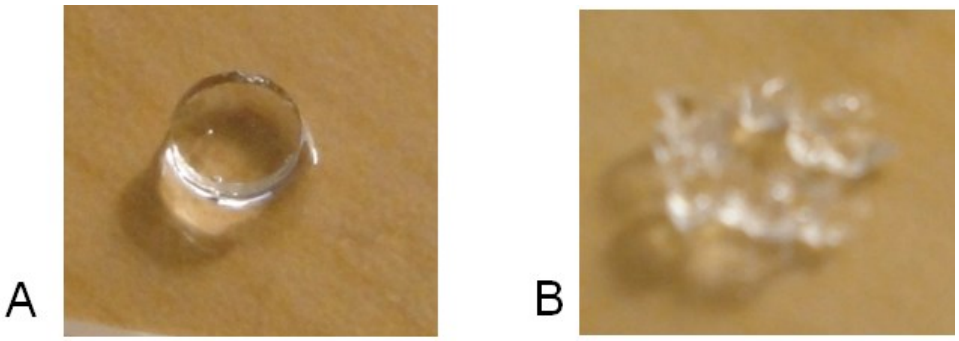

Figure 27: Pictures of an N1 gel before and after compression; $\dot{\varepsilon}_t = 1.5 \times 10^{-4}\ s^{-1}$

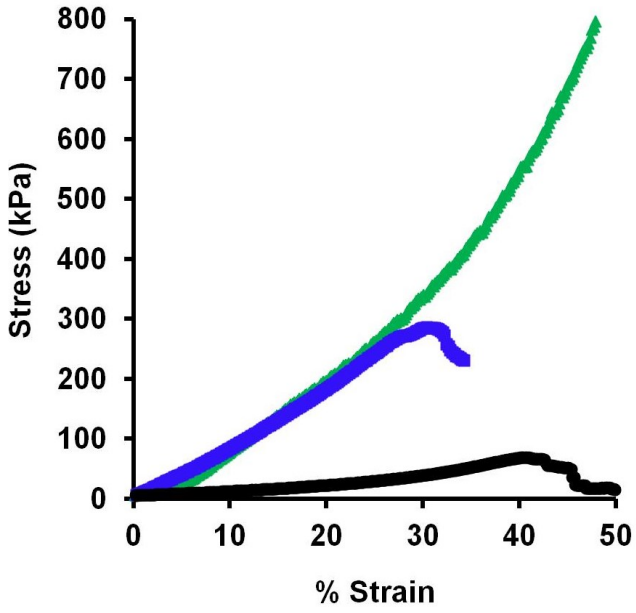

Figure 28: Representative stress – strain compression curves for N1 (black), N2 gel (blue), and N1•10d gel (green); $\dot{\varepsilon}_t = 1.5 \times 10^{-4}\ s^{-1}$

Table 4: E_c and ε_b for gels compressed at $\dot{\varepsilon}_t = 1.5 \times 10^{-4}\ s^{-1}$

	N1	**N2**	**N1•10d**
E_c (kPa)	1.2 ± 0.1	12.0 ± 0.7	14.0 ± 0.6
ε_b	42 ± 2 %	30 ± 1 %	> 80%

As expected, **N2** shows an increase in E_c and decrease in ε_b due to the increase in covalent cross-linking.[139] When the **10d** was incorporated into **N1** to form **N1•10d**, the E_c increased to 14.02 ± 0.59 kPa as is expected with the addition of cross-linkers. This increase in E_c mimics the behavior that was observed in the **N2** samples. **N1•10d** survives past the point of failure for both **N1** and **N2**. In fact, **N1•10d** was compressed without breaking at the maximum attainable load on the rheometer (50N).

The average initial height of **N1•10d** gels is 1,957 ± 72 μm, but after compression they were on average less than 1,000 μm tall. When the disks are then soaked again in DMSO, they recover their original height (1965 ± 52 μm) and modulus (1.2 ± 0.1 kPa), indicating no permanent damage to the gels. The decrease in height was attributed to the solvent that was squeezed out of the gel during the compression studies. If the solvent is replaced, then the material regains its original size, shape, and modulus.

When the gels are compressed rapidly on the timescale of pincer dissociation ($\dot{\varepsilon}_\iota$ = 1.25 x 10^{-2} s^{-1} vs. k_d = 6 x 10^{-4} s^{-1}), the hybrid networks behave like analogous covalent networks (Figure 28; Table 5).

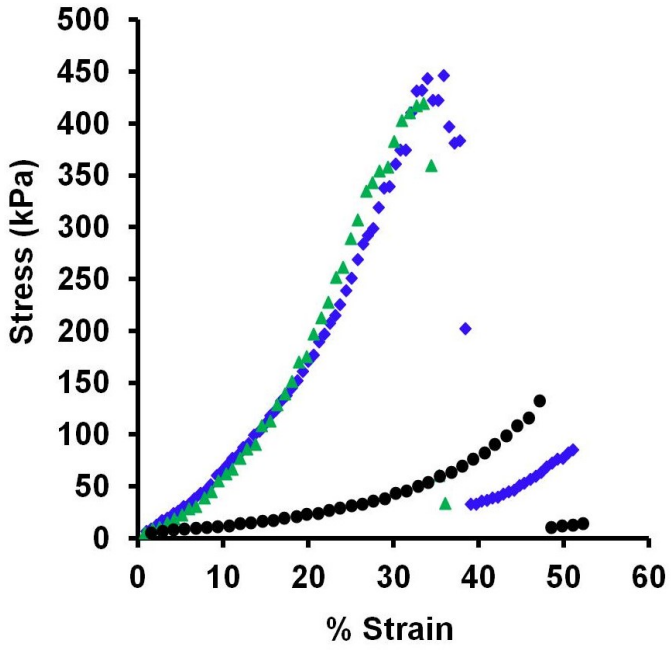

Figure 29: Representative compression curves for three gels; $\dot{\varepsilon}_\iota$ = 1.25 x 10^{-2} s^{-1}
N1 (black, ε_b = 47%); **N2** (blue, ε_b = 32%); **N1•10d** (green, ε_b= 32%).

Table 5: E_c and ε_b for gels compressed at $\dot{\varepsilon}_\iota$ =1.25 x 10^{-2} s^{-1}

	N1	N2	N1•10d
E_c (kPa)	1.1 ± 0.1	6.5 ± 0.5	6.3 ± 0.2
ε_b	46 ± 2%	32 ± 0.7%	36 ± 0.5%

The hybrid **N1●10d** has an average E_c of 6.3 ± 0.2 kPa, similar to the value of E_c for **N2** and suggesting a comparable number of intact cross-linkers. The strain at break (ε_b = 36 ± 0.5%) is also similar to that of **N2** (ε_b = 32 ± 0.7%). This suggests that as the reversible cross-linkers remain intact on the timescale of the compression, they behave as if they were permanent covalent bonds. To test this relationship further, the disks were compressed at initial strain rates ranging from 1.25 x 10^{-2} s^{-1} to 5.00 x 10^{-5} s^{-1}. Results are shown in the Figure 30.

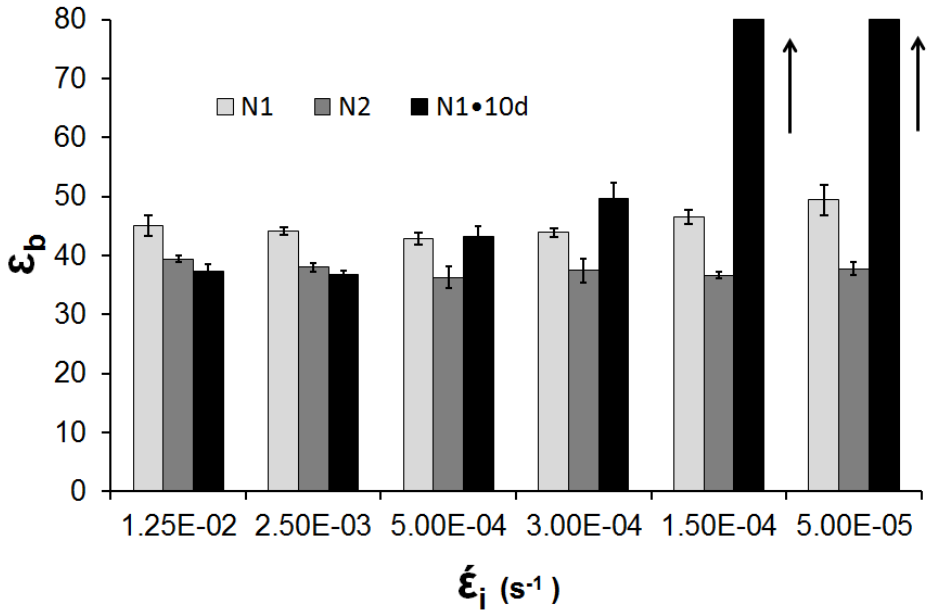

Figure 30: ε_b as a function of $\dot{\varepsilon}_\iota$
N1 (light gray), **N2** (medium gray), and **N1•10d** (black).

At high $\dot{\varepsilon}_\iota$, **N2** and **N1•10d** have similar values of ε_b that are both less than that of **N1**. As $\dot{\varepsilon}_\iota$ decreases, ε_b for the hybrid gels begins to increase while those of the purely

covalent gels change very little. For the slowest compression rates tested, the hybrid gels survive even once the instrument's maximum applied normal force is reached, at which point the experiment was terminated. It should be noted that **N1•10d** begins to survive past the point of failure for **N1** when $\dot{\varepsilon}_t$ has been lowered to around 5.00×10^{-4} s^{-1}. This rate is on the same order of magnitude as the k_d reported for the **10d** cross-linker (6×10^{-4} s^{-1}). The point of transition would suggest that the dynamics of the reversible cross-linker should be on the same timescale as the compression rate in order to extend the ε_b for the network. If this hypothesis is true, there should be a shift in the $\dot{\varepsilon}_t$ at which the transition occurs if the pincer cross-link is changed from **10d** to a pincer complex with a different k_d. This hypothesis is tested in the following section.

3.4 Comparison of Hybrid Systems with Different Pincer Complexes

Previous work in our laboratory probed the structure activity relationship between the dynamics of the compounds **10a-d** and the rheological properties of reversible networks formed from them.[83-84] Compounds **10a, 10b,** and **10c**, shown above, have similar structures to **10d** but very different rates of pyridine exchange. They can therefore be used to create similar hybrid networks through which to study the contribution of cross-linker reversibility to the mechanical response of the hybrid gels.

As shown in Table 2, when the metal center stays the same but the alkyl stubstituents change from methyl to ethyl, K_{eq} (association equilibrium constant, see Figure 16) remains relatively constant, but the rate constants for the pyridine

association/dissociation change substantially. The large change in rate constants is attributed to steric effects in the association exchange mechanism.[83] For example, when compound **10c** is compared to **10d**, there is an approximate 40 fold increase in k_d from 2.6 x 10^{-2} s^{-1} to 6 x 10^{-4} s^{-1} (see Table 2 and Figure 16). If the strain rate dependence of ε_b is due to cross-linker dissociation, then increasing k_d by a factor of 40 should shift the protective effect by a comparable amount of the extension of life to a faster $\dot{\varepsilon}_i$.

N1•10c networks were created similarly to **N1•10d**, and UV-Vis studies again confirmed that the pincer uptake reached equilibrium at 6 days (see Appendix 1). The new hybrid gels were then compressed to failure at various $\dot{\varepsilon}_i$, and results are shown in Figure 31.

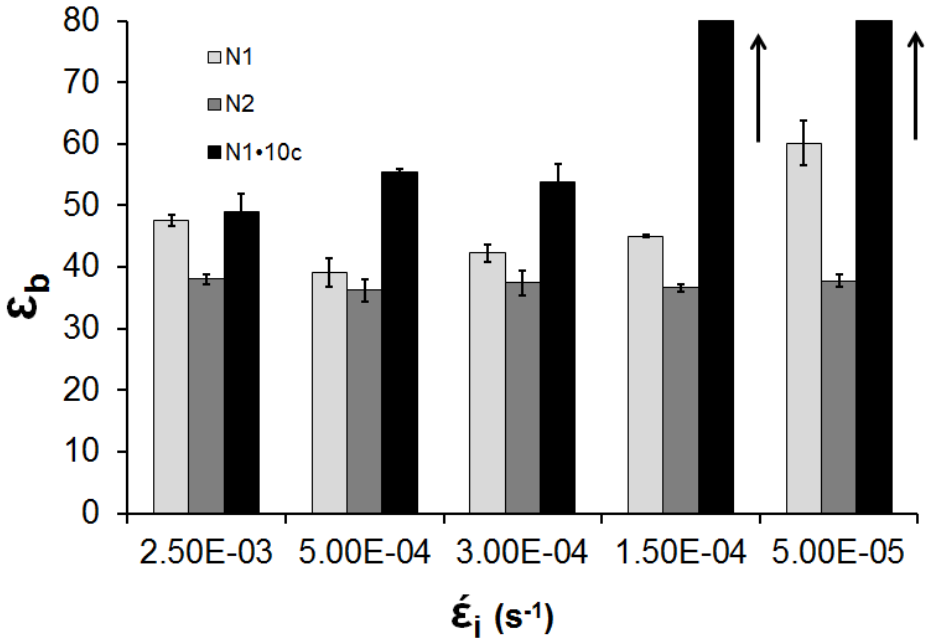

Figure 31: ε_b as a function of $\dot{\varepsilon}_i$
N1 (light gray), **N2** (medium gray), and **N1•10c** (**black**).

As the data in Figure 31 show, the failure behavior for the **N1•10c** gels is similar to the failure behavior observed in the **N1•10d** gels. The notable difference in behavior is observed for the higher $\dot{\varepsilon}_\iota$, where the **N1•10c** gels survive to higher ε_b when compared with the covalent **N1** and **N2** gels. This suggests that the dynamics of the reversible cross-linkers may influence the failure behavior on different timescales. Whereas **N1•10c** survival starts to improve at higher $\dot{\varepsilon}_\iota$ than observed in **N1●10d**, the difference is less than a factor of ~10 and not the full factor of 40 expected from the difference in k_d values. The difference in behavior is even less obvious at lower $\dot{\varepsilon}_\iota$. The ambiguity in the influenc of k_d is driven home in Figure 32, which shows the ratio of hybrid networks **N1●10** relative to that of **N1**. This ratio is plotted as a function of normalized strain rate ($\dot{\varepsilon}_\iota/k_d$) . If cross-linker dissociation on the timescale of deformation were the sole determining factor in dictating fracture strain, these data should collapse on a single master plot. As seen in Figure 32, however, they do not. This result raises some additional questions with regards to the behavior of the gels, especially at small $\dot{\varepsilon}_\iota$. It should be noted that for the lowest $\dot{\varepsilon}_\iota$, the compressions take over an hour to complete and there is solvent lost due to the diffusion out of the gel and/or evaporation. These additional factors likely influence the failure behavior and create ambiguity in the interpretation.

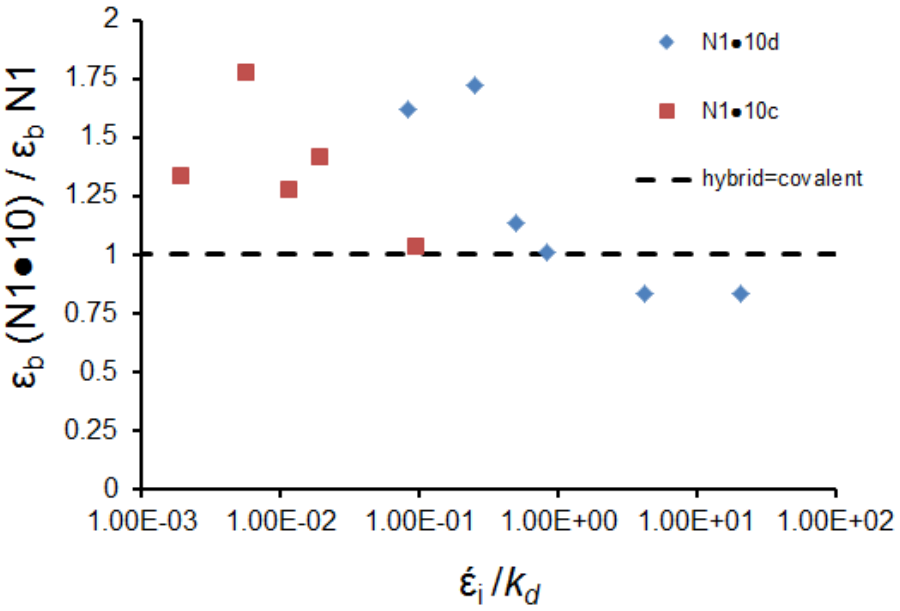

Figure 32: Relative ε_b for both hybrid gels as a function of relative strain rate

To further probe the structure activity relationship suggested in the studies carried out with **N1•10d**, the k_d value was increased by an even larger magnitude. As reported in Table 2, compound **10a** has a k_d of 1450 s^{-1} while **10b** has a k_d of 17 s^{-1}. This corresponds to an approximate increase of 2.5 x 10^6 fold for **10a** and 2 x 10^4 fold for **10b** when compared with the k_d value for **10d**. It should be noted that by switching to the **10a** and **10b** cross-linkers, the K_{eq} pyridine coordination is also changing (therefore increasing the amount of reversible cross-linkers present in the networks). Compounds **10a** and **10b** have values of k_d that are much greater than that of **10d,** and so when **N1** gels are soaked in solutions of either **10a** or **10b,** the solutions reached a stable

concentration after only 3 days (as confirmed via UV-Vis data in Appendix 1) which became the standard minimum equilibrium time for this set of gels.

N1 disks were prepared as above and soaked in 5 mM solutions of either **10a** or **10b** in DMSO to create the respective hybrid networks **N1•10a** and **N1•10b.** The hybrid gels were then compressed at 1.25 x 10^{-2} s^{-1} until failure was observed. Figure 33 shows representative compression curves for each of the 3 types of gels compared in this study. Table 6 summarizes the E_c and ε_b data that were compiled for all three types of gels.

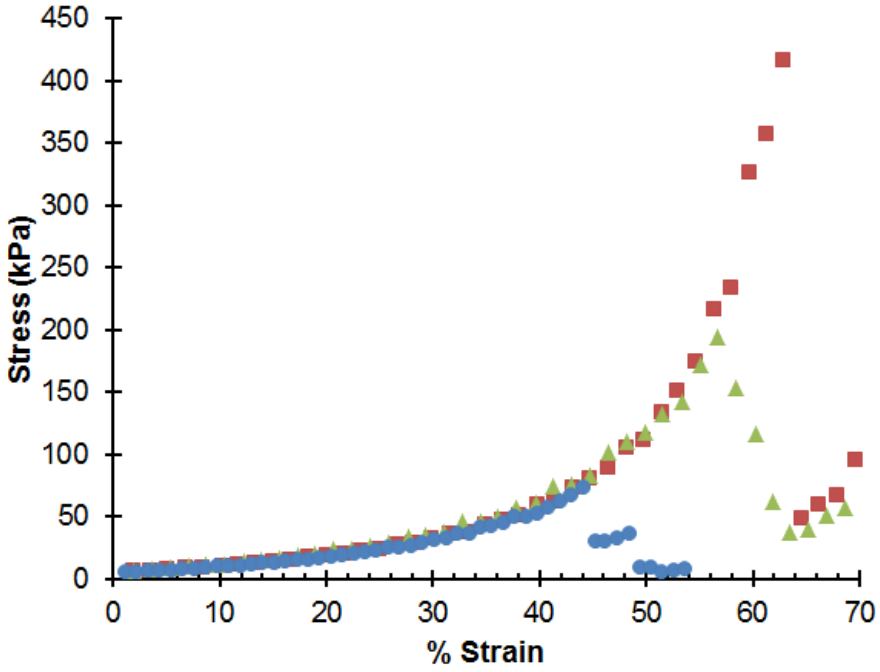

Figure 33: Compression curves for N1 (blue circles), N1•10a (red squares), N1•10b (green triangles); $\dot{\varepsilon}_t$ = 1.25 x 10^{-2} s^{-1}

Table 6: E_c and ε_b for three types of gels compressed at $\dot{\varepsilon}_t = 1.25 \times 10^{-2}\ s^{-1}$

	N1	N1•10a	N1•10b
E_c (kPa)	1.1 ± 0.1	1.2 ± 0.3	1.2 ± 0.2
ε_b	46 ± 1.8 %	61 ± 2.1 %	55 ± 1.4 %

Unlike the cases discussed above, the addition of either **10a** or **10b**, does not have a measurable influence on E_c within the measured standard deviation (Table 6). Both hybrid networks, however, have a larger ε_b than **N1** despite the fact that they do not contribute significantly to the modulus: **N1•10a** $\varepsilon_b = 61 \pm 2.1\%$, and for **N1•10b** $\varepsilon_b = 55 \pm 1.4$ %. It is also interesting to note that the pincer complex with the larger k_d value (**10a**) has a larger effect.

These observations are independent of compression rate across the range studied. When disks are compressed $\dot{\varepsilon}_t = 1.5 \times 10^{-4}\ s^{-1}$ no influence on ε_b was observed, see Table 7.

Table 7: E_c and ε_b for gels compressed at $\dot{\varepsilon}_t = 1.5 \times 10^{-4}\ s^{-1}$

	N1	N1•10a	N1•10b
E_c (kPa)	1.4 ± 0.1	1.3 ± 0.4	1.2 ± 0.2
ε_b	43 ± 2 %	56 ± 4 %	52 ± 1 %

The E_c showed no increase for either hybrid network, however, they did survive to higher strains when compared with the **N1** gels. This indicated that during the slower compressions the faster reversible cross-linkers (**10a** and **10b**) were still active at protecting against failure. More surprisingly, these results indicate that **10a** and **10b** influence the failure behavior of the gels *without* contributing to the overall E_c or supporting stress within the network. As discussed in Chapter 1, many different types of hybrid networks have been shown to have enhanced properties when compared to covalent networks with similar cross-linking densities. In most cases, the addition of the reversible component does contribute to the material properties of the system. In contrast, our system demonstrates that incorporating highly dynamic and weak reversible bonds can still protect against failure at strains previously unattainable to the parent covalent networks, even when they do not contribute to the modulus. The hybrid networks **N1•10a** and **N1•10c** are essentially the same mechanically as the **N1** gels. All three gels support the same stresses and strains (at low strain values), but the two hybrid networks survive to higher strains, past the point of failure of the original gel.

3.5 Discussion

These initial studies showed that a hybrid network could be successfully created using a network of PVP covalently cross-linked with DBH and incorporating the *bis*-functional pincer complexes (**10a-d**). The addition of these reversible cross-links was

shown to enhance the failure properties of the polymer network. The covalent network successfully provided a permanent shape for the material that could remain intact over a large range of strains. In the cases of the slow compressions where deformations were observed, these deformations were not permanent and could be easily reversed by reswelling the gels in solvent. The reversible nature of the pincer complexes offered a mechanism that prevented failure from occurring in the covalent network.

Further studies probed the influence of the kinetic behavior of the pincer complexes on the macroscopic properties of the material. The studies carried out with different cross-linkers and different values of $\dot{\varepsilon}_\iota$ demonstrated that the timescale of the strain matters. As previously reported by our group, the PVP – pincer dissociation essentially follows first order kinetic behavior.[83] Therefore the varying k_d values for each of the pincer complexes can be used to determine the half-life for each of the pincer complexes. For example, compound **10d** ($k_d = 6 \times 10^{-4}$ s^{-1}) the approximate half-life is 20 min. Assuming that each pincer complex has two pincer ends that need to be intact for the cross-link to bear stress, if just one of those pincer – pyridine coordination sites dissociates, the cross-link is broken within the network. When the **N1•10d** gels were compressed at the higher $\dot{\varepsilon}_\iota = 1.25 \times 10^{-2}$ s^{-1}, the average gel broke within 30 seconds. Using the first order integrated rate law, after 30 seconds, approximately 1% of all the pincers units have dissociated. This requires that 99% of all of the pincer complexes remained coordinated during that time period and behaved similar to an intact covalent

bond. This mathematical probability was observed when the gels compressed at this $\dot{\varepsilon}_t$ still broke like the covalent gels.

As the $\dot{\varepsilon}_t$ is decreased over the range of values studied, the ε_b begins to increase for the hybrid **N1•10d** gel. The **N1•10d** are first observed to survive past the parent **N1** gel at a $\dot{\varepsilon}_t = 5.00 \times 10^{-4}\ s^{-1}$, this roughly correlates to the k_d value for **10d** ($6 \times 10^{-4}\ s^{-1}$). This result initially suggested that the protective behavior was related to the dynamics of the reversible cross-linker. As the $\dot{\varepsilon}_t$ is decreased further, the ε_b continues to increase, until the maximum load (50 N) that can be applied with the instrument is reached.

When the $\dot{\varepsilon}_t$ was reduced to the lowest rate $\dot{\varepsilon}_t = 5 \times 10^{-5}\ s^{-1}$, the average compression to 40% strain lasted 8,000 seconds, or 133 min. This is over 6 times the half-life of the dissociation of **10d**. After 8,000 seconds over 99% of all of the pincer complexes have dissociated and broken and therefore broken their cross-link at least once. Because the cross-links had been given enough time to break and reform over the length of the compression, the reversibility of the pincer interactions protected the covalent network from breaking. If a buildup of stress was localized on a pincer cross-link, and then that cross-link broke, the stress would be dissipated. That cross-link could, however, easily reform within the network and bear stress again. Given enough time, the cross-links can break and reform several times and therefore extend the life of the covalent network by presumably relieving some of the stress being supported by the covalent cross-links.

Additional considerations must be taken into account when interpreting the data for the two lowest $\dot{\varepsilon}_t$. For these long timescales, there may be contributions do to solvent loss. It was noted that there is some solvent that is pushed out of the gels during the compression. This most likely leads to the observed shape deformation that can be simply reversed by reswelling the gels in solvent. Solvent evaporation could also be a factor, though not as likely due to the low vapor pressure and high boiling point of DMSO. The addition of the reversible cross-linkers may extend the ε_b to high enough values, until the effect of solvent loss takes over and produces the pronounced spike in ε_b when the $\dot{\varepsilon}_t$ is decreased by only a factor of 2 from 3.00×10^{-4} s^{-1} to 1.5×10^{-4} s^{-1}.

Initially, it was hypothesized that the dynamics of the reversible cross-linkers directly influenced the failure behavior of the gels. When the k_d was increased by a factor of 40 by changing the reversible component in the network to **10c** there was a shift in the failure behavior as a function of $\dot{\varepsilon}_t$. Now, the **N1•10c** gels begin to survive past the **N1** gels at a higher $\dot{\varepsilon}_t = 2.5 \times 10^{-3}$ s^{-1}. While this shift in ε_b is suggestive of a relationship between the k_d for the reversible cross-linker and the $\dot{\varepsilon}_t$ where protection begins, there was no corresponding shift in the maximum survival. The gels did not survive past the maximum load until the two lowest $\dot{\varepsilon}_t$ (as was observed for **N1•10d**). Taken together, these results do not provide a definitive relationship between the dynamics of the reversible cross-linker and the failure behavior.

To further probe the influence of the kinetic behavior on the failure behavior of the gels, even larger values of k_d were used by incorporating the **10a** and **10b** compounds. It should be noted that when switching from the **10c/d** pair of cross-linkers to the **10a/b** pair, there is a significant change in the K_{eq}. The K_{eq} for the **10c/d** pair of cross-linkers is 2 orders of magnitude greater than the K_{eq} for the **10a/b** pair (see Table 2). The higher values of K_{eq} indicate that for a given concentration of cross-linker, the number of active cross-links formed is higher. While this is important to note, concentration studies discussed in Chapter 4, show that with increasing amounts of **10a** or **10b**, the ε_b increases as well, indicating that a higher K_{eq} would positively influence the failure behavior.

When **N1•10a** and **N1•10b** were compared with their parent **N1**, it was observed that the addition of these dynamic and weak reversible cross-links did not contribute to the modulus of the material, yet they still protect the network against failure at increased ε values. These reversible cross-links essentially "dance" through the network, forming and breaking during the compression. Their protective effect is most likely due to their ability to dissipate energy without causing permanent damage to the covalent network. Because their k_d values are higher than those of the **10c** and **10d** cross-linkers, they are able to more effectively dissipate energy at the higher $\dot{\varepsilon}_i$.

The idea that the dissociation kinetics of the reversible cross-links influence the failure behavior of the network is suggested by these studies. There are, however, many

questions that remain regarding these hybrid networks. In the case of the addition of **10c** and **10d**, there is an increase in E_c as well as ε_b, but this was not the case with the addition of **10a** and **10b**. How do **10a** and **10b** increase ε_b if they are not supporting stress within the network (as evidenced by an increase in E_c)? How does the covalent network fail in the presence of the fast acting reversible cross-linkers? Do the reversible cross-links merely delay the onset of covalent bond failure? Do they slow down the rate of covalent bond failure? To probe what is occurring within the covalent network, a modified system was needed that could be used to further investigate the mechanism of protection in the hybrid networks. The studies involving the modified mechanchemical system are discussed in Chapter 4.

3.6 Control Experiments for Gel Preparation

To rule out alternative hypotheses with regards to the changes observed in the failure properties, a series of control experiments were performed. Chapter 4 describes studies with mono-functional pincer complexes to rule out the influence of charged species and co-solvent swelling studies rule out effects from differential swelling. Here, supplementary control studies are described that rule out the influence of excess silver triflate (AgOTf) and possible triflate ligand blocking.

It is possible that silver impurities remain with the pincer complexes after the synthesis. To rule out an influence from silver, excess silver triflate (AgOTf) was added to the **N1** networks. AgOTf was added in varying amounts from 1 % up to ~ 34 wt%

when compared with the mass of **10d** added. The disks were allowed to soak for a full 7 days, compressed at $\dot{\varepsilon}_t = 1.5 \times 10^{-4}\ s^{-1}$, and ε_b was determined. Table 8 summarizes the ε_b for the gels that broke and notes the gels that survived.

Table 8: Summary of ε_b for gels with excess AgOTf
N1 disks were soaked in solutions of DMSO, DMSO and AgOTf, or DMSO/AgOTf/**10d** in various ratios. All disks were compressed at $\dot{\varepsilon}_t = 1.5 \times 10^{-4}\ s^{-1}$.

Gel	% AgOTf	ε_b
N1•10d	0	Survived > 80%
N1•10d	1	Survived > 80%
N1•10d	5	Survived > 80%
N1•10d	34	Survived > 80%
N1	0	41 ± 2.1 %
N1	1	40.5 ± 1.5 %
N1	5	43.5 ± 2.0 %
N1	34	42 ± 1.8 %

All of the disks that had **10d** present survived until the instrument's maximum force (50 N) was reached; no change was observed in the presence of AgOT. Likewise, the **N1** disks with added AgOTf, broke at strain values consistent with the original **N1** disks. These results indicate no contribution to ε_b from AgOTf.

3.7 Experimental Procedures

3.7.1 General Considerations

All rheological experiments were carried out on an AR-G2 Rheometer from TA Instruments. Unless otherwise stated, all reagents were used as received from their respective suppliers. All cross-linker compound **10a-d** were synthesized in house using methods detailed previously.[140] At various times, **10a-d** was contributed by David Loveless, Sung Lan Jeon, Donghua Xu, and Zach Kean for the studies carried out in this chapter and Chapters 4 and 5.

Glass molds were prepared as follows: Glass TLC plates purchased from Silacycle were cleared of their silica gel with a razor blade and water to produce clean sheets of glass. A small amount of water was placed on the back of 4 glass microscope slides. The slides were placed on the larger piece of glass (from the TLC plate) to create a mold of approximately 25 mm x 75 mm x 1 mm in size. The small amount of water trapped in between the plates created a tension that allowed the plates to be moved initially, but held them in place after the mold was formed. Once the polymer sample is transferred to the mold, an additional microscope slide is used to scrape excess polymer material from the top of the mold. That slide then forms the top of the mold.

3.7.2 Making Solutions and Gels with PVP and DBH

Poly-4-vinylpyridine (PVP) was purchased from Sigma and reported by Sigma with a M_w = 60,000. It was previously reported in literature to have a M_n = 22,000 g/mol

and M_w = 64,300 g/mol with a polydispersity index (PDI) of 2.92.[141] Studies carried out in our lab determined that M_n = 33,000 g/mol and M_w = 44,500 g/mol with a PDI of 1.35.[79]

PVP (0.1 – 0.5 g) was added to standard 25 mL scintillation vials. ACS grade DMSO (VWR) was added by pipet to achieve the desired concentrations of PVP. The vials were then placed on a stir plate at room temperature and allowed to stir for several hours until a uniform solution was achieved. To this solution was added 1,6-dibromohexane (DBH; Across Organics). The vials were then capped and vortexed for 30 seconds to mix. After mixing, the solution was transferred by glass pipet to the glass molds. Samples were either allowed to polymerize at room temperature or the glass mold was heated on a hot plate.

Vials were heated by suspending them in an oil bath. The bottom of the vials was not in contact with the bottom of the oil bath or the heating element. The oil bath was kept at steady temperature throughout the experiment and constantly stirred.

Gel preparation: Solutions of PVP and DBH were transferred to the prepared glass molds and covered with a glass slide. The glass molds were then placed on a hot plate and heated at 90 °C for 5 min. After cooling, the top slide was removed and the gel was removed from the mold with a razor blade or spatula. The gel was then placed into a glass petri dish and covered in fresh DMSO. The DMSO was then changed every few hours, during which time the slabs of polymer swell. After swelling for 3 days, the slabs are removed from the DMSO and placed on a clean glass surface using a spatula and/or

tweezers. Biopsy punches purchased from Health Med Ex ® are used to punch uniform disks with a 5 mm diameter. Using tweezers, the disks are then placed in glass scintillation vials and covered in DMSO. The disks are stored in the closed vials with DMSO until they are used for experiments.

Synthesis of hybrid networks: 5 mM solutions of the desired reversible cross-linker (compounds **10a-d**) were made using fresh DMSO. 10 disks of **N1** were added to 2 mL of the **10** solution in a small vial. The vial was capped and covered in foil.

3.7.3 Compression Experiments

The 8 mm parallel plate geometries were used for all compression experiments. Experiments on submerged samples were carried out using a solution cup with a flat bottom, and unsubmerged samples were compressed with the simple parallel plate geometries. The parallel plate geometries were attached to the rheometer using the standard TA Instruments procedure reported in the manual. The normal force and gap distance were zeroed and the sample is placed on the bottom plate. The normal force was then zeroed again. Studies were carried out to determine if the sample must be centered on the plate before compression. It was determined that as long as the entire sample was placed on the plate, it did not matter if the sample was centered for compression.

Disk Handling: To transfer a disk to the rheometer, a single disk was removed from the vial of solution or solvent using tweezers or a small spatula. The gel was

placed on a dry Kimwipe® that was used to gently tap dry the top of the disk. The diameter of the disk is measured with digital calipers by gripping the disk with the calipers, which are then expanded until gel dropped from between the calipers. The distance where the disk drops from the calipers was noted as the diameter of the disk. The gel was then placed on the bottom plate (or in solution cup). The height of the disk was determined by lowering the top plate to the surface of gel until a normal force of 0.1 N is achieved.

Compressive Modulus (E_c) Procedure: Gels were compressed at a constant velocity. Table 9 below summarizes the actual v_c values used compared to the reported values of $\dot{\varepsilon}_t$.

Table 9: Actual v_c values set on rheometer for the values of $\dot{\varepsilon}_t$ reported above.

v_c (μm/s)	Approximate $\dot{\varepsilon}_t$ (s^{-1})
25	1.25×10^{-2}
5	2.50×10^{-3}
1	5.00×10^{-4}
0.6	3.00×10^{-4}
0.3	1.50×10^{-4}
0.1	5.00×10^{-5}

Data were collected at specified time increments depending on the length of the test. The normal force was collected as a function of the height which was converted to % strain, while the normal force is used to calculate the stress. The stress v. strain curve is plotted and the slope of the line is taken to be the E_c. Usually there is a non-linear

initial compression region followed by the linear region. The E_c is always taken from the linear portion of the graph.

Compression to Failure: All initial instrumental set up and gel preparation is the same as reported above for the Compressive Modulus Test. Unlike the E_c test, the disk is compressed until the disk actually fails. Because the point of failure is unknown, the instrumental procedure is modified to continue compressing until 100% strain is achieved. Therefore, the compression must be manually terminated. The compression was stopped when a drop in stress was observed, and the failure of the disk was visually confirmed.

4. Probing Covalent Network Failure in Hybrid Networks

4.1 Mechanochemical Probe for Failure

The effect of mechanically invisible reversible cross-links on gel fracture was unexpected, so a greater understanding what was happening to the covalent framework in the hybrid systems was needed. For example, do the reversible cross-linkers prevent the scission of covalent bonds, or do they allow the material to maintain its integrity even as the covalent framework breaks down? In order to answer these questions, a chemiluminescent dioxetane probe for bond scission developed by our collaborator Rint Sijbesma at Eindhoven University of Technology was ustilized.[142]

This diadamantyl dioxetane probe (shown in Figure 34) is a mechanophore – a functional group that undergoes an accelerated chemical reaction in response to an applied force.[143] In this case, the scission of the dioxetane into a pair of ketones (via a retro-[2+2]cycloaddition) can be accelerated by tension, for example that experienced by the unit incorporated into a polymer main chain or polymer cross-linker. The ketones are produced in an electronically excited state that emits a photon of blue light as a signal of molecular fracture.

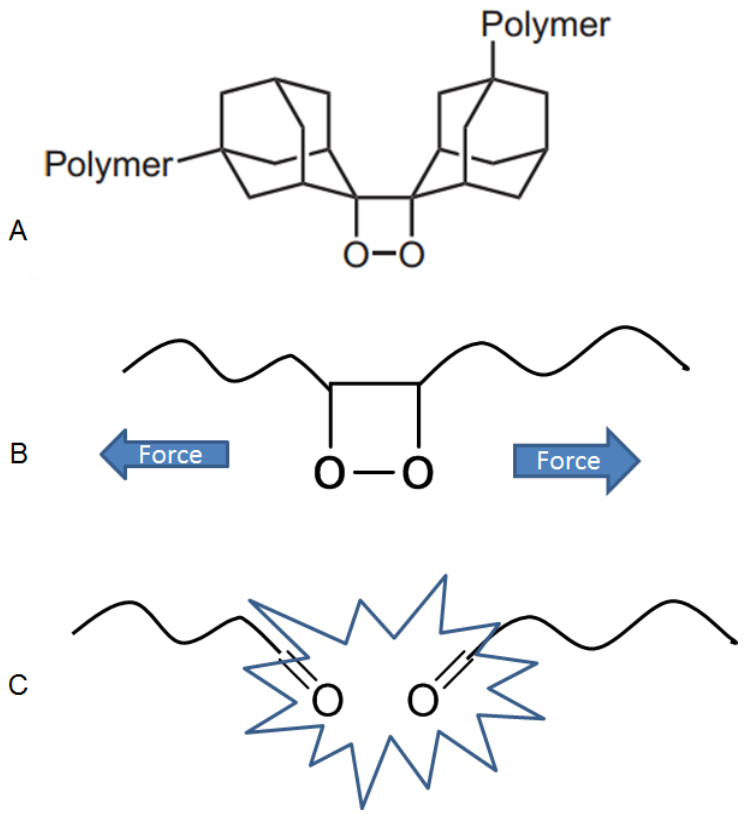

Figure 34: 1,2 dioxetane unit developed by Chen et. al.
The 1,2 dioxetane unit (in **A)** is a mechanically active functional group that when placed under tension in a polymer chain (in **B**) undergoes a chemical transformation and emits light (in **C**).[142]

Chen *et al*, previously demonstrated that additional light could be harvested from the triplet and singlet excited states of the ketone by incorporating an efficient energy transfer acceptor that subsequently fluoresces with high quantum efficiency.[142] By selecting different acceptor compounds they could tune the wavelength of light ultimately collected from the transition. They also showed that the dioxetane mechanophore could be successfully incorporated into a polymer network as a covalent cross-link that is activated under macroscopic stress.

The 1,2 dioxetane was incorporated into the covalent networks, using it as a real-time probe of covalent cross-link scission under load to characterize the effect of reversible cross-linker addition on the fracture of the covalent framework. This light emission could indicate how much fracture was occurring within the covalent network, and perhaps more importantly when it was occurring, as a function of added reversible cross-linker.

4.2 Characterization of a Dioxetane/PVP Covalent Network

Covalent network **N3** was synthesized using the 1,2-dioxetane unit shown in Figure 35 as a covalent cross-linker.

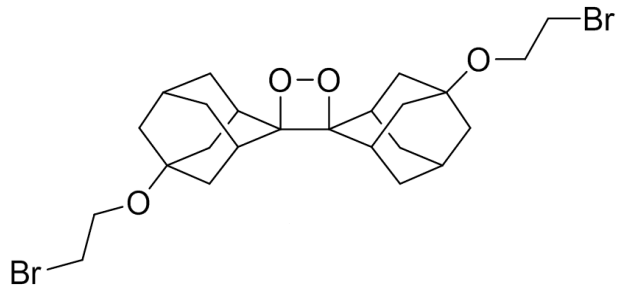

Figure 35: Modified 1,2-dioxetane covalent cross-linker

PVP was reacted with 4% dioxetane cross-linker (cross-linker per pyridine repeat unit) of dioxetane (see Experimental, Section 4.5). The resulting gels were cut and swollen in DMSO following the procedures described in Chapter 3, with a few minor differences in procedure as noted in Section 4.5, below. As in Chapter 3, the failure of the new **N3** gels was characterized under compression. In general, the **N3** networks behave similarly to the other covalent networks **N1** and **N2**, in that the gels are

transparent and sufficiently robust as to be manipulated with spatulas and tweezers without breaking. Initial studies confirmed that the dioxetane mechanophores are active as desired; disks compressed between a finger and a thumb in a dark room emitted light as the gel was crushed into small pieces.

9,10-Bis(phenylethynyl)anthracene (DPEA, Figure 36) was employed as an energy transfer acceptor. The **N3** networks were swollen in a 1 mg/mL DMSO solution of DPEA. Unless otherwise stated, **N3** will refer to a network that has been soaked in the DPEA solution prior to experimentation.

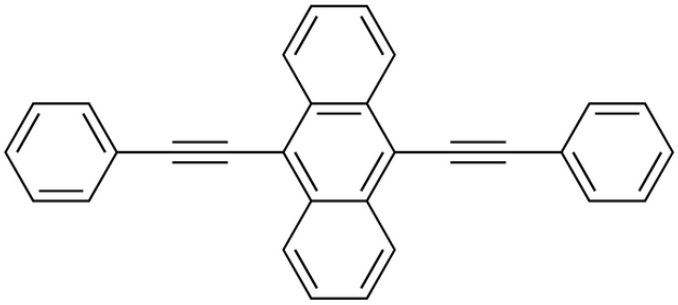

Figure 36: *9,10*-Bis(phenylethynyl)anthracene

Once soaked in the DPEA solution, the gels have the same "highlighter green/yellow" color as the DPEA solution, confirming that the dye was taken up into the gels. As shown in Table 10, the DPEA does not change the critical mechanical properties

(ε_b, maximum stress at break (σ_b), and E_c) of the gel, based on a comparison of identical disks soaked in DMSO with and without the dye.

Table 10: Influence of DPEA on gel properties compressed at $\dot{\varepsilon}_t = 6.0 \times 10^{-2}\ s^{-1}$

Gel	ε_b	σ_b (kPa)	E_c (kPa)
N3, no DPEA	50.0 ± 2.6 %	240 ±14	2.3 ± 0.4
N3 + DPEA	52.1 ± 1.7 %	240 ± 47	2.2 ± 0.6

To confirm that the dioxetane is necessary for light emission, network **N4** was formed by cross-linking PVP with 4% of the cross-linker shown in Figure 37. This cross-linker lacks the central 1,2-dioxetane ring that is necessary for light emission. Crushing **N4** to failure resulted in no detectable emission, confirming that the dioxetane functionality is responsible for the observed luminescence.

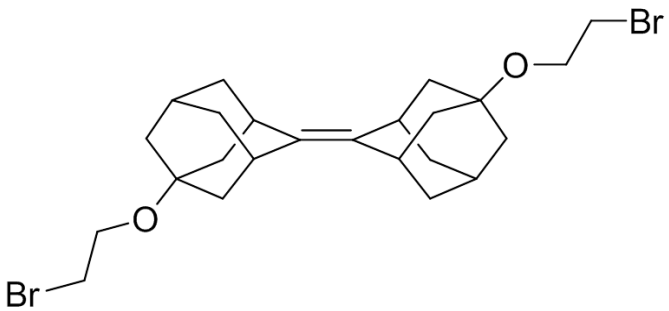

Figure 37: Adamantane cross-linker used in control studies

Since changes in intensity as a function of adding reversible cross-linkers were expected, initial characterization in the presence of other cross-linkers was needed to determine the influence on the observed emission from the dioxetanes, independent of the influence of reversibility. A series of gels in which the dioxetane content was diluted with other covalent cross-linkers was prepared. The total amount of cross-linking was held constant at 4%, but the composition of the total cross-linking was varied by adding different amounts of the dioxetane cross-linker, *1,6*-dibromohexane and *1,12*-dibromododecane. Table 1 shows the composition of the 5 different sets of gels constructed including the original **N3** gels.

Table 11: Composition of covalent cross-linking for various gels

Gel Name	% Dioxetane Cross-linking	% Dibromododecane Cross-linking	% Dibromohexane Cross-linking
N3	4	0	0
N5	2	2	0
N6	2	0	2
N7	1	3	0
N8	1	0	3

All 5 sets of gels were compressed to failure at a $\dot{\varepsilon}_l = 6.0 \times 10^{-2}\ s^{-1}$. Figure 38 shows a representative compression curve for each of the 5 types of networks.

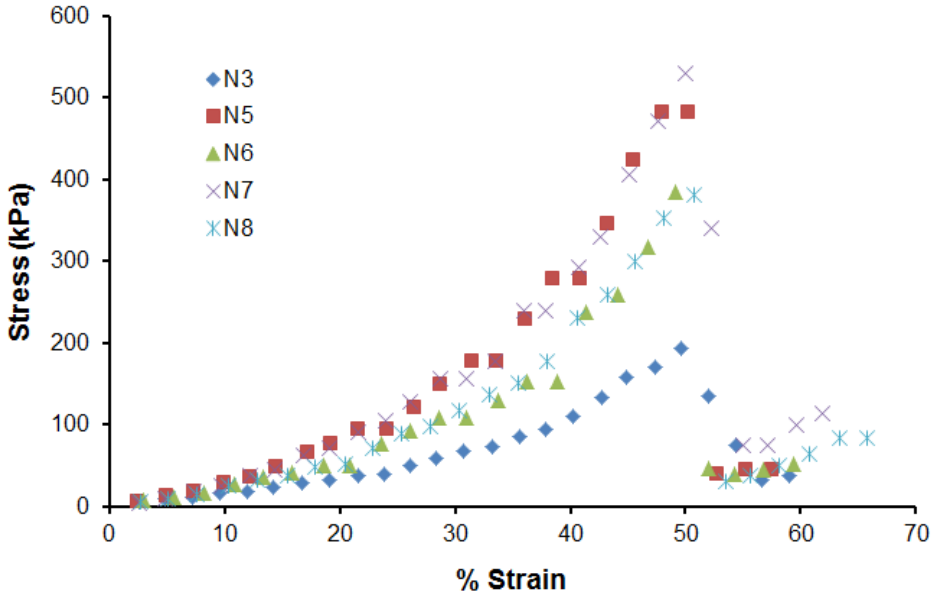

Figure 38: Representative compressions, $\dot{\varepsilon}_t$ = 6.0 x10^{-2} s^{-1}
N3 and **N5-N8** disks were compressed until failure. The networks formed with shorter cross-linkers (**N6** and **N8**) showed lower E_c and σ_b than those formed with the longer cross-linker (**N5** and **N7**).

The average ε_b for the different compositions of cross-linker are summarized in Figure 39

and the average moduli are summarized in Figure 40.

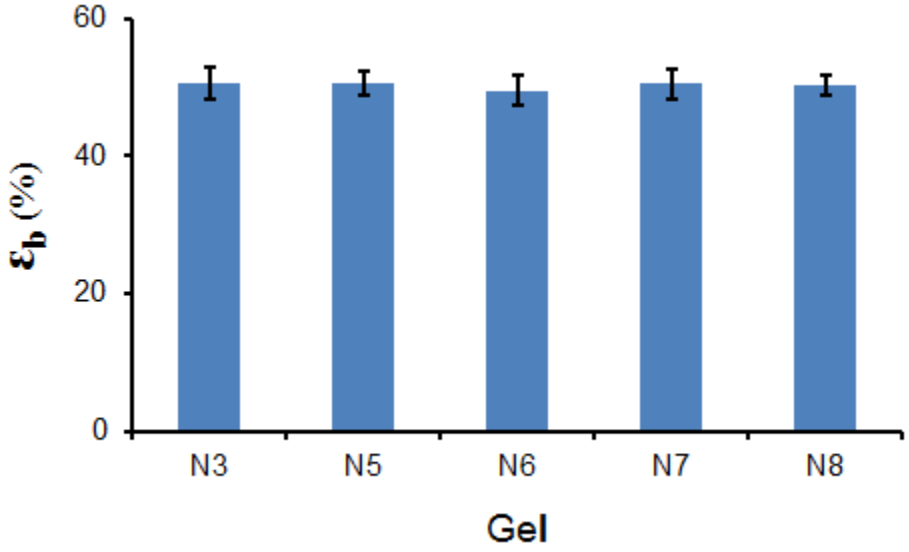

Figure 39: ε_b as a function of covalent cross-linker content
Gels formed with 4% dioxetane cross-linker (relative to pyridine) of different cross-linkers and mixtures of cross-linkers were compressed at 6.0×10^{-2} s^{-1}. The average ε_b does not depend on the type of cross-linker or the length of the cross-linker chain.

The ε_b does not depend on the relative composition of the cross-linking. Neither the amount of dioxetane nor the length of the additional cross-linker influences the ε_b. The E_c, however, does depend on the length of the additional cross-linker, and the lower modulus of **N3** suggests that it is a slightly less effective cross-linker than the simple dibromoalkanes.

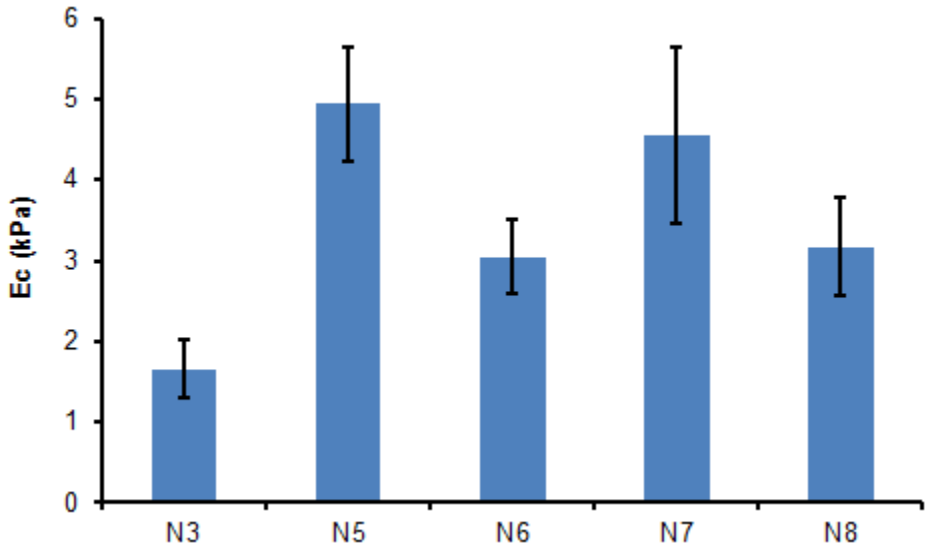

Figure 40: E_c as a function of covalent cross-linker content
Gels formed with a total of 4% cross-linking (relative to pyridine) of different cross-linkers and mixtures of cross-linkers were compressed at $\dot{\varepsilon}_t = 6.0 \times 10^{-2}\ s^{-1}$. Unlike ε_b, E_c of the gel does depend on the covalent cross-linker employed. Gels synthesized with the longer dibromododecane cross-linkers (**N5** and **N7**) have a larger E_c.

Light emission data were collected as the gels were compressed. Figure 41 below shows a representative compression curve and light emission intensities plotted as a function of strain for **N3**. Across multiple compositions, the strain at which the maximum light intensity of the emission (ε_{em}) is observed is well correlated with ε_b (Figure 42).

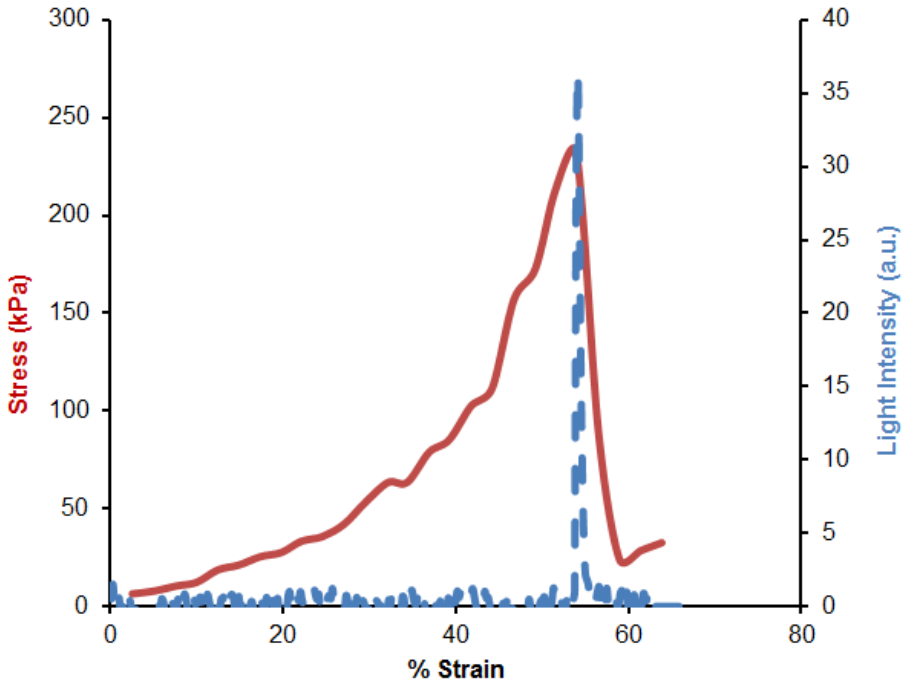

Figure 41: Representative stress and light intensity as a function of strain for a N3 gel Light intensity collected as **N3** was compressed at $\dot{\varepsilon}_t$ = 6.0 x10^{-2} s^{-1}. The stress is shown as a solid red line and the light intensity is shown as a dashed blue line.

The scission of the underlying covalent network occurs almost entirely in concert with the failure of the gel and further supports the definition of "failure" in Chapter 3. Once it was observed that the maximum light emission occurs with the failure of the gel, how the intensity of light emitted depends on the amount of mechanophore incorporated into the network was investigated. The maximum light intensities for gels **N3** and **N5-N8** were compared. Figure 42 summarizes the intensities of light emission for different gels.

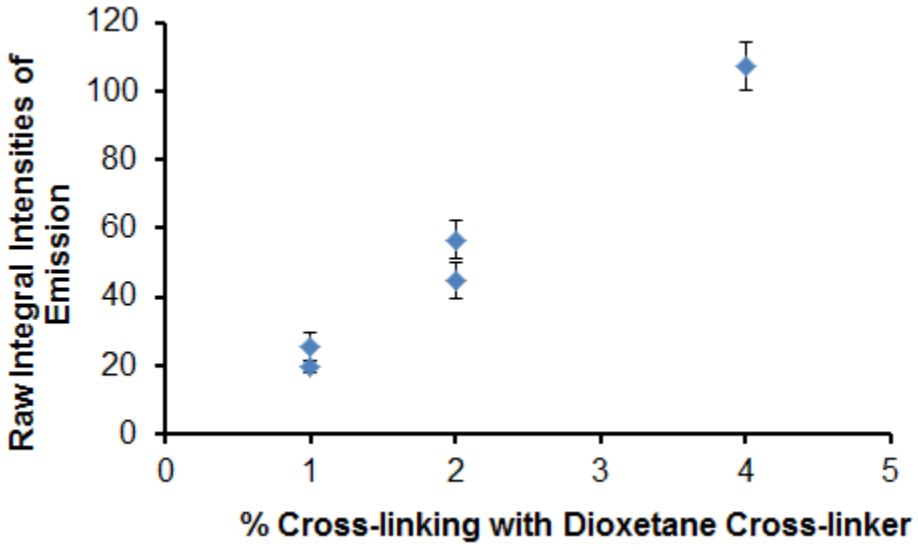

Figure 42: Light emission as a function of equivalents of dioxetane
Gels **N3** and **N5-N8** were compressed at $\dot{\varepsilon}_t = 6.0 \times 10^{-2}\ s^{-1}$. The maximum intensity of light emission depends directly on the amount of dioxetane cross-linker in the gels, and not on the length of the additional cross-linker.

The **N3** gels exhibited the highest maximum light emission intensity. The **N5** and **N6** gels that were cross-linked with only half as much dioxetane had a maximum light intensity that was approximately half as intense as the **N3** gels. Similarly, the **N7** and **N8** gels that were cross-linked with only ¼ the amount of dioxetane had a maximum light intensity that was approximately ¼ the intensity of the **N3** gels. The length of the additional cross-linker (either dibromododecane or dibromohexane) did not influence the maximum intensity of light emission. Assuming that the incorporation of the dioxetane is proportional to the amount added in the cross-linking step, these data demonstrate that the probabilyt of dioxetane scission during fracture is not influenced by the presence of other cross-linkers.

4.3 Mechanical Characterization of Hybrid Networks

Hybrid networks were created using the **N3** gels in a manner similar to the procedure described in Chapter 3. The **N3** gels were soaked in 5 mM DMSO solutions of **10a** or **10b** to form the hybrid networks **N3•10a** and **N3•10b**, respectively. The gels were then compressed at $\dot{\varepsilon}_t = 6.0 \times 10^{-2}\ s^{-1}$. As seen in Table 12, ε_b, σ_b, and E_c, varied as observed for **N1** in Chapter 3.

Table 12: Average ε_b σ_b, and E_c for N3 gels; $\dot{\varepsilon}_t = 6.0 \times 10^{-2}\ s^{-1}$

Gel	ε_b	σ_b (kPa)	E_c (kPa)
N3	53.5 ± 3.7 %	180 ± 60	1.2 ± 0.5
N3•10a	68.9 ± 3.2 %	520 ± 160	1.2 ± 0.3
N3•10b	70.8 ± 1.1 %	509 ± 170	0.83 ± 0.4

Importantly, the moduli of the two hybrid networks again showed no statistically significant change when compared with the parent **N3** gels, consistent with the rapid dissociation kinetics of the **10a** and **10b** cross-linkers. Also, as before, an increase in σ_b and ε_b was observed for the hybrid gels relative to the purely covalent **N3.** The reversible cross-links do not contribute to E_c, and they prevent failure from occurring at and beyond strains at which the **N3** networks would fail.

Several observations confirm that the reversible cross-linking is responsible for the higher ε_b. First, as shown in Figure 43, ε_b increases monotonically with cross-linker

concentration. It should be noted that at concentrations lower that 2 mM, there is a sufficient amount of residual bromide ions present in the gels to bind with the pincer complexes. The presence of bromide ions effectively "blocks" the pincer complexes from forming metal-ligand interactions with the pyridine residues.

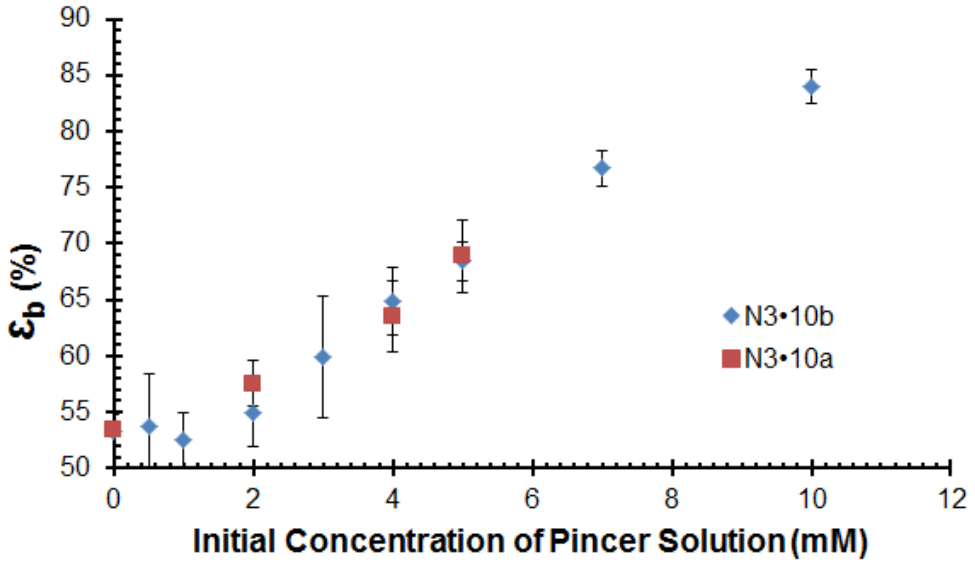

Figure 43: ε_b as a function of concentration of reversible cross-linker
Disks from **N3•10a** and **N3•10b** were soaked in solutions of **10a** and **10b** of varying concentrations. They were then compressed at $\dot{\varepsilon}_t = 6.0 \times 10^{-2}$ s^{-1} to failure. As the concentration of cross-linker solution is increased beyond 2 mM, the ε_b increases for both hybrid networks.

Second, to rule out the influence of the additional charges in the network, mono-functional pincer complexes **6a** and **6b** (Figure 44) were incorporated into **N3** gels. The **N3** gels were soaked in 10 mM solutions (same functional group concentration as 5 mM **10a** or **10b**) of **6a** or **6b**. When compressed at 6.0 x10^{-2} s^{-1} there was no statistically

significant difference in the ε_b of **N3•6a** and **N3•6b** relative to **N3** (Figure 45). The *bis*-functionality of the **10a** and **10b** cross-linkers is necessary for the hybrid networks to survive past the ε_b of the original covalent **N3** gels.

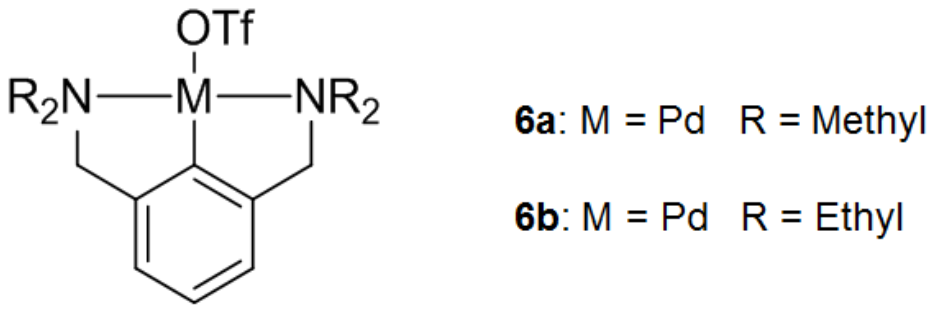

Figure 44: Monofunctional versions of the pincer complexes 6a and 6b

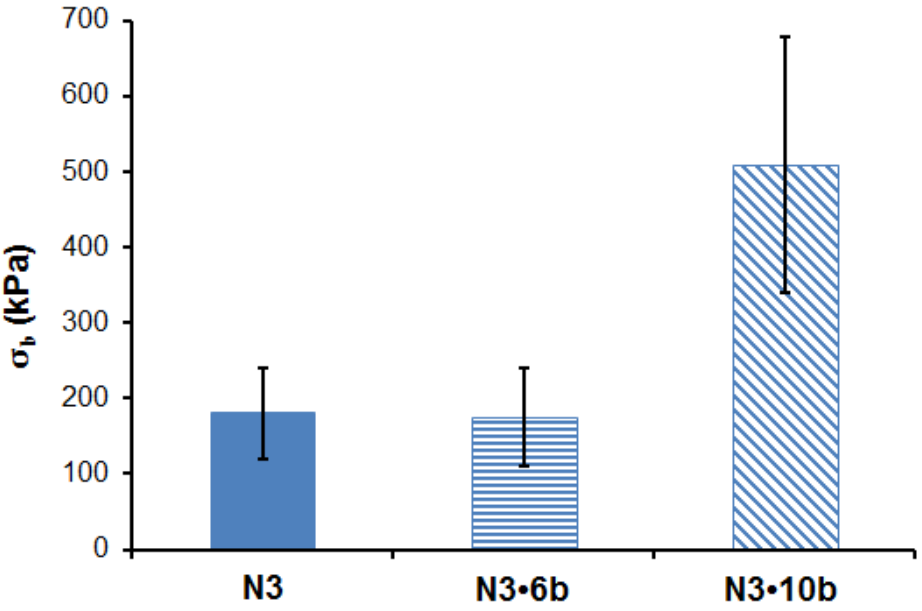

Figure 45: σ_b at break for N3, N3•6b, and N3•10b gels
N3, **N3•6b**, and **N3•10b** gels were compressed at 6.0 x10^{-2} s^{-1} to failure. **N3•6b** gels show no difference when compared to the **N3** gels. **N3•10b** gels, however, show a drastic increase when compared to both the **N3** and **N3•6b** gels

Third and finally, the effect of differential swelling was considered. It is often observed that the sizes of gels soaked in solutions of **10a-d** are different than those of gels soaked in pure DMSO. The size of the disks decreases (both in height and diameter) once they are soaked in the solutions of **10a-d**. **N3** disks that are punched using a 5 mm biopsy punch and then soaked in pure DMSO have an average diameter of 5.03 ± 0.04 mm. When disks from the same **N3** gel, and cut with the same biopsy punch, are soaked in a 5 mM solution of **10b** in DMSO, the average diameter decreased to 4.83 ± 0.05 mm. As the concentration of pincer is increased, the diameter of the disks decreases. To rule out the influence of differential swelling, **N3** gels were soaked in mixtures of DMSO and diglyme (*bis*-(2-methoxyethyl) ether) of varying ratios. As the ratio of diglyme to DMSO increases, the diameter of the disks decreases. The relative volume fraction (ϕ_{rel}) is calculated for each disk relative to the average volume of a gel swollen in DMSO. Figure 46 shows a plot of the ϕ_{rel} as a function of the diglyme in solution.

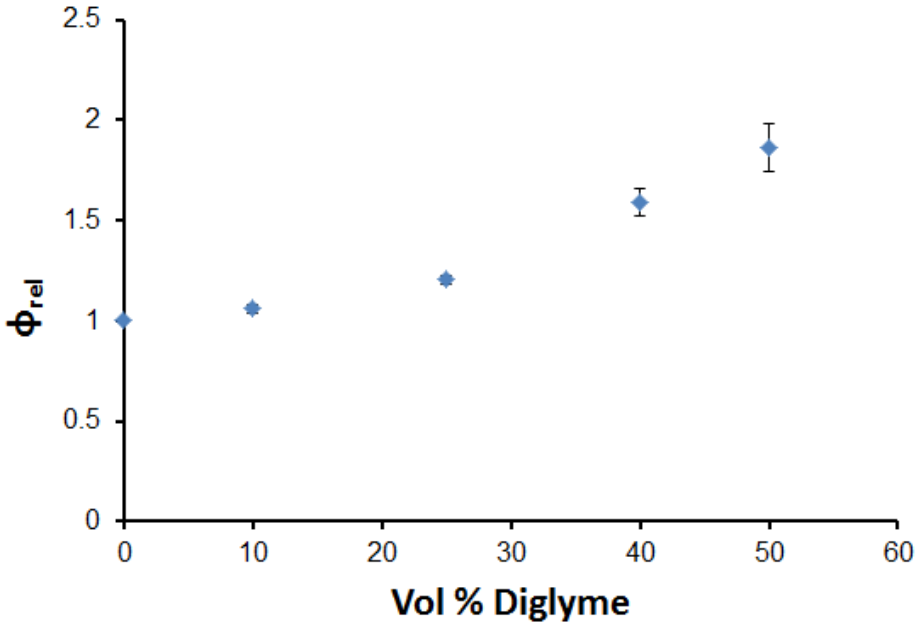

Figure 46: ϕ_{rel} as a function of diglyme in DMSO swelling solution
N3 gels were first swollen in DMSO, and then placed into solutions of DMSO and diglyme in various ratios. As the volume % of diglyme increases, the diameters of the disks decrease. ϕ_{rel} is calculated relative to the average volume of the gels swollen in just DMSO.

Using the different ratios of diglyme and DMSO, ϕ_{rel} was varied over the range observed in the **N3•10b** gels (ϕ_{rel} = 1 – 2). All of the **N3** disks were compressed under the conditions described above. ε_b data were compared for the **N3** gels soaked in various ratios of diglyme, and the **N3•6b** and **N3•10b** data previously collected. Figure 47 shows the values of ε_b as a function of the ϕ_{rel} for all gels.

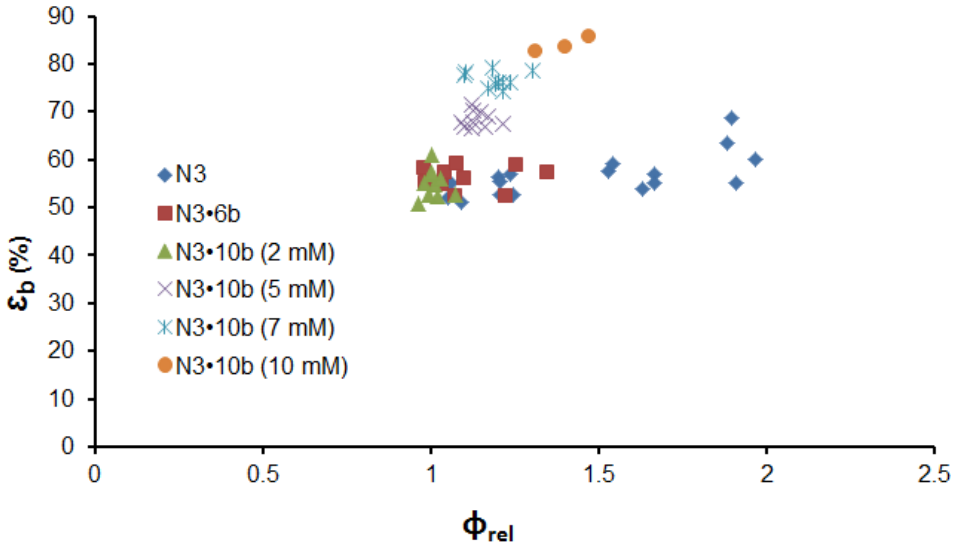

Figure 47: ε_b as a function of ϕ_{rel} for several sets of gels

For **N3** (blue diamonds Figure 46), there is no increase in ε_b as ϕ_{rel} was increased (ε_b = 56.5 ± 4 %). Data from gels soaked in the mono functional compound **6b** also showed no dependence of ε_b on ϕ_{rel}. As seen in Figure 47, the increase in ε_b observed for the **N3•10b** gels is not easily accounted for by the observed differences in swelling.

Table 13 summarizes the average E_c, ε_b and σ_b for the **N3** gels compared with the hybrid **N3•10c**. As expected, E_c increases (from 1.4 ± 0.2 kPa to 2.8 ± 0.6 kPa) when **10c** is incorporated into the network. Simultaneously, ε_b decreases from 53 ± 4 % to 37 ± 2 % and σ_b decreases from 200 ± 70 kPa to 105 ± 10 kPa. The behavior of the hybrid **N3•10c** gels is close to that of a network with more covalent crosslinking (such as **N2**). Recall that **10c** has a k_d of 0.026 s^{-1} (see Table 2 in Chapter 3), of the same order of magnitude as

$\dot{\varepsilon}_\iota$. A significant fraction of cross-linkers therefore remain intact on the timescale of the compression.

Table 13: Properties of N3 and N3•10c compressed at $\dot{\varepsilon}_\iota = 6.0 \times 10^{-2}\ s^{-1}$

Gel	E_c (kPa)	ε_b	σ_b (kPa)
N3	1.4 ± 0.2	53 ± 4 %	200 ± 70
N3•10c	2.8 ± 0.6	37 ± 2 %	105 ± 10

4.4 Discussion of Light Emission Results for Hybrid Networks

To probe the mechanism of failure in the systems described above, light emission data were collected for the **N3**, **N3•10a,** and **N3•10b** gels as the disks were compressed. The mechanically induced light emission can be used to determine when the covalent cross-links are breaking within the various networks, and whether/how it changes upon the addition of the reversible cross-links. **N3, N3•10a,** and **N3•10b** gels were all compressed at $\dot{\varepsilon}_\iota = 6.0 \times 10^{-2}\ s^{-1}$ to failure. Both the light emission and the stress were collected as a function of the strain. When ε_{em} was compared to ε_b, a direct correlation was observed. The ε_{em} peak shifts to the new observed ε_b in both **N3•10a** and **N3•10b** gels. Figure 48 shows representative compression data for **N3** and **N3•10b** overlaid with their light emission data.

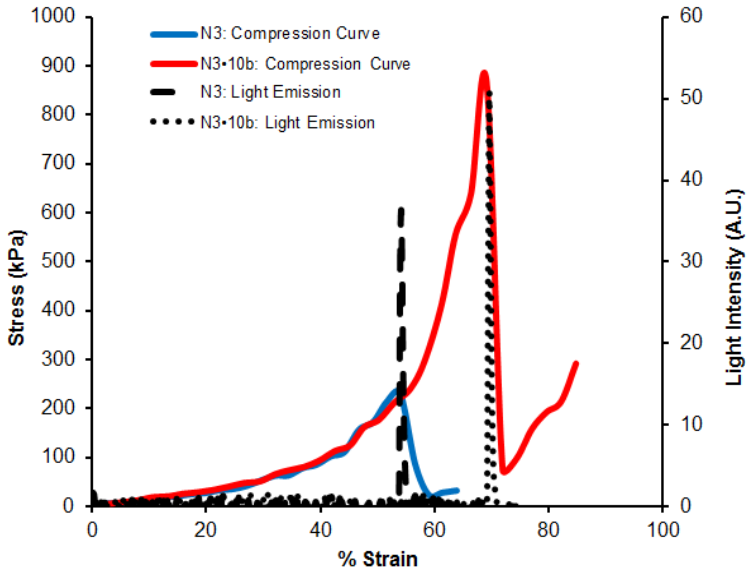

Figure 48: Representative stress-strain and light emission data under compression **N3** (blue line stress and dashed light emission peak) and **N3•10b** (red line stress and dotted light emission peak); $\dot{\varepsilon}_l = 6.0 \times 10^{-2}\ s^{-1}$

One important feature to note is the absence of light emission in the 55% - 70% range for the hybrid network. This is a region where the **N3** gels doesn't survive, but the hybrid **N3•10a** and **N3•10b** do. The breakage of the covalent bonds has been prevented in the hybrids in this region.

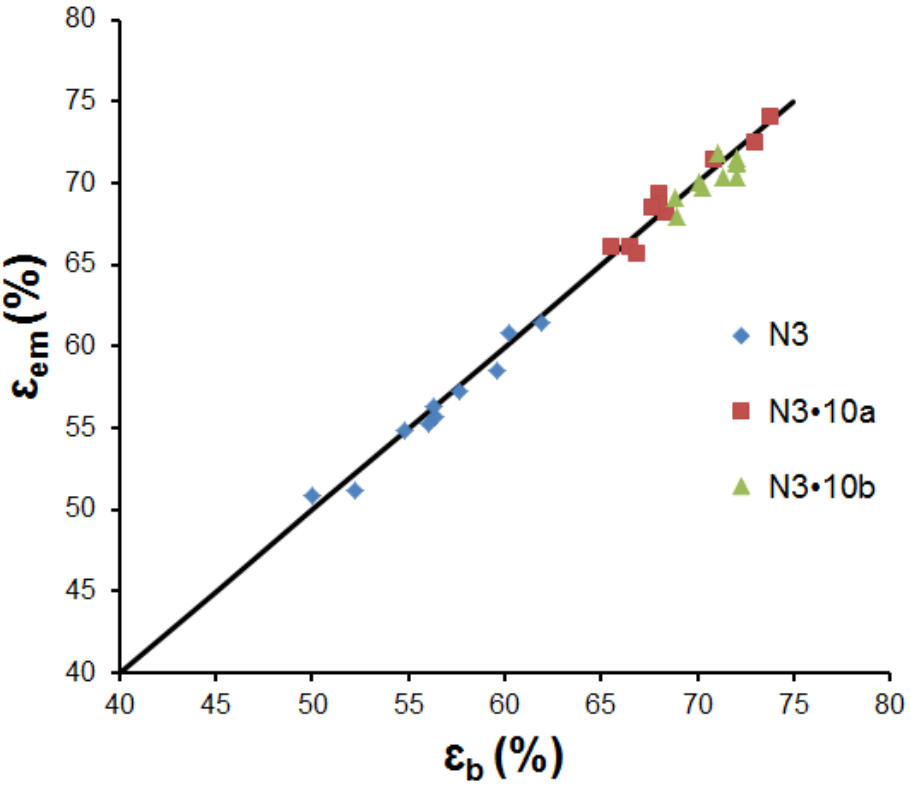

Figure 49: ε_b and ε_{em} for three sets of gels
N3, N3•10a, and **N3•10b** gels were all compressed at $\dot{\varepsilon}_t = 6.0 \times 10^{-2}\ s^{-1}$ to failure; $\varepsilon_b = \varepsilon_{em}$ within their calculated standard deviations. Line is $\varepsilon_b = \varepsilon_{em}$.

Figure 49 shows the relationship of ε_b and ε_{em} for **N3**, **N3•10a**, and **N3•10b**. The data fall along the $\varepsilon_b = \varepsilon_{em}$ line. As discussed before, this both validates the characterization of failure, and also shows that the same fracture behavior is occurring, just at a higher strain the hybrid network. This conclusion is further supported by the total light intensity. **N3** gels soaked in solutions of different concentrations of **10b** and compressed under the same conditions as above.

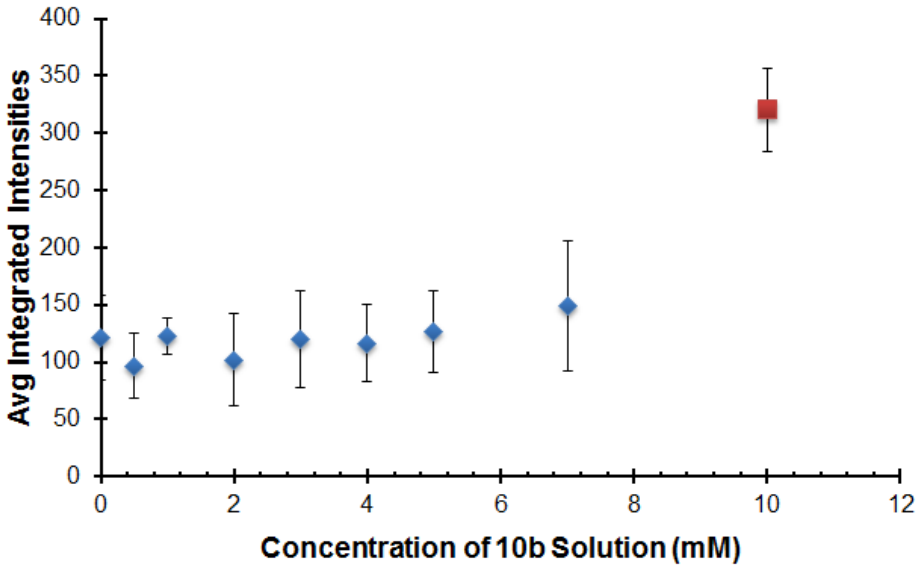

Figure 50: Average integrated intensities as a function of 10b concentration
N3 gels were soaked in varying concentrations of **10b** and compressed at $\dot{\varepsilon}_t$ = 6.0 x10^{-2} s^{-1} to failure.

The integrated emission intensities are shown in Figure 50. As the concentration of reversible cross-linker increases, there is no significant change in the integrated light intensity. The increase in average light emission for the highest concentration (10 mM) is attributed to the fact that the diameter or the gel increases as the gel is compressed and the height decreases, assuming that the volume of the disk remains constant throughout the entire experiment. When the disk has been compressed to approximately 62% strain, the diameter of the disk approaches that of the parallel plates that are being used to compress the disk. At strains higher than 62%, the disk begins to expand past the plate boundary and the top plate now indents and pushes into the middle of the disk. It is possible that this change in strain influences the light emission

data at the highest strains and therefore can account for the uncharacteristic behavior at the higher concentrations of **10b**.

4.5 Conclusions

To study the mechanism of failure within the covalent networks and the effect of the reversible cross-linkers on that failure mechanism, a mechanochemical probe was incorporated into our covalent networks. The modified dioxetane cross-linking unit emits light upon bond scission and was used as a quantitative signal for the breakage of the covalent network. The observed light emission is directly correlated with the amount of dioxetane incorporated into the network. The ε_{em} coincides with the ε_b.

As was observed in the **N1** gels, adding the reversible cross-linkers **10a** or **10b** had no effect on the modulus of the gels, but did increase the ε_b. After incorporating the reversible cross-linker **10a** and **10b** into the networks, the ε_b shifted to a higher ε and was accompanied by a shift in the ε_{em}. This confirmed that the failure event is prevented from occurring at the earlier strains. The fact that no major change is observed in the intensity of light emitted or the width of the emission peak indicates that the mechanism of failure remains unchanged and is simply delayed. The addition of reversible cross-linkers provides a mechanism of protecting against failure at the lower strain values, but does not influence the mechanism of failure.

Control experiments demonstrated that the ability to form cross-links within the network is essential to the observed failure protection. When mono-functional analogs are introduced into the networks instead of the *bis*-functional **10a** or **10b**, the networks fail as the pure covalent networks. Additionally, the influence of swelling or charged environments was systematically ruled out.

To our knowledge this set of studies is the first of its kind to quantitatively probe the failure of the covalent component of hybrid networks. The addition of the highly dynamic and weak reversible cross-linkers provides an effective way to dissipate energy within the network without inducing failure in the covalent network. These reversible cross-linkers are essentially invisible to the mechanical properties of the gel. As they dissipate energy, they allow the gels to withstand greater strains than previously attainable. This energy dissipation does not change the way in which the gels ultimately fail (in an instantaneous catastrophic event), but delays the event from occurring.

4.6 Experimental Procedures

All compression and light emission studies were conducted in collaboration with Zach Kean. The majority of the light emission data was analyzed by Kean. Kean also contributed the synthesis of the dioxetane cross-linkers, polymer networks, and compounds **6a** and **6b**.

4.6.1 Gel Synthesis

The dioxetane cross-linker (Figure 35) was mixed with 300 mg/mL PVP solutions in DMSO and cast in a glass mold. The system was heated to ~ 90 °C for 5 min. The resulting gel was removed from the mold and swollen in DMSO for 3 days in a glass petri dish. The DMSO was changed twice daily to remove any unreacted units from the system. After the gels had reached a stable size, the slabs were punched into 5 mm disks using a biopsy punch. These 5 mm disks were transferred to a 25 mL vial and stored in DMSO at room temperature until use in further experiments.

DPEA acceptor solution: A 1 mg/mL solution of DPEA (Figure 36) was stirred in dry DMSO for one hour at room temperature to saturate. The solution was then passed through a teflon syringe filter (200 μm pore size) to remove undissolved DPEA. The solution was allowed to sit overnight at room temperature then filtration was repeated before use. **N3** disks were then removed from the vials of DMOS and placed into vials with the DPEA solution. They were allowed to soak for 3 days.

4.6.2 Incorporating the Reversible Cross-linker

5 mM solutions of **10a** and **10b** were made in the DPEA/DMSO solutions. Ten **N3** disks were transferred into 2 mL volumes of the respective solutions in small 7 mL vials. The vials were sealed with parafilm, wrapped in foil, and stored in a modified desiccator that was sealed with parafilm. The disks were soaked at room temperature for 3 days.

4.6.3 Mechanical Testing

The compression experiments discussed in this chapter were carried out in a manner similar to the compression testing described in Chapter 3. Prior to mechanical testing, the disks were removed from their respective solutions treated as outlined in Chapter 3 . The diameter and height of each disk was measured as detailed in previous chapters. Individual disks were compressed at a constant v_c of 50 μm/s between 8 mm parallel plate geometries on an ARG2 TA Instruments Rheometer. The disks were compressed until failure was observed. Once failure was observed the compression was stopped and the plates were separated. The crushed bits of gel were discarded and the plates were cleaned.

4.6.4 Light Emission Collection

Light emission data was collected using a pco.edge camera. The stage of the rheometer was surrounded with a black plastic shield that prevented ambient light from the room from influencing the recordings. Once the disk is placed on the rheometer geometry, the shield and camera were covered with black-out fabric clipped into place. Compression studies were carried out using the procedures outlined in Chapter 3. The following standard operating procedure was used to operate the pco.edge camera.

- Connect communications cables A and B to appropriate ports.
- Set lens aperture to F1.2 (manually).
- Connect trigger cable to port 2.

- Plug in power cable.
- Turn camera on then open pco.edge operating software.
- Ensure that the following settings are correct:

  >Camera Control > Continuous Autorange OFF

  Set image size to 160 x 112

  33 ms exposure, 0 ms delay (FPS based off)

  >Convert Control BW > Min 80 Max 178 (Can be changed according to brightness, BE CONSISTENT)
- Open View B/W window
- Click Live Preview to see live images
- Stop live preview and hit "Start Record" to arm the camera. The dot will turn red and recording will start once triggered by the rheometer.

5. Additional Related Studies: Incorporating Reversible Cross-linkers into a HEMA/PVP Copolymer Network

5.1 Introduction

In this chapter, we report relaxation studies that probe the contributions of the reversible cross-linking on gels made from a copolymer system of both 4-vinyl pyridine (VP) and 2-hydroxyethylmethacrylate (HEMA) monomers. For purely historical reasons, these gels differ from those in previous chapters and are included here for supplementary purposes only. From a fundamental standpoint, the addition of HEMA into the polymer changes the polymer-solvent interactions, and the direct incorporation of cross-linker via free radical polymerization likely results in a somewhat different cross-linking architecture than was the case in Chapters 3 and 4. In addition, elastomeric materials made with HEMA are often used as a starting material for modification and studied in many systems due to their low cost, potential biocompatibility, and versatility.[144-145] Polymerized HEMA, or pHEMA, is not overly chemically sensitive or excessively reactive and can be easily polymerized under mild conditions. pHEMA is often used in systems where eventual applications in a biological system are important. pHEMA has been used in studies to mimic cartilage[146] or tissue with biocompatible hydrogels.[147] I originally intended to take my Ph.D work in the direction of biomaterials, and so working with pHEMA in these studies was therefore potentially advantageous in laying a foundation for that transition.

5.2 Building the PVP/HEMA Copolymer Network

Covalent network, **N9**, was formed from the free radical polymerization of approximately 29.5 % 4-VP, 69 % HEMA, and 1.5 %EGDMA. This recipe gave a gel that could be swollen nicely in DMSO and easily manipulated and punched into disks. The covalent **N9** networks were then swollen in DMSO. The reversible *bis*-metallic pincer complexes (**10a-d**) were incorporated by soaking the disks of **N9** in 3 mM DMSO solutions of the individual complexes, during which time the disks changed color. UV-Vis spectroscopy was used as before to monitor the uptake as a function of time. Both E_c data and oscillation storage modulus (G') data were used to confirm the time dependence of the uptake which varied for the four different metal complexes. As observed in previous hybrid networks, **N9•10a** and **N9• 10b** gels were saturated after 3 days of soaking, while **N9•10c** and **N9•10d**, required 7 days.

5.3 Mechanical Response of Hybrid Gels Under Compression

Compression studies were carried out to determine if these networks would behave similarly to the **N1** and **N3** gels. **N9** gels and hybrid gels **N9•10a-d** were each compressed at $\dot{\varepsilon}_t = 2 \times 10^{-3}\ s^{-1}$, and the moduli determined (Table 14).

Table 14: Average E_c for N9 and its hybrids; $\dot{\varepsilon}_t = 2 \times 10^{-3}\ s^{-1}$

Gel	E_c (kPa)
N9	10.4 ± 0.4
N9•10a	12.6 ± 0.2
N9•10b	19.4 ± 0.7
N9•10c	18.6 ± 0.3
N9•10d	17.5 ± 0.5

Each hybrid network **N9•10a-d** showed increased compressive moduli when compared to the **N9** covalent network. This showed that the cross-linkers also bear stress within the hybrid networks under compression. As is shown in Table 14, the increase in E_c was more pronounced for the slower pincer complexes (**10b-d**). Unlike the studies carried out with the **N1•10a** or **N3•10a** gels, there was actually a small influence observed in the **N9•10a** hybrid networks. Clearly, the copolymer networks' behavior is different than that of the behavior observed in the other networks. This observation raises several questions when expanding our previous work to new systems. The change in environment (copolymer, swelling, etc) has influenced the effect of the reversible cross-links on the material. How much can the system be altered from the **N1** or **N3** compositions before it hinders the positive contributions from the reversible cross-linkers observed in previous studies. Additional studies should be carried out to further confirm the observed increase in E_c and probe the influence as a function of co-polymer mixture.

5.4 Relaxation Under Compression

As discussed in Chapter 2, the molecular kinetics of the **10a-d** compounds are seen in the dynamic mechanical properties of hybrid gels similar to the **N9•10a-d** set.[92] The influence of molecular dynamics on the relaxation behaviors of **N9•10a-d** were studied with a compression relaxation test. Disks from all **N9** hybrid gels were compressed at $\dot{\varepsilon}_l$ = 2.5 s^{-1} to 20 % strain and the resulting stress was monitored over time. As seen in Figure 51, no substantial relaxation is observed in **N9** gel over the initial 15 seconds.

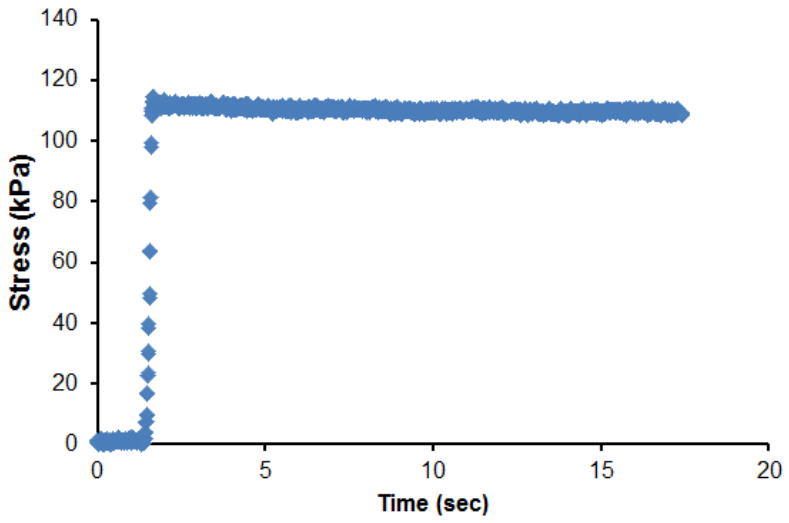

Figure 51: Stress vs. time for N9 at 20% strain; $\dot{\varepsilon}_l$ = 2.5 s^{-1}

When the hybrid networks **N9•10a-d** were compressed under the same conditions, however, different relaxation behaviors were observed (Figure 52). The hybrid networks **N9•10a, N9•10b, and N9•10c** all relax to the ~ 110 kPa stress of **N9,**

but on different timescales. **N9•10d** gels showed drastically slower relaxation behavior and needed a longer time to relax back to the covalent values. In all cases, the transient cross-links initially bear stress within the network, as shown in Figure 53.

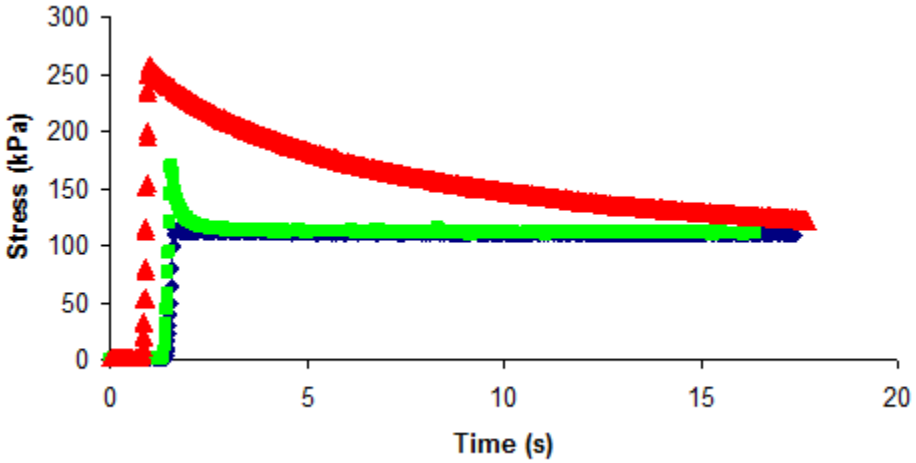

Figure 52: Stress vs. time for the N9•10a-c **networks after a 20% strain;** $\dot{\varepsilon}_i$ **= 2.5 s^{-1} N9•10a (blue), N9•10b (green), and N9•10c (red)**

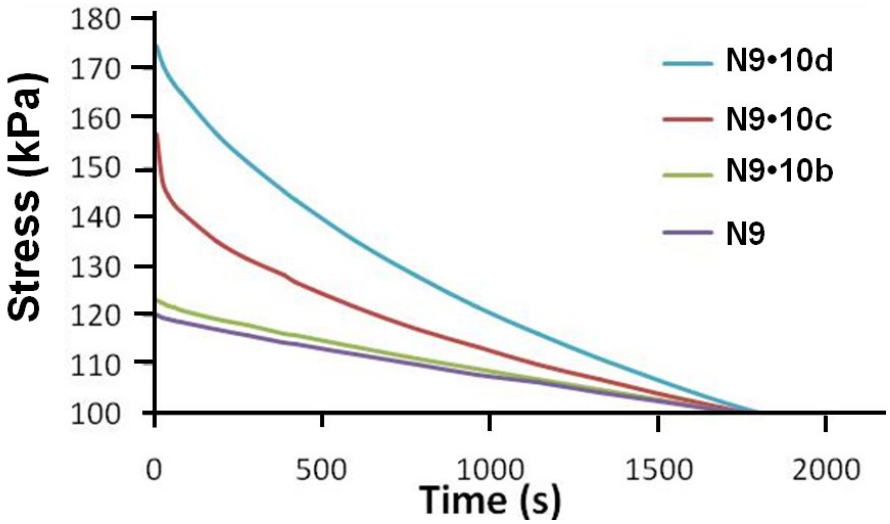

Figure 53: Stress relaxation for hybrid networks at a fixed strain
Stress vs. time for **N9 (purple), N9•10b (green), N9•10c (red),** and **N9•10d (blue)** gels were each compressed at $\dot{\varepsilon}_i$ = 2.5 s^{-1} to 20% strain and held at room temperature.

Drastically different relaxation times were observed for the four hybrid gels. When the **N9•10a** hybrid networks were tested, any relaxation of the network occurred faster than could be recorded given the temporal resolution of our experiment (ms timescale). Therefore, the collected data appeared like the pure covalent network. This observation calls into the question the increase in modulus for the **N9•10a** networks reported in Table 14. In the other three hybrid networks, the relaxation curves fall back to that of the covalent gel on time scales that are qualitatively consistent with the relative dissociation rates of their reversible cross-linkers.

5.5 Behavior Under Repeated Compressions

We wanted to further investigate if the reversible cross-linkers would have a similar protective effect in these new systems. The **N9, N9•10a,** and **N9•10c** gels were compressed at $\dot{\varepsilon}_t = 2.2 \times 10^{-3}\ s^{-1}$ to 20% strain for 20 cycles with no rest period in between compression. Figure 54 shows moduli as a function of compression cycle for the covalent **N9** gel and hybrid networks **N9•10a** and **N9•10c.**

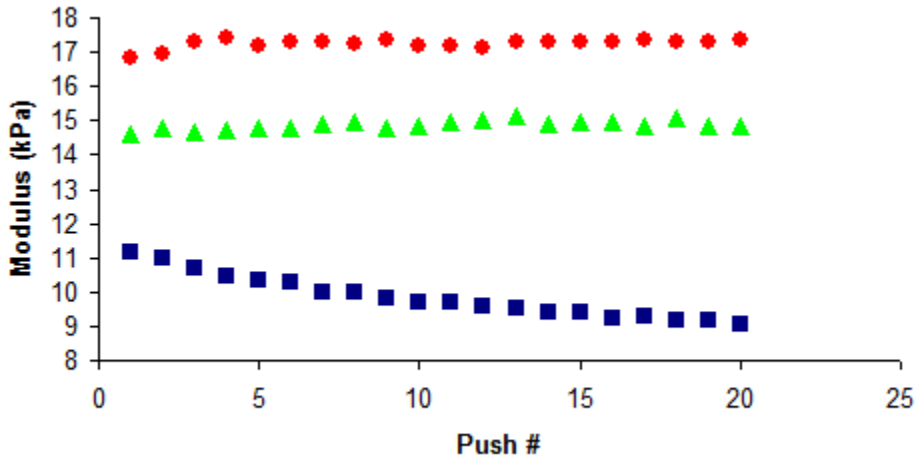

Figure 54: Compressive modulus as a function of compression cycle
N9 (■), **N9•10a** (▲) and **N9•10c** (●); compressed to 20% strain at $\dot{\varepsilon}_t = 2.2 \times 10^{-3}\ s^{-1}$.

The **N9** gel showed a decrease in compressive modulus over the 20 repeated compressions. The compressive modulus of **N9** decreased by approximately 18% (~2 kPa) over 20 cycles, whereas, the moduli of **N9•10a** and **N9•10c** remained relatively constant. When the test was extended to 100 cycles, a decrease in modulus was observed in both the **N9** gels as well as the hybrid **N9•10b** (Figure 55).

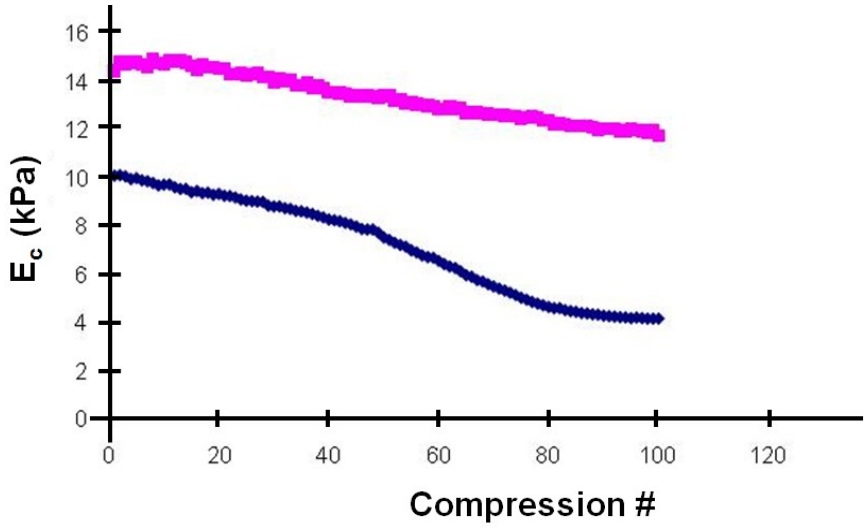

Figure 55: Compressive modulus as a function of 100 compressions
Gels **N9 (blue)** and **N9•10b (purple)** were compressed to 20%, at $\dot{\varepsilon}_t = 2.2 \times 10^{-3}\ s^{-1}$ with no rest time in between cycles.

When **10b** is incorporated into the covalent gel, the loss in modulus was retarded. As shown in Figure 55, the modulus of **N9** decreased by approximately 60% (~ 6 kPa), while that of hybrid **N9•10b** decreased by less than 13% (~2 kPa). When the samples are returned to their respective soaking solutions (either DMSO for the covalent network, or the solution of **10b** in DMSO) overnight, both samples showed a restoration of modulus when tested the next day. This indicates that the observations are not relevant to the fracture behavior described in Chapters 3 and 4.

5.6 Summary

Transient cross-links were successfully incorporated into the covalent copolymer networks of varying compositions. The timescales observed for stress relaxation in the

hybrid materials differ with the lifetimes of the transient cross-linkers that were incorporated into the network. Additionally, when studied under repeated compressions, the networks exhibited viscoelastic relaxation that was slower for the hybrid networks. All of the different gels were able to recover their loss in modulus with a simple reswelling in solvent. This indicates that lasting deformations were not being induced in any of the gels. While these results suggest some structure activity relationships, a more systematic and quantitative study is needed to better elucidate this relationship in the co-polymer networks.

5.6. Experimental

Covalent N9 Network Synthesis: All reagents were used as purchased from Sigma unless noted differently. By pipet, deionized water (400 μL), ethylene glycol (600 μL), distilled hydroxyethyl methacrylate (HEMA) (1400 μL), distilled 4-vinyl pyridine (4-VP) (200 μL), ethylene glycol dimethacrylate (EGDMA) (30 μL), ammonia persulfate (150 mg/mL) (100 μL), and sodium metabisulfate (150 mg/mL) (100 μL) were added to a large (20mL) glass scintillation vial. The vial was capped and shaken by hand for 30 seconds. The solution was then transferred via glass pipet to a glass mold approximately 5 cm x 1 cm x 0.1 cm in size. A glass microscope slide was slid across the top of the mold to obtain a gel of uniform thickness. The solution was allowed to polymerize overnight (~15-20 hours). The next day the gel was removed from the mold

and cut in half using a razor blade. The pieces of gel were then soaked in DMSO. The DMSO was changed twice daily for 3-4 days to remove any small molecular weight components. The gels were then punched into 5 mm disks using standard biopsy punches. Unless otherwise noted the cut disks were stored in DMSO in capped vials.

Inserting metal cross-linkers: 10 disks formed as described above were removed from DMSO and placed in 2 mL of 3 mM solutions of metal cross-linkers (**10a-10d**) in DMSO. The disks were allowed to soak in the metal solutions for a week before material testing.

Mechanical Testing: All testing was performed on AR G2 Rheometer from TA Instruments using the 8 mm parallel plate geometry as the upper geometry and a solution cup as the lower geometry. Prior to compression, the diameter of the gel was measured using digital calipers. To determine the height of the disk, the top geometry was lowered just until coming in contact with the top of the gel and registers a normal force of 0.1 N. All compressions were performed at 25 °C (as modulated by the Peltier plate base). The disks were compressed at a constant velocity, typically 3 μm/s (see earlier compression rate discussions in Chapter 3). The resulting normal force was collected as a function of gap distance between the geometries. Normal force and gap distance values were then converted to stress and strain values based on the diameter and height measurements performed before the experiment was carried out. Compressive modulus measurements were carried out as described in Chapter 3. For

relaxation measurements, gels were submerged in 1 mL of either DMSO (for **N9** gels) or a 3 mM DMSO solution of the appropriate metal complex (**N9•10a-d**). Gels were compressed at v_c = 25 μm/s to a strain of 20% and the resulting stress measured over 30 min. The first 45 seconds were collected using high-speed data acquisition software from TA Instruments .

6. General Conclusions and Future Directions

The work discussed in this dissertation explores the relationship between the kinetics of reversible interactions in hybrid polymer networks and the failure behavior under compression of gels made from those networks. The hybrid networks comprised covalent frameworks and any of a family of four different reversible cross-linkers based on pincer complexes.

For more slowly dissociating pincer complexes (**10c** and **10d**), it was shown that: (1) the passive reversibility of the pincer complexes provided a means for protecting the covalent network from failure; and (2) the failure behavior of the hybrid networks depends on the $\dot{\varepsilon}_t$. More interesting were the networks formed with rapidly dissociating complexes (**10a** and **10b**), which did not contribute in a measureable way to compressive modulus but nonetheless had a substantial impact on the fracture strain of the gels. The delay in covalent bond failure was observed through the emission of light from the covalent bond scission event.

The enhancements in strain at break observed in hybrid networks are typically attributed to non-destructive dissipation of energy through dissociation of the reversible cross-linkers on the timescale of deformations. A correlation between fracture strain and both $\dot{\varepsilon}_t / k_d$ and modulus enhancement was therefore expected. Neither was observed, and one hypothesis as to why is that the time scale relevant to fracture is not related to strain rate, but to the rate of crack propagation. During propagation, two components

contribute to the overall fracture energy: the intrinsic fracture energy (the energy required to break bonds) and the fracture energy due to mechanical dissipation in a plastic zone surrounding the crack.[65] If the reversible bonds remain intact on the time scale of the crack propagating through the material (i.e. the rate of crack- propagation is faster than the k_d), then the reversible cross-links act as permanent bonds and contribute to the intrinsic fracture energy component (small number of bonds) while also limiting the size of the plastic zone. If, however, the reversible bonds break on the timescale of the crack propagation through the material (i.e. the rate of crack-propagation is slower than the k_d) then reversible bonds contribute to dissipation of energy and the reversible cross-links retard the breaking of covalent bonds and ultimately the failure of the material.

Looking ahead, the rate of crack propagation could be measured using the light emission data and compared to the k_d of the reversible cross-linkers. Because the cross-linkers and their behavior in transient networks are so well characterized[74-75, 77-81, 83-85, 140, 148] these systems offer great potential for quantitative structure-activity studies that test long-standing models of fracture in polymer gels.

On a practical level, the hybrid networks formed with rapidly dissociating cross-linkers **10a** and **10b** are interesting in that they and their pure covalent analogs have identical moduli and bulk mechanical properties at low strains, but show drastic differences in fracture strain. This ability to vary the maximum achievable fracture

strain without paying a cost in increase modulus could lend itself to interesting applications in soft active materials. For that to happen, the generality of the findings needs to be established. How can appropriate combinations of covalent network and reversible cross-linkers be determined for a specific design challenge or application? What happens if hybrid networks are created with more than one hybrid component? And how does this behavior be extend to other types of strain (i.e. tensile or shear)?

Appendix: Ultraviolet Spectroscopy Studies of the Pincer Complexes

Ultraviolet (UV) spectroscopy was used to study the uptake of the pincer complexes (**10a-d**) in the **N1** gels. Each of the pincer complexes **10a-d** has a unique peak absorbance on the UV-Vis spectrum that can be monitored as a function of concentration. Standard solutions were prepared for each of the pincer complexes, then used to create a calibration curve and calculate a molar absorptivity for each compound. Table 15 below summarizes the λ_{max} monitored and the calculated molar absorptivity (a) for each compound.

Table 15: λ_{max} and molar absorptivity (a) data for compounds 10a-d

Compound	λ_{max} (nm)	a (cm^{-1} M^{-1})
10a	269	10.8
10b	265	15.4
10c	303	13.3
10d	292	17.4

Figures 62 - 65 provide the calibration curves for **10d, 10c, 10a,** & **10b**,in order of the experiments discussed in chapter 3.

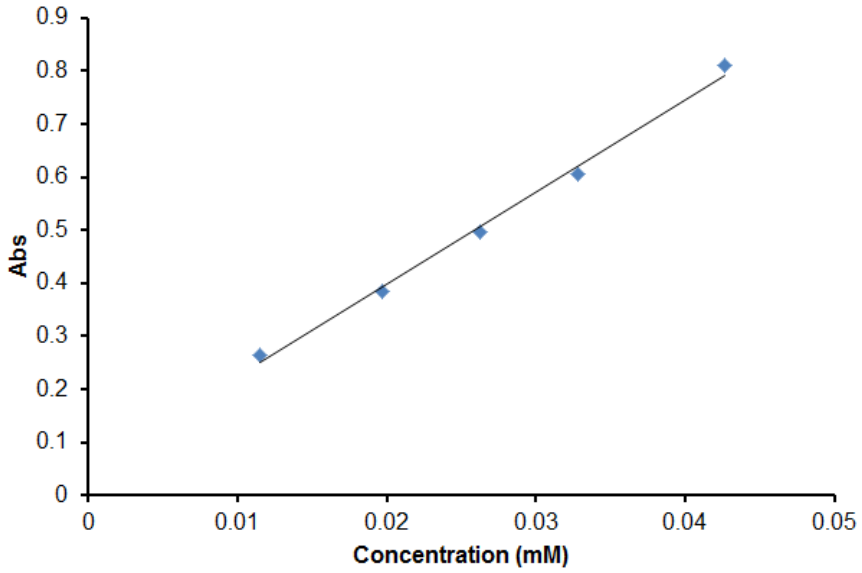

Figure 56: Calibration curve for 10d performed in DMSO at 292 nm.

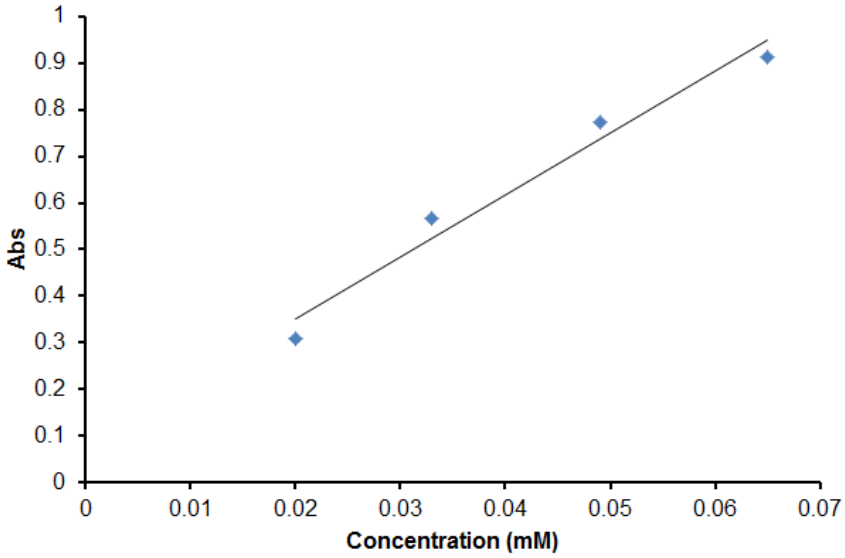

Figure 57: Calibration curve for 10c performed in DMSO at 303 nm.

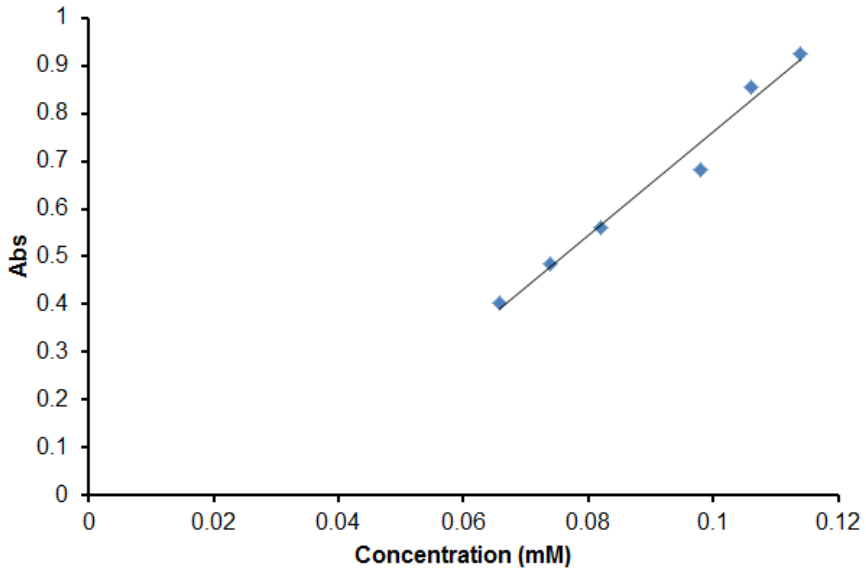

Figure 58: Calibration curve for 10a performed in DMSO at 269 nm.

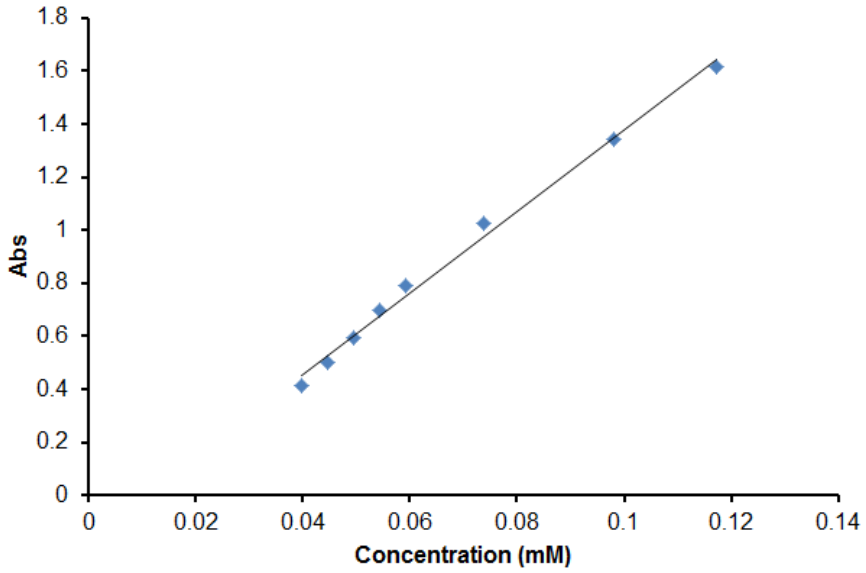

Figure 59:Calibration curve for 10b performed in DMSO at 265 nm.

Disks of **N1** were placed in individual 5 mM solutions of **10a-d** in DMSO. Aliquots were removed from the solution at various time intervals. UV spectroscopy was then used to monitor the concentration of the solution as a function of time to determine how long it took for the concentration to reach equilibrium. Figure 60 plots the concentration of **10c** and **10d** as a function of time.

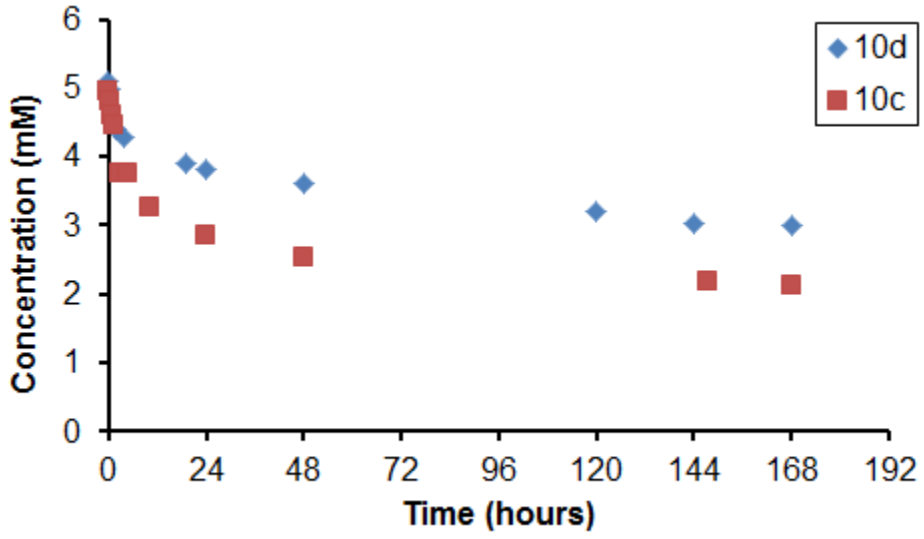

Figure 60: Concentration of 10c and 10d as a function of soak time
N1 disks were soaked in either a solution of **10c** or **10d** with initial concentrations of 5 mM in DMSO. The concentration of the solutions were monitored via UV spectroscopy. The concentration of the solution decreases over time and reaches equilibrium by 168 hours.

As expected, the concentration of the surrounding solution decreases as a function of time. This indicates that the pincer complexes are being taken into the gels. The time it takes to reach equilibrium could also be observed for the concentration data.

It was determined that the system reaches equilibrium after 6 days. Therefore, for the remaining studies carried out with **10d** and **10c**, the **N1** disks were soaked for a full 7 days before mechanical testing.

Figure 61 shows the concentration of **10a** and **10b** as a function of time.

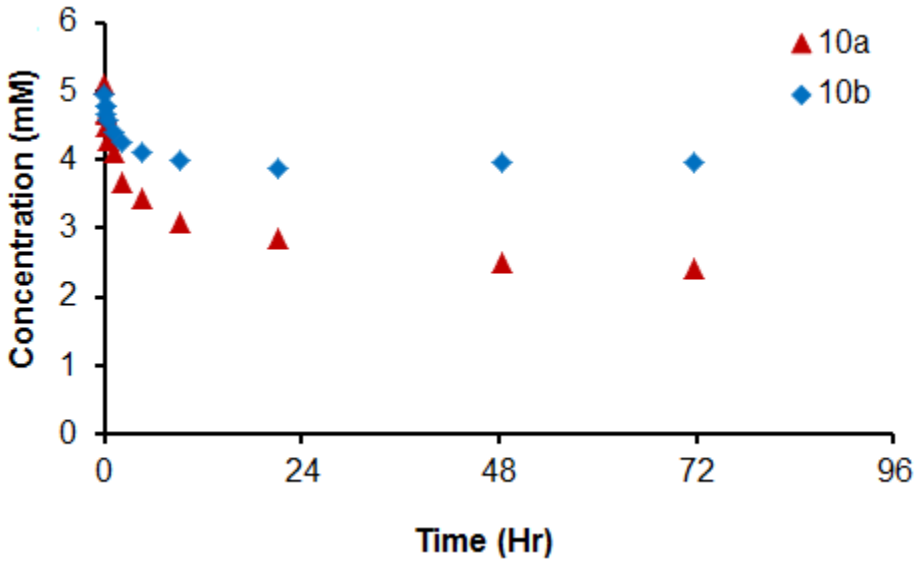

Figure 61: Concentration of 10a or 10b as a function of soak time
N1 disks were soaked in either a solution of **10a** or **10b** with initial concentrations of 5 mM in DMSO. The concentration of the solutions were monitored via UV spectroscopy. The concentration of the solution decreases over time and reaches equilibrium by 72 hours.

The concentration of **10a** and **10b** both decrease with time. Due to the significantly larger k_a values for **10a** and **10b**, the concentration reaches equilibrium between 48 and 72 hours. Therefore, for the remainder of the studies, disks were soaked in solutions of either **10a** or **10b** for at least 3 days before carrying out mechanical

testing. It should be noted that the UV cut off wavelength for DMSO is around 268-265 nm. Unfortunately, this coincides with the wavelength peaks of interest for both **10a** and **10b**. Also, several calibration curves do not pass through the origin, and so the molar absorptivities reported in Table 15 are surely incorrect. The concentration data is a little suspect in that it was expected the uptake to be more similar based on the similar K_{eq} values for **10a** and **10b**. While the concentrations of the soak solutions may not be exact, the general trends observed in the concentration are reliable. The approximate equilibrium times have been confirmed with compression data. The modulus increases with time until the equilibrium has been reached.

Works Cited

1. Erman, B.; Flory, P. J., *Macromolecules* **1982,** *15*, 806-811.

2. Grest, G. S.; Pütz, M.; Everaers, R.; Kremer, K., *J. Non-Cryst. Solids* **2000,** *274*, 139-146.

3. Klusák, J.; Knésl, Z., *Comp. Mater. Sci.* **2007,** *39*, 214-218.

4. Meissner, B., *Polymer* **2000,** *41*, 7827-7841.

5. Seitz, M. E.; Martina, D.; Baumberger, T.; Krishnan, V. R.; Hui, C.-Y.; Shull, K. R., *Soft Matter* **2009,** *5*, 447-456.

6. Bonderer, L. J.; Studart, A. R.; Gauckler, L. J., *Science* **2008,** *319*, 1069-1073.

7. Burnworth, M.; Knapton, D.; Rowan, S.; Weder, C., *J. Inorg. Organomet. P.* **2007,** *17*, 91-103.

8. Rowan, S. J.; Beck, J. B., *Faraday Discuss.* **2005,** *128*, 43-53.

9. Thompson, R. B.; Ginzburg, V. V.; Matsen, M. W.; Balazs, A. C., *Macromolecules* **2002,** *35*, 1060-1071.

10. Baekeland, L. H., *J. Ind. Eng. Chem.* **1909,** *1*, 149-161.

11. Flory, P. J.; Erman, B., *Macromolecules* **1982,** *15*, 800-806.

12. Erk, K. A.; Henderson, K. J.; Shull, K. R., *Biomacromolecules* **2010,** *11*, 1358-1363.

13. Jan, H. v. E.; Ben, L. F., Gels. In *Encyclopedia of Supramolecular Chemistry*, Taylor & Francis: 2007; Vol. null, pp 586-596.

14. Hirst, A. R.; Smith, D. K.; Feiters, M. C.; Geurts, H. P. M.; Wright, A. C., *J. Am. Chem. Soc.* **2003,** *125*, 9010-9011.

15. Rees, G. D.; Robinson, B. H., *Adv. Mater.* **1993,** *5*, 608-619.

16. Martens, P.; Blundo, J.; Nilasaroya, A.; Odell, R. A.; Cooper-White, J.; Poole-Warren, L. A., *Chem. Mater.* **2007,** *19*, 2641-2648.

17. Calvert, P., *Adv. Mater.* **2009,** *21*, 743-756.

18. Hoffman, A. S., *Adv. Drug Deliver. Rev.* **2002,** *54*, 3-12.

19. Bray, J. C.; Merrill, E. W., *J. Biomed. Mat. Res.* **1973,** *7*, 431-443.

20. Tomatsu, I.; Peng, K.; Kros, A., *Adv. Drug Deliver. Rev.* **2011,** *63*, 1257-1266.

21. Lee, K. Y.; Mooney, D. J., *Chem. Rev.* **2001,** *101*, 1869-1880.

22. Hyon, S.-H.; Cha, W.-I.; Ikada, Y.; Kita, M.; Ogura, Y.; Honda, Y., *J. Biomat. Sci-Polym. E.* **1994,** *5*, 397-406.

23. Hicks, C. R.; Crawford, G. J.; Lou, X.; Tan, D. T.; Snibson, G. R.; Sutton, G.; Downie, N.; Werner, L.; Chirila, T. V.; Constable, I. J., *Eye* **0000,** *17*, 385-392.

24. Vintiloiu, A.; Leroux, J.-C., *J. Control. Release* **2008,** *125*, 179-192.

25. Hughes, N. E.; Marangoni, A. G.; Wright, A. J.; Rogers, M. A.; Rush, J. W. E., *Trends Food Sci. Tech.* **2009,** *20*, 470-480.

26. Fadnavis, N. W.; Koteshwar, K., *Biotechnol. Progr.* **1999,** *15*, 98-104.

27. Ajayaghosh, A.; Praveen, V. K.; Vijayakumar, C., *Chem. Soc. Rev.* **2008,** *37*, 109-122.

28. Ajayaghosh, A.; Praveen, V. K., *Acc. Chem. Res.* **2007,** *40*, 644-656.

29. Brown, H. R., *Macromolecules* **2007,** *40*, 3815-3818.

30. Ha, S. M.; Yuan, W.; Pei, Q.; Pelrine, R.; Stanford, S., *Smart Mater. Struct.* **2007,** *16*, S280.

31. Gong, J. P., *Soft Matter* **2010,** *6*, 2583-2590.

32. Gong, J. P.; Katsuyama, Y.; Kurokawa, T.; Osada, Y., *Adv. Mater.* **2003,** *15*, 1155-1158.

33. Liao, I. C.; Moutos, F. T.; Estes, B. T.; Zhao, X.; Guilak, F., *Adv. Funct. Mater.* **2013,** *23*, 5833-5839.

34. Ciferri, A., *Supramolecular Polymers*. Marcel Dekker: New York, 2000.

35. Lehn, J. M., *Makromol. Chem., Macromol. Symp.* **1993,** *69*, 1-17.

36. Lehn, J. M., *Supramolecular Chemistry : Concepts and Perspectives : a Personal Account Built Upon the George Fisher Baker Lectures in Chemistry at Cornell University [and the] Lezione Lincee, Accademia nazionale dei Lincei, Roma*. VCH: Weinheim ; New York, 1995.

37. Noro, A.; Hayashi, M.; Matsushita, Y., *Soft Matter* **2012,** *8*, 2416-2429.

38. Castellano, R. K.; Clark, R.; Craig, S. L.; Nuckolls, C.; Rebek, J. *Proc. Natl. Acad. Sci.* **2000,** *97*, 12418-12421.

39. Scherer, M.; Caulder, D. L.; Johnson, D. W.; Raymond, K. N., *Angew. Chem. Int. Ed.* **1999,** *38*, 1588-1592.

40. Sijbesma, R. P.; Beijer, F. H.; Brunsveld, L.; Folmer, B. J. B.; Hirschberg, J. H. K. K.; Lange, R. F. M.; Lowe, J. K. L.; Meijer, E. W., *Science* **1997,** *278*, 1601-1604.

41. Pei, X.; Zhao, J.; Ye, Y.; You, Y.; Wei, X., *Soft Matter* **2011,** *7*, 2953-2960.

42. Scherman, O. A.; Ligthart, G. B. W. L.; Ohkawa, H.; Sijbesma, R. P.; Meijer, E. W., J. *Proc. Natl. Acad. Sci.(USA)* **2006,** *103*, 11850-11855.

43. Calzia, K. J.; Tew, G. N., *Macromolecules* **2002,** *35*, 6090-6093.

44. Schubert, U. S.; Hien, O.; Eschbaumer, C., *Macromol. Rapid Commun.* **2000,** *21*, 1156-1161.

45. Wang, S.; Chen, C.-C.; Dormidontova, E. E., *Soft Matter* **2008,** *4*, 2039-2053.

46. Yan, Y.; Besseling, N. A. M.; de Keizer, A.; Marcelis, A. T. M.; Drechsler, M.; Cohen Stuart, M. A., *Angew. Chem. Int. Ed.* **2007,** *46*, 1807-1809.

47. Burattini, S.; Greenland, B. W.; Merino, D. H.; Weng, W.; Seppala, J.; Colquhoun, H. M.; Hayes, W.; Mackay, M. E.; Hamley, I. W.; Rowan, S. J., *J. Am. Chem. Soc.* **2010,** *132*, 12051-12058.

48. Wang, X. L.; Lin, H. Y.; Hu, T. L.; Tian, J. L.; Bu, X. H., *J. Mol. Struct.* **2006,** *798*, 34-39.

49. Cordier, P.; Tournilhac, F.; Soulie-Ziakovic, C.; Leibler, L., *Nature* **2008,** *451*, 977-980.

50. Wilson, G. O.; Andersson, H. M.; White, S. R.; Sottos, N. R.; Moore, J. S.; Braun, P. V., Self-Healing Polymers. In *Encyclopedia of Polymer Science and Technology*, John Wiley & Sons, Inc.: 2002.

51. Syrett, J. A.; Becer, C. R.; Haddleton, D. M., *Polymer Chemistry* **2010,** *1*, 978-987.

52. Skrzeszewska, P. J.; Sprakel, J.; de Wolf, F. A.; Fokkink, R.; Cohen Stuart, M. A.; van der Gucht, J., *Macromolecules* **2010,** *43*, 3542-3548.

53. Blaiszik, B. J.; Kramer, S. L. B.; Olugebefola, S. C.; Moore, J. S.; Sottos, N. R.; White, S. R., *Annu. Rev. Mater. Res.* **2010,** *40*, 179-211.

54. Zhang, M.; Xu, D.; Yan, X.; Chen, J.; Dong, S.; Zheng, B.; Huang, F., *Angew. Chem.* **2012,** *124*, 7117-7121.

55. Hentschel, J.; Kushner, A. M.; Ziller, J.; Guan, Z., *Angew. Chem.* **2012,** *124*, 10713-10717.

56. Sijbesma, R. P.; Meijer, E. W., *Chem. Commun.* **2003**, 5-16.

57. Chiang, D.; Crary, P. C.; Li, J. C. M., *Polymer* **1994,** *35*, 4110-4114.

58. Chen, X.; Wudl, F.; Mal, A. K.; Shen, H.; Nutt, S. R., *Macromolecules* **2003,** *36*, 1802-1807.

59. Nettles, D. L.; Vail, T. P.; Morgan, M. T.; Grinstaff, M. W.; Setton, L. A., *Ann. Biomed. Eng.* **2004,** *32*, 391-397.

60. White, S. R.; Sottos, N. R.; Geubelle, P. H.; Moore, J. S.; Kessler, M. R.; Sriram, S. R.; Brown, E. N.; Viswanathan, S., *Nature* **2001,** *409*, 794-797.

61. Flory, P. J., *Principles of Polymer Chemistry*. Ithaca, Cornell University Press, 1969, 1953.: 1969.

62. Baumberger, T.; Caroli, C.; Martina, D., *Nature Mater.* **2006,** *5*, 552-555.

63. Baumberger, T.; Caroli, C.; Martina, D., *Eur. Phys. J. E* **2006,** *21*, 81-89.

64. Fantner, G. E.; Hassenkam, T.; Kindt, J. H.; Weaver, J. C.; Birkedal, H.; Pechenik, L.; Cutroni, J. A.; Cidade, G. A. G.; Stucky, G. D.; Morse, D. E.; Hansma, P. K., *Nature Mater.* **2005,** *4*, 612-616.

65. Zhao, X., *Soft Matter* **2014,** *10*, 672-687.

66. Leibler, L.; Rubinstein, M.; Colby, R. H., *Macromolecules* **1991,** *24*, 4701-4707.

67. Kushner, A. M.; Vossler, J. D.; Williams, G. A.; Guan, Z., *J. Am. Chem. Soc.* **2009,** *131*, 8766-8768.

68. Kushner, A. M.; Gabuchian, V.; Johnson, E. G.; Guan, Z., *J. Am. Chem. Soc.* **2007,** *129*, 14110-14111.

69. Dimopoulos, A.; Wietor, J.-L.; Wübbenhorst, M.; Napolitano, S.; van Benthem, R. A. T. M.; de With, G.; Sijbesma, R. P., *Macromolecules* **2010,** *43*, 8664-8669.

70. Wietor, J.-L.; Dimopoulos, A.; Govaert, L. E.; van Benthem, R. A. T. M.; de With, G.; Sijbesma, R. P., *Macromolecules* **2009,** *42*, 6640-6646.

71. Henderson, K. J.; Zhou, T. C.; Otim, K. J.; Shull, K. R., *Macromolecules* **2010,** *43*, 6193-6201.

72. Sun, J.-Y.; Zhao, X.; Illeperuma, W. R. K.; Chaudhuri, O.; Oh, K. H.; Mooney, D. J.; Vlassak, J. J.; Suo, Z., *Nature* **2012,** *489*, 133-136.

73. Loveless, D. M.; Abu-Lail, N. I.; Kaholek, M.; Zauscher, S.; Craig, S. L., *Angew. Chem. Int. Ed.* **2006,** *45*, 7812-7814.

74. Loveless, D. M.; Jeon, S. L.; Craig, S. L., *Macromolecules* **2005,** *38*, 10171-10177.

75. Loveless, D. M.; Jeon, S. L.; Craig, S. L., *J. Mater. Chem.* **2007,** *17*, 56-61.

76. Serpe, M. J.; Craig, S. L., *Langmuir* **2006,** *23*, 1626-1634.

77. Xu, D.; Craig, S. L., *J. Phys. Chem. Lett.* **2010,** *1*, 1683-1686.

78. Xu, D.; Craig, S. L., *Macromolecules* **2011,** *44*, 7478-7488.

79. Xu, D.; Craig, S. L., *Macromolecules* **2011,** *44*, 5465-5472.

80. Xu, D.; Hawk, J. L.; Loveless, D. M.; Jeon, S. L.; Craig, S. L., *Macromolecules* **2010,** *43*, 3556-3565.

81. Xu, D.; Liu, C.-Y.; Craig, S. L., *Macromolecules* **2011,** *44*, 2343-2353.

82. Yount, W. C.; Juwarker, H.; Craig, S. L., *J. Am. Chem. Soc.* **2003,** *125*, 15302-15303.

83. Yount, W. C.; Loveless, D. M.; Craig, S. L., *J. Am. Chem. Soc.* **2005,** *127*, 14488-14496.

84. Yount, W. C.; Loveless, D. M.; Craig, S. L., *Angew. Chem. Int. Ed.* **2005,** *44*, 2746-2748.

85. Kersey, F. R.; Loveless, D. M.; Craig, S. L., *J. R. Soc. Interface* **2007,** *4*, 373-380.

86. Hawk, J.; Craig, S., Physical and Materials Applications of Pincer Complexes. In *Organometallic Pincer Chemistry*, van Koten, G.; Milstein, D., Eds. Springer Berlin Heidelberg: 2013; Vol. 40, pp 319-352.

87. Pollino, J. M.; Stubbs, L. P.; Weck, M., *J. Am. Chem. Soc.* **2004,** *126*, 563-567.

88. Huck, W. T. S.; van Veggel, F. C. J. M.; Reinhoudt, D. N., *Angew. Chem. Int. Ed. Engl.* **1996,** *35*, 1213-1215.

89. Huck, W. T. S.; Hulst, R.; Timmerman, P.; van Veggel, F. C. J. M.; Reinhoudt, D. N., *Angew. Chem. Int. Ed. Engl.* **1997,** *36*, 1006-1008.

90. Nair, K. P.; Pollino, J. M.; Weck, M., *Macromolecules* **2006,** *39*, 931-940.

91. South, C. R.; Weck, M., *Langmuir* **2008,** *24*, 7506-7511.

92. Kersey, F. R.; Loveless, D. M.; Craig, S. L., *J. R. Soc. Interface* **2007,** *4*, 373-380.

93. Huck, W. T. S.; Snellink-Ruel, B. H. M.; Lichtenbelt, J. W. T.; van Veggel, F. C. J. M.; Reinhoudt, D. N., *Chem. Commun.* **1997**, 9-10.

94. Huisman, B. H.; Schonherr, H.; Huck, W. T. S.; Friggeri, A.; van Manen, H. J.; Menozzi, E.; Vancso, G. J.; van Veggel, F. C. J. M.; Reinhoudt, D. N., *Angew. Chem. Int. Ed.* **1999,** *38*, 2248-2251.

95. Huck, W. T. S.; van Veggel, F. C. J. M.; Sheiko, S. S.; Moller, M.; Reinhoudt, D. N., *J. Phys. Org. Chem.* **1998,** *11*, 540-545.

96. Huck, W. T. S.; Hulst, R.; Timmerman, P.; van Veggel, F. C. J. M.; Reinhoudt, D. N., *Angew. Chem. Int. Ed.* **1997,** *36*, 1006-1008.

97. Huck, W. T. S.; Snellink-Ruel, B.; van Veggel, F. C. J. M.; Reinhoudt, D. N., *Organometallics* **1997,** *16*, 4287-4291.

98. Huck, W. T. S.; Prins, L. J.; Fokkens, R. H.; Nibbering, N. M. M.; van Veggel, F. C. J. M.; Reinhoudt, D. N., *J. Am. Chem. Soc.* **1998,** *120*, 6240-6246.

99. Huck, W. T. S.; van Veggel, F. C. J. M.; Kropman, B. L.; Blank, D. H. A.; Keim, E. G.; Smithers, M. M. A.; Reinhoudt, D. N., *J. Am. Chem. Soc.* **1995,** *117*, 8293-8294.

100. Huck, W. T. S.; van Veggel, F. C. J. M.; Reinhoudt, D. N., *J. Mater. Chem.* **1997,** *7*, 1213-1219.

101. Albrecht, M.; van Koten, G., *Angew. Chem. Int. Ed.* **2001,** *40*, 3750-3781.

102. Wieczorek, B.; Dijkstra, H. P.; Egmond, M. R.; Klein Gebbink, R. J. M.; van Koten, G., *J. Organomet. Chem.* **2009,** *694*, 812-822.

103. Stiriba, S.-E.; Slagt, M. Q.; Kautz, H.; Klein Gebbink, R. J. M.; Thomann, R.; Frey, H.; van Koten, G., *Chem. Eur. J.* **2004,** *10*, 1267-1273.

104. van de Coevering, R.; Alfers, A. P.; Meeldijk, J. D.; Martínez-Viviente, E.; Pregosin, P. S.; Klein Gebbink, R. J. M.; van Koten, G., *J. Am. Chem. Soc.* **2006,** *128*, 12700-12713.

105. South, C. R.; Pinon III, V.; Weck, M., *Angew. Chem. Int. Ed.* **2008,** *47*, 1425-1428.

106. South, C. R.; Higley, M. N.; Leung, K. C. F.; Lanari, D.; Nelson, A.; Grubbs, R. H.; Stoddart, J. F.; Weck, M., *Chem. Eur. J.* **2006,** *12*, 3789-3797.

107. South, C. R.; Leung, K. C. F.; Lanari, D.; Stoddart, J. F.; Weck, M., *Macromolecules* **2006,** *39*, 3738-3744.

108. Burd, C.; Weck, M., *J. Polym. Sci.: Part A: Polym. Chem.* **2008,** *46*.

109. Whitesides, G. M.; Mathias, J. P.; Seto, C. T., *Science* **1991,** *254*, 1312-1319.

110. Davis, A. V.; Yeh, R. M.; Raymond, K. N., *Proc. Natl. Acad. Sci. U.S.A* **2002,** *99*, 4793-4796.

111. Ziegler, M.; Brumaghim, J. L.; Raymond, K. N., *Angew. Chem. Int. Ed.* **2000,** *39*, 4119-4121.

112. Kang, J.; Rebek Jr., J., *Nature* **1997,** *385*, 50-52.

113. Kang, J.; Hilmersson, G.; Santamaria, J.; Rebek Jr., J., *J. Am. Chem. Soc.* **1998,** *120*, 3650-3656.

114. Yoshizawa, M.; Kusukawa, T.; Fujita, M.; Sakamoto, S.; Yamaguchi, K., *J. Am. Chem. Soc.* **2001,** *123*, 10454-10459.

115. Rivera, J. M.; Craig, S. L.; Martin, T.; Rebek Jr., J., *Angew. Chem. Int. Ed.* **2000,** *39*, 2130-2132.

116. Kersting, B.; Meyer, M.; Powers, R. E.; Raymond, K. N., *J. Am. Chem. Soc.* **1996,** *118*, 7221-7222.

117. Chen, J.; Korner, S.; Craig, S. L.; Rudkevich, D. M.; Rebek Jr., J., *Nature* **2002,** *415*, 385-386.

118. Fujita, M.; Umemoto, K.; Yoshizawa, M.; Fujita, N.; Kusukawa, T.; Biradha, K., *Chem. Commun.* **2001**, 509-518.

119. Seidel, S. R.; Stang, P. J., *Acc. Chem. Res.* **2002,** *35*, 972-983.

120. Rodriquez, G.; Albrecht, M.; Schoenmaker, J.; Ford, A.; Lutz, M.; Speck, A. L.; van Koten, G., *J. Am. Chem. Soc.* **2002,** *124*, 5127-5138.

121. Dijkstra, H. P.; Chuchuryukin, A.; Suijkerbuijk, B. M. J. M.; van Klink, G. P. M.; Mills, A. M.; Spek, A. L.; van Koten, G., *Adv. Synth. Catal.* **2002,** *344*.

122. Sijbesma, R. P.; Beijer, F. H.; Brunsveld, L.; Folmer, B. J. B.; Ky Hirschberg, J. H. K.; Lange, R. F. M.; Lowe, J. K. L.; Meijer, E. W., *Science* **1997,** *278*, 1601-1604.

123. Burnworth, M.; Knapton, D.; Rowan, S. J.; Weder, C., *J. Inorg. Organomet. Polym Mater.* **2007,** *17*, 91-103.

124. Burke, K. A.; Sivakova, S.; McKenzie, B. M.; Mather, P. T.; Rowan, S. J., *J. Polym. Sci.: Part A: Polym. Chem.* **2006,** *44*, 5049-5059.

125. Botterhuis, N. E.; van Beek, D. J. M.; van Gemert, G. M. L.; Bosman, A. W.; Sijbesma, R. P., *J. Polym. Sci.: Part A: Polym. Chem.* **2008,** *46*, 3877-3885.

126. Fox, J.; Wie, J. J.; Greenland, B. W.; Burattini, S.; Hayes, W.; Colquhoun, H. M.; Mackay, M. E.; Rowan, S. J., *J. Am. Chem. Soc.* **2012,** *134*, 5362-5368.

127. Botterhuis, N. E.; van Beek, D. J. M.; van Gemert, G. M. L.; Bosman, A. W.; Sijbesma, R. P., *J. Polym. Sci., Part A: Polym. Chem.* **2008,** *46*, 3877-3885.

128. Kersey, F. R.; Yount, W. C.; Craig, S. L., *J. Am. Chem. Soc.* **2006,** *128*, 3886-3887.

129. Jeon, S. L.; Loveless, D. M.; Craig, S. L., *Supramol. Chem* **2010,** *22*, 698-703.

130. Loveless, D. M.; Jeon, S. L.; Craig, S. L., *J. Mater. Chem.* **2007,** *17*, 56-61.

131. Lodge, A. S., *T. Faraday Soc.* **1956,** *52*, 120-130.

132. Tanaka, F.; Edwards, S. F., *Macromolecules* **1992,** *25*, 1516-1523.

133. Jongschaap, R. J. J.; Wientjes, R. H. W.; Duits, M. H. G.; Mellema, J., *Macromolecules* **2001,** *34*, 1031-1038.

134. Furukawa, H.; Kuwabara, R.; Tanaka, Y.; Kurokawa, T.; Na, Y.-H.; Osada, Y.; Gong, J. P., *Macromolecules* **2008,** *41*, 7173-7178.

135. Kong, H. J.; Wong, E.; Mooney, D. J., *Macromolecules* **2003,** *36*, 4582-4588.

136. Mooney, M., *J. Appl. Phys.* **1940,** *11*, 582-592.

137. Rivlin, R. S., *Philos. T. R. Soc. Lond. A.* **1948,** *241*, 379-397.

138. Gent, A. N.; Thomas, A. G., *J. Appl. Polym. Sci.* **1959,** *1*, 107-113.

139. Kong, H. J.; Wong, E.; Mooney, D. J., *Macromolecules* **2003,** *36*, 4582-4588.

140. Jeon, S. L.; Loveless, D. M.; Yount, W. C.; Craig, S. L., *Inorg. Chem.* **2006,** *45*, 11060-11068.

141. Chen, D.; Handa, H.; Wan, L.; Mao, G., *Macromol. Rapid Commun.* **2007,** *28*, 1619-1623.

142. Chen, Y.; Spiering, A. J. H.; KarthikeyanS; Peters, G. W. M.; Meijer, E. W.; Sijbesma, R. P., *Nature Chem.* **2012,** *4*, 559-562.

143. Beyer, M. K.; Clausen-Schaumann, H., *Chem. Rev.* **2005,** *105*, 2921-2948.

144. Corkhill, P. H.; Hamilton, C. J.; Tighe, B. J., *Biomaterials* **1989,** *10*, 3-10.

145. Meakin, J. R.; Hukins, D. W. L.; Aspden, R. M.; Imrie, C. T., *J.Mater. Sci.: Mater. Med.* **2003,** *14*, 783-787.

146. Kon, M.; de Visser, A. C., *Plast. Reconstr. Surg.* **1981,** *67*, 289-293.

147. McFarland, C. D.; Mayer, S.; Scotchford, C.; Dalton, B. A.; Steele, J. G.; Downes, S., *J. Biomed. Mater. Res.* **1999,** *44*, 1-11.

148. Jeon, S. L.; Loveless, D. M.; Craig, S. L., *Supramol. Chem.* **2010,** *22*, 697-703.

Biography

Born: March 8, 1984 in Akron, Ohio

Education:

B.S. in Chemistry and Physics, Hillsdale College, Hillsdale, M.I., 2006

Ph.D. in Chemistry, Duke University, Durham, N.C. , expected 2014

Awards:

Pelham Wilder Teaching Award, Duke University, 2007 and 2010

3rd Place in the **Richard D. Gilbert Award Symposium for Students in Polymer Science –** North Carolina Section of the ACS Polymer Discussion Group, Raleigh, NC, 2010

National Science Foundation - Integrative Graduate Education and Research Traineeship Program (IGERT), Duke University, 2008

LAUREATES, undergraduate research award, Hillsdale College, 2005

Professional Memberships:

Phi Lambda Upsilon, Duke University Chapter, 2006-2013

American Chemical Society, N.C. section and Polymer Division, 2007-2014

Publications:

Jennifer L. Hawk and Stephen L. Craig **Physical and Materials Applications of Pincer Complexes,** *Top Organomet Chem,* **2013**, 40, pp 319-352

Xu, D., Hawk, J.L., Loveless, D.M., Jeon, S.L., and Craig, S. L. **Mechanism of Shear Thickening in Reversibly Cross-Linked Supramolecular Polymer Networks** *Macromolecules,* **2010**, 43 (7), pp 3556-3565